Hmx1 Function In Lateral Facial Development

Wenjie Li

A thesis

submitted in partial fulfillment of the

requirements for the degree of

Master of Science

University of Washington

2016

Committee:

Timothy Cox

Eric E. Turner

Richard Presland

Anne-Marie Bollen

Program Authorized to Offer Degree:

School of Dentistry

University of Washington

ABSTRACT

Hmx1 Function In Lateral Facial Development

Wenjie Li

Chair of the Supervisory Committee:

Professor Timothy Cox

Department of Oral Health Sciences, Pediatrics

The oculoauricular syndrome (OAS) in humans, the "*dumbo*" and "*misplaced ears*" strains in mice, the "*dumbo*" strain in rats, and the "crop ear" phenotype in cattle, all converge on a single gene - Hmx1. It encodes a homeodomain transcription factor expressed in the developing eyes, peripheral nervous system, and posterior aspects of the first and second branchial arches (BA1 and BA2) which give rise to lateral craniofacial structures including the external ear. Current published literature on lateral craniofacial development and its associated anomalies is scarce. To enhance the knowledge in this field, we used high-resolution imaging tools and performed 3D morphological studies on staged

mouse embryos and also on postnatal day 28 (adult) mice to characterize in detail the phenotype of the *dumbo* mutants. In addition to the rotated low-set position of the *dumbo* ear, a novel ear tag was found at the lower back of the pinna when *dumbo* mice were examined in a pure C57Bl6/N background. This structure could be identified as early as embryonic day (E)12. Abnormalities were also uncovered in adult *dumbo* mice: fusion in the squamosal and parietomastoid sutures, shape changes in the cranium and mandible, paraoccipital process hypoplasia, auriculofacial nerve deficits, and a lack of response to an air-blowing test. These all suggest Hmx1 is required for the development of lateral facial structures and proper neuromuscular reflex. Unlike the Hmx1 coding region mutations which were found responsible for the mouse phenotype and human OAS, our study with the *dumbo* rat strain showed that a 5.7 kb deletion, ~80 kb distal to the Hmx1 locus, is responsible for the rat *dumbo* phenotype. Transient transgenesis tests demonstrate that this deleted non-coding sequence encompasses a 594 bp Evolutionarily Conserved Region (ECR) that functions as an Hmx1 tissue-specific enhancer regulating the development of specific lateral and frontonasal mesenchyme. Future fate-mapping studies using this tissue-specific ECR will ultimately determine the specific craniofacial tissue types derived from the embryonic Hmx1-expressing mesenchyme. Studies of the Hmx1 regulatory network could provide a defined blueprint to interpret the genetic contribution to pinna morphogenesis and other birth defects associated with the lateral facial structures.

TABLE OF CONTENTS

ABBREVIATIONS

BABB:	benzyl alcohol/benzyl benzoate
BSA:	bovine serum albumin
bp:	base pair
CNE:	conserved non-coding element
CTAn:	CT Analyzer
DNA:	deoxyribonucleic acid
ssDNA:	single-stranded DNA
dsDNA:	double-stranded DNA
dNTP:	deoxyribonucleoside triphosphate
dH_2O:	deionized H_2O
dpc:	days post-coitum
E:	embryonic day
ECR:	evolutionarily conserved region
EDTA:	ethylene-diamine-tetra-acetic acid
ENU:	n-ethyl-n-nitrosourea
EtOH:	ethanol
GFP:	green fluorescent protein
hrs:	hours
HCl:	hydrochloric acid
IHC:	immunohistochemistry
IKI:	iodine potassium iodide
kb:	kilobase pairs
LB medium:	Luria-Bertani medium
LiCl:	lithium chloride
MeOH:	methanol
$MgCl_2$:	magnesium chloride
min:	minute
microCT:	microcomputed tomography
NaCl:	sodium chloride

Na_2CO_3:	sodium carbonate
$NaHCO_3$:	sodium bicarbonate
NaOH:	sodium hydroxide
O/N:	overnight
OPT:	optical projection tomography
PBFS:	phosphate buffered formal saline
PBS:	phosphate buffered saline
PCR:	polymerase chain reaction
PFA:	paraformaldehyde
PTAH:	phosphotungstic acid hematoxylin
RNA:	ribonucleic acid
RNAseq:	RNA sequencing, also called whole transcriptome shotgun sequencing (WTSS)
sec:	second
TAE:	tris-acetate-EDTA buffer
TBE:	tris-borate-EDTA buffer
TE:	tris-EDTA
TG:	trigeminal ganglion
OAS:	oculo-auricular syndrome
UV:	ultraviolet light
V:	volts
v/v:	volume per volume
w/v:	weight per volume
X-gal, BCIG:	5-bromo-4-chloro-3-indolyl-β-D-galactopyranoside

CHAPTER ONE: GENERAL INTRODUCTION AND BACKGROUND

1.1 Early patterning of the human ear development

The vertebrate ear is divided into the external, middle, and inner ear. The external ear, which consists of the auricle and the external acoustic meatus (EAM), plays an essential role in auditory function by protecting the tympanic membrane and receiving sound from the environment. Both genetic and environmental factors contribute to the development of malformation of the ear and its surrounding lateral facial structures [1]. Defects of the ear and its related lateral facial region have profound aesthetic, functional, and psychosocial impacts in patients' lives.

The emergence of the ear in humans starts at the end of the fourth week of gestation, during which four well-defined branchial arches (BA), also known as pharyngeal arches, are visible in the neck region of the embryo. The first (mandibular) and second (hyoid) arches contribute to the development of the external ear. During the 5th gestational week, six hillocks (the "Hillocks of His", three on each side) on the first and second branchial arches (BA1 and BA2) can be distinguished at the edge adjacent to the first branchial cleft. By the 20^{th} week of gestation, the auricle, which was initially located in the neck area, has moved upward to attain its adult location and overall configuration.

Developmental disturbance in the BA1 and BA2 regions can cause a common congenital defect in the structure of the external ear (pinna) and/or internal ear. The severity of the defect ranges from absence of the pinna (anotia), to a smaller pinna (microtia), or other minor structural abnormalities such as ear tags or absence of the ear lobe. The data collected from birth defects surveillance programs around the world shows that the overall prevalence of microtia and/or anotia is 2.06 per 10,000

births (CI: 2.02-2.10) [2]. Americans and Asians seem to have higher rates of microtia when compared to Europeans [2]. Similar to many other structural defects, microtia can be seen as an isolated anomaly or as an identifiable syndrome in approximately 20-60% of cases [1–3]. Even when not associated with other defects, individuals with microtia require surgical interventions for reconstruction and treatment of hearing loss. New genetic methods, including the identification of genes associated with human craniofacial syndromes, has shed light on normal and abnormal ear development. Potential environmental factors that can lead to the development of microtia include maternal diabetes [4], maternal age [5], and altitude [6, 7]. Epidemiological data have shown inherited mutations in *HOXA2* [8], *TBX1* [9], *SIX* [10], and *IRF6* [11] that lead to microtia, but they could only explain a small portion of the microtia cases. Developmental pathways for understanding lateral facial growth and pinna morphogenesis require further genetic investigations and related animal model studies.

1.2 The Oculo-Auricular Syndrome (OAS) is associated with Hmx1

Malformation or displacement of the ear occurs in many complex developmental syndromes, yet little is known about the specific mechanisms that underlie the development of the pinna. OAS, a rare autosomal recessive disease in humans, with profound ocular anomalies, malformed external ears but otherwise normal hearing in affected individuals, provides an entry point into understanding the developmental mechanism and associated deformities of the ear and lateral facial structures. It was first described in a reinvestigation of a consanguineous Swiss family in 2008 [12, 13]. Through sequence analysis, all the affected OAS members in this Caucasian family were found to have a homozygous deletion of 26 nucleotides (c.215-240 del) in a

gene encoding the Homeobox transcription factor *HMX1* (*NKX5-3*). Hmx1 has two exons; the deletion in exon one created a frameshift, generating a stop codon that abolished the translation of the homeobox domain in exon two [12]. Apart from the characteristic eyes and low-set ears, an individual patient designated as VII.8 (see **Fig. 1**) was found to have three rows of maxillary permanent teeth. In addition, spina bifida occulta and moderate dyscrania with flattening of the cranial base and short mandibular rami were found in another patient designated as VII.9 (see **Fig. 1**).

A second report from the study of a consanguineous family of Asian (Pakistani) background confirmed that the Hmx1 gene is associated with the OAS [14]. Genetic analyses in this study identified a homozygous c.650A>C; p.(Gln217Pro) missense mutation within the highly conserved homeodomain of Hmx1 gene of Patients I and II (homozygous) and parental sample (heterozygous). Protein structural modeling predicted the detrimental effect on protein folding and/or stability, which was further confirmed by in vitro dual luciferase assays. Both affected male patients were found to have similar complex eye defects, similar to the Swiss family report. Meanwhile, they were also recognized to have a highly unusual ear phenotype of malformed, low-set pinna with crumpled helix, narrow external acoustic meatus (EAM) and deficient lobule (see **Fig. 2 A, B, D**). It indicated that the developmental deficiency in both the BA1 and BA2 are associated with developmental deficiency of the EAM, and abnormalities of the helix and anti-tragus lobe, respectively [15]. Minor external ear abnormalities and marked bilateral posterior corneal abnormality seen on slit lamp examination called embryotoxon [16] were found in the father of Patient I, suggesting manifestations of a carrier. Protein function analyses supported previous findings that the evolutionarily constrained homeodomain, including parts that do not establish

direct DNA contact, is critical to HMX1 function [17]. The phenotypic details of all the patients are listed in **Table 1**.

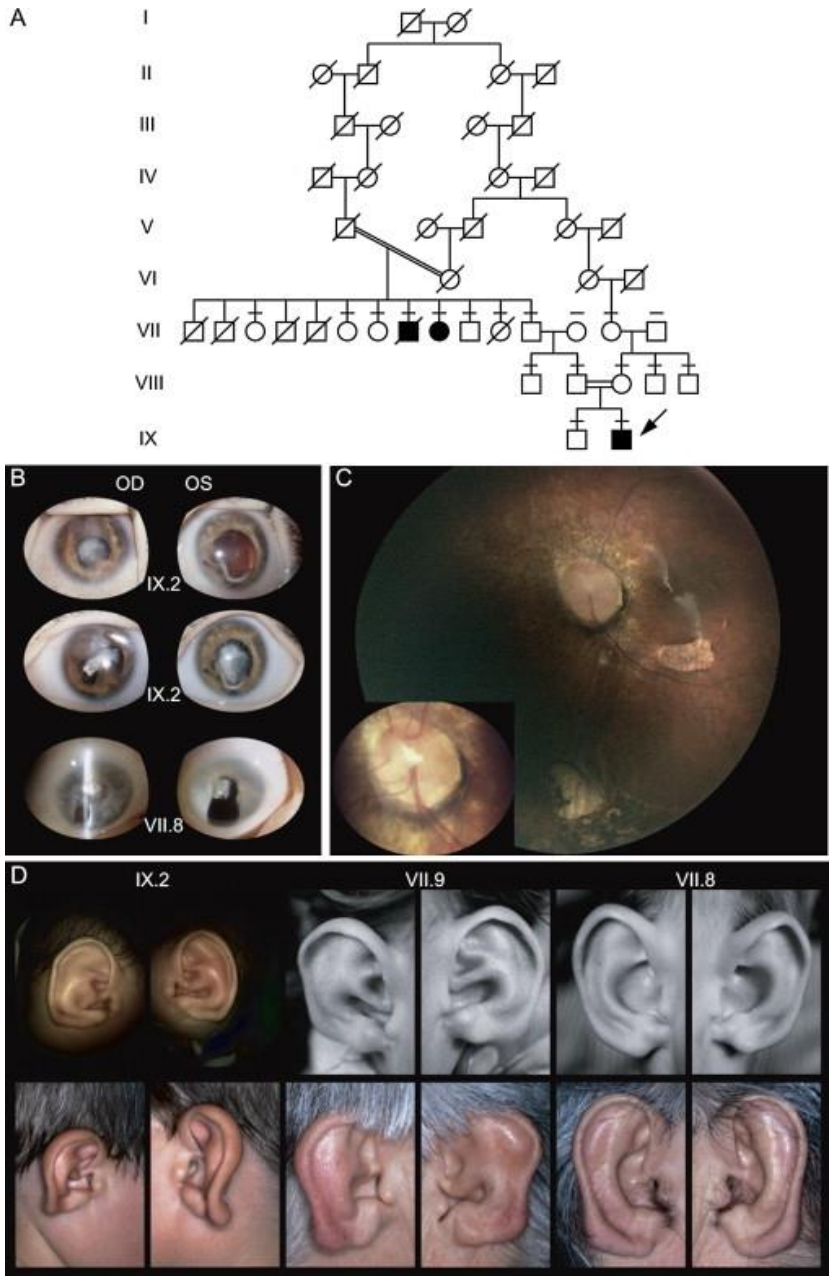

Figure 1. The deletion in the coding region of *HMX1* led to the Oculo-Auricular Syndrome in the Swiss family (adapted from Schorderet DF and et al [12]).
(A) Pedigree of consanguineous family with autosomal recessive oculo-auricular syndrome. Affected individuals are indicated by black symbols, and the proband is indicated by an arrow. Individuals with a line above the symbol have been tested for the mutation. (B) Top: Eyes of two affected patients. Middle: Eyes of the proband a few months later with advanced cataract. Bottom: Eyes of VII.8 presenting cataract and coloboma. (C) Fundus photography of irido-corneal adherences in the left eye (Retcam II) showing the macular hypoplasia, inferior chorio-retinal coloboma, retinal dysplasia, and Morning Glory-like optic nerve head, with a magnified view of the latter (lower left corner). (D) External ear of the three affected patients at two different ages. The three ear pinnas present a deformation of the lobule. Left: Patient IX.2. Middle: Patient VII.9. Right: Patient VII.8.

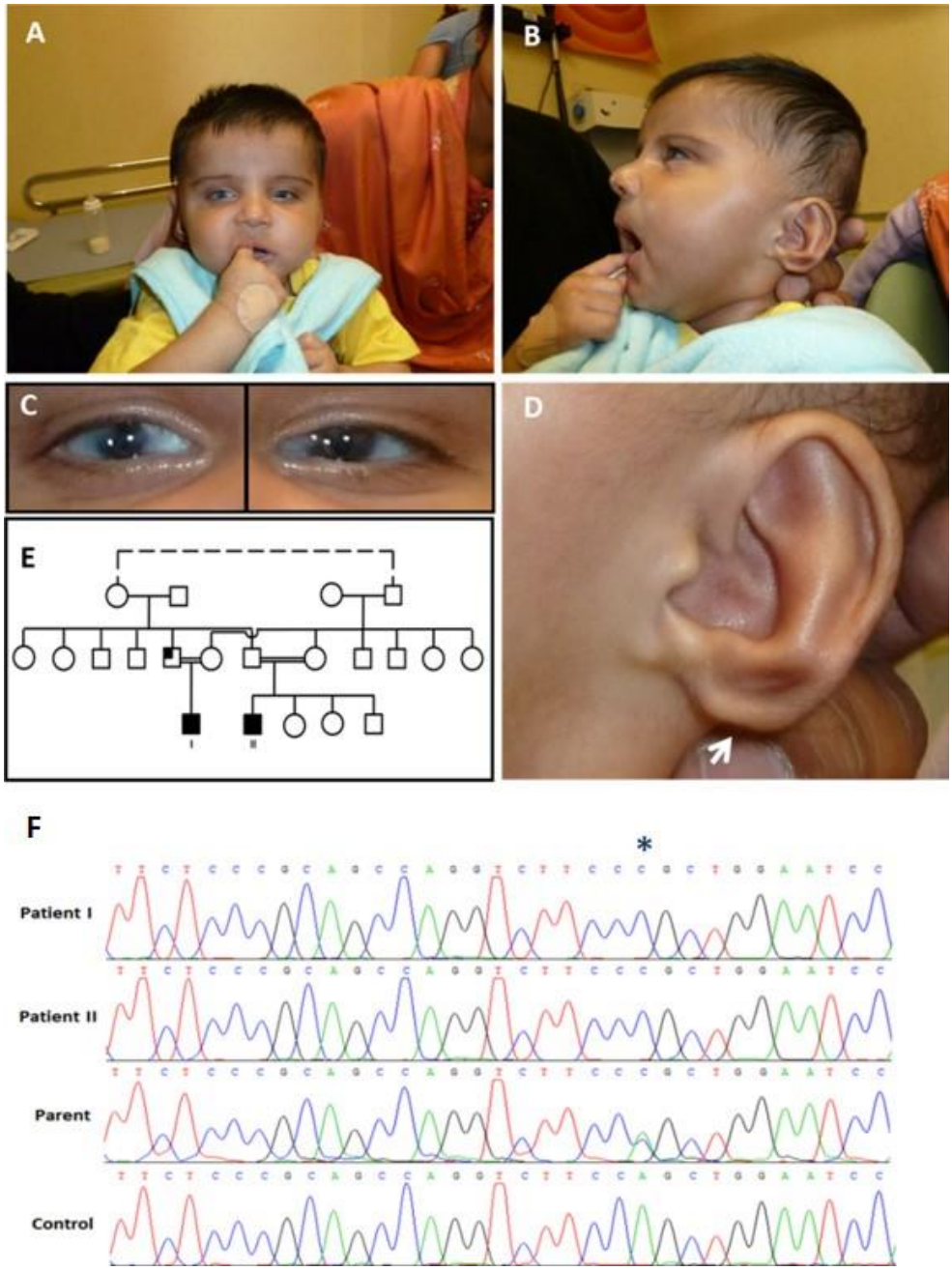

Figure 2. The Pakistani family with Oculo-Auricular Syndrome originating from a non-tolerable homozygous missense mutation within the highly conserved homeodomain of HMX1 (adapted from Gillespie R.L. et al [14]). (A) Patient I presenting with bilateral microcornea, microphthalmia, coloboma, and congenital cataract. (B) Profile view of Patient I demonstrating an unusual ear morphology. (C) Close-up view of the ocular features in Patient I: bilateral microcornea, microphthalmia, coloboma, and congenital cataract. (D) Close-up view of the unusual ear morphology in Patient I. The deficient lobule is indicated by a white arrow. (E) Three generation family pedigree with affected family members represented by black squares. Father of Patient I with carrier manifestations is represented by a white square with a black insert. (F) HMX1 Sanger sequencing results. Chromatogram depicting the homozygous HMX1 c.650A>C (p.Gln217Pro) sequence change (indicated by an asterisk) that is homozygous in Patients I and II, heterozygous in the parental sample and absent in the control.

	Patient I	Patient II	Proband*	Individual 1 (VII.8)*	Individual 2 (VII.9)*
Eye					
Anterior segment					
Cornea	Posterior embryotoxon (L)	Posterior embryotoxin (L)	Microcornea	Sclerocornea	Microcornea
	Localized sclerocornea (R)	Gross sclerocornea (opaque and vascularized in [R])			
	Microcornea (7 mm [R]; 8 mm [L])	Microcornea (6 mm [R]; 6.75 mm [L])			
Lens	Bilateral dense CC	Dense central & nuclear bilateral CC	Rapidly progressive bilateral CC	Cataract (onset not clear)	Cataract (onset not clear) Microphakia
Iris	Inferior iris coloboma	Inferior iris coloboma	Posterior synechiae	Inferior iris coloboma	Iris coloboma
		Anterior synechiae (L)	Incomplete iris coloboma		
Posterior segment					
Retina	Bilateral uveoretinal coloboma	Small, tilted, dysplastic optic discs	Bilateral optic nerve dysplasia	Inferior chorioretinal coloboma (R)	Retinal detachment
	Small dysplastic optic discs		Macular hypoplasia	Inferior chorioretinal atrophy	
			Peripheral infero-nasal chorioretinal coloboma	Lacunae (L)	
			Circumferential abnormalities of the RPE	Pigment deposits within the RPE	
			Mottled RPE appearance (aged 4 y)		
			Equatorial chorioretinal atrophic lacunae		
			Thinning of the retinal vessels		
ERG	N/A	Significantly attenuated light & dark ERGs (age 14 y)	Moderately severe, generalized retinal dystrophy, apparent loss of rod photoreceptor function, mild cone abnormality (aged 6 y). Rod-cone dystrophy (aged 7 y)	N/R	N/R
			Almost undetectable rod specific ERG, severe cone ERG abnormalities (aged 12 y)		
Other					
Globe	Colobomatous microphthalmia	Gross microphthalmia	Colobomatous microphthalmia (R)	Microphthalmia	Microphthalmia
	Short axial length (13.9 mm [R]; 14.9 mm [L])	Slightly short axial length (17 mm [L]; 16.9 mm [R])	Esotropia (R) (aged 4 y)	Increased IOP	
		Enophthalmos			
Other	Congenital nystagmus	x-NEW-CELL-x	Congenital nystagmus	Nystagmus	(L) eye enucleated due to painful complications of partially calcified phthisis bulbi
	Divergent strabismus (R)				
	Naso-lacrimal duct obstruction				
Visual symptoms	Poor peripheral vision	Good light response, poor dark adaptation (age 5 mo)	Poor visual acuity from infancy, marked visual field constriction (aged 9 y)	Vision limited to light perception (aged 6 y).	N/R
	Poor dark adaptation (age 2.5 y)			Normal eye tension and some vision maintained through inferior iris coloboma until aged 65 y when cataracts progressed	
Ear					
Phenotype	Low-set	Low-set	Lobule aplasia	Strikingly abnormal appearance of the pinna	Strikingly abnormal appearance of the pinna
			Narrow intertragic incisures		
	Lobule aplasia	Lobule aplasia	Abnormal bridging between the crus of helix and antihelix	Lobule aplasia	Lobule aplasia
	Narrow external acoustic meatus	Narrow external acoustic meatus	Narrow external acoustic meatus		
		'Crumpled' appearance	Small eardrum with normal appearance		
Hearing	Normal	Normal	Normal	N/R	N/R
Other	Excessive sweating	Excessive sweating	N/R	3 maxillary dental rows	Spina bifida occulta
		High palate			Moderate dyscrania with flattening of the cranial base
		Extra dentition			
		Small atrial septal defect			Short mandibular rami
		Micrognathia			
		Mild plagiocephaly			

Table 1. Summary of phenotypic details of patients I and II reported (adapted from Gillespie R.L. et al [14] and the original OAS family reported by Schorderet et al [12])**.** R, right eye; L, left eye; N/A, not available; N/R, not reported. * Indicates affected individuals described in the original OAS family.

1.3 Hmx1 - an entry point to understand lateral facial development

The *HMX1* (*NKX5-3*) with three other transcription factors: *HMX2* (*NKX5-2*), *HMX3* (*NKX5-1*), and *SOHO1* in vertebrates comprise the NKX5 homeodomain family [18]. The H6 homeobox genes *Hmx1*, *Hmx2* and *Hmx3* compose a family within the NKL subclass of the ANTP (Antennapedia) class of homeobox genes [19]. This Homeobox family is a large group of genes, each containing the homeobox domain, which is approximately 180 base pairs in length and encodes a highly conserved, functional helix-turn-helix motif. Specificity of the DNA binding motif allows Homeobox proteins to regulate expression of other genes [20]. *HMX1* can act as a transcriptional repressor and has a preferential binding for the consensus sequence 5′-CAAGTG-3′ [21].

In the mouse, *Hmx1* expression in the craniofacial mesenchyme (CM) can be detected at E10.5 in the dorsal part of BA1, the caudal half of BA2, the peripheral nervous system, and the eye [22–25]. In the peripheral nervous system, the *Hmx1* expression is restricted to the mandibular lobe of the trigeminal ganglion (TG), geniculate (facial) ganglion and the dorsal root ganglia. The mouse models such as the "dumbo" (*dmbo*) and "misplaced ears" (*mpe*) mutant lines represent two mutations in *Hmx1* [26]. The *dmbo* model was found to have a C→T mutation corresponding to amino acid 193 in the *Hmx1* exon 1, changing GLU65 to an amber stop codon (CAG→UAG), which abolished the protein function. The *mpe* line arose from a spontaneous mutation in C3H/HeJ colony mice at the Jackson Laboratory [26]. An 8 bp deletion in the exon 2 homeodomain was found in the $Hmx1^{mpe}$ allele. Homozygotes of this mutation also have the similar low-set external ear phenotype with a shortfall of homozygotes from intercrosses [26]. The hearing and inner ear structures of the homozygous mice were no different from the controls, similar to the reports of OAS patients [12, 14, 26, 27].

Similar ear phenotypes found in rats led to the discovery of a mutation in the highly conserved non-coding element downstream from the *Hmx1* gene [28]. Strongly resembling the mouse counterpart [29], the autosomal recessive rat *dumbo* phenotype was found to be caused by a 5,777 bp deletion residing ~80 Mb downstream from the *Hmx1* transcription unit which houses a Evolutionarily Conserved Region (ECR) common to all mammalian species [28], which is about ~600 bp [28, 30] in length. The loss of HMX1 protein expression in branchial arch mesenchyme but not in sensory neurons strongly suggested that the deletion region could function as an *Hmx1* tissue-specific enhancer of the lateral facial mesenchyme [28]. Interestingly, a recent report of the common "crop ear" trait in Highland cattle showed that the truncated ear phenotype is caused by a 76 bp duplication within the most highly conserved part of the ~600 bp ECR found in the *dumbo* rat (see **Fig. 22, 23**) [31]. These cross-species models reinforced the ECR's role in conserved developmental processes and Hmx1's function in the ear and lateral facial development.

The common phenotype associated with loss of *Hmx1* in different species is distinct from all other known syndromes affecting ear development, which have more extensive craniofacial malformations. For example, a mutation in *HOXA2*, a classical gene in ear development, was reported to cause autosomal recessive bilateral microtia with hearing impairment and partial cleft palate [8]. Similar to the human condition, the *Hoxa2* deficient mice also exhibit external and middle ear deformities together with other craniofacial defects including bilateral cleft of the secondary palate [32, 33]. A Treacher Collins-Franceschetti Syndrome 1 (*TOCF1*) mutation is responsible for Treacher Collins Syndrome (TCS), and apart from microtia, affected patients have middle ear defects that result in conductive deafness and other phenotypes such as cleft palate [34, 35]. Transcription factor *TFAP2A* is associated with the human

Branchio-Oculo-Facial Syndrome (BOFS), which has the characteristic defects of the outer and middle ear as well as the conductive hearing loss [36]. Mutations in the *Bmp5* gene, which belongs to the Bone Morphogenetic Proteins (BMP) family, results in a reduction of pinna size accompanied by the congenital absence of a pair of ribs and other bony defects in mice [37]. Thus, Hmx1's patterning suggests a more specific and distinctive role in the development of the lateral facial region which may be relevant to the subtle craniofacial malformations that are commonly seen in pediatric practice.

Attempts have been made to characterize *Hmx1*'s function in retinogenesis and neurogenesis in *Drosophila,* zebrafish, and mice [17, 23, 38]. A combination of *in silico* and *in vitro* techniques have identified Hmx1 target genes such as *Ptpro* and *Sema3f* in retinogenesis [39]. While still under investigation, Hmx1 could play a role in the establishment of retinal polarity [17]. In lateral facial development, *Hmx1* is found to be essential for the early development of the geniculate ganglion and facial nerve [25]. One report based on a small number of mixed strain animals described hypertrophy of the gonial bone and exencephaly due to *Hmx1* mutation [26]. However, none of these studies provided a clear understanding of Hmx1's function in lateral craniofacial development. Hence this study aims to address this issue by using the *dumbo* mouse model and transgenic assay studies.

1.4 Working hypotheses and research aims

Based on the literature review, we hypothesize that: the Hmx1 gene plays a significant role in the development of lateral facial structures especially the ear (pinna); and that loss of Hmx1 could lead to severe malformation of these structures; and that the deleted region in the *dumbo* rat contains the regulatory elements necessary to drive Hmx1 expression in craniofacial tissues.

To test these hypotheses, the aims of this research project are:

<u>Aim 1:</u> To determine the craniofacial/skeletal features in the presence and absence of Hmx1 in mice.

In this project, computer-based three-dimensional (3D) morphometric methods and histochemistry tests will be used to carefully characterize affected craniofacial structures in Hmx1 *dumbo* mice at different embryonic stages as well as in adulthood. Behavioral tests will be used to investigate neuromuscular function in adult *dumbo* mice.

<u>Aim 2:</u> To test the function of the dumbo rat Hmx1 downstream deletion region and to explore the Hmx1 gene regulatory elements.

In this study, transgenic analyses will be used to determine the enhancer activities of the *dumbo* rat Hmx1 downstream deletion region. The ECR region within the *dumbo* rat Hmx1 deletion will be carefully analyzed by using the transgenic essay. Attempts will be made to explore the possible upstream regulators and downstream targets of Hmx1 in the craniofacial mesenchyme.

CHAPTER TWO: MATERIALS AND METHODS

2.1 Materials

2.1.1 Drugs, chemicals, and reagents

All chemicals and reagents were of analytical grade or other highest grade obtainable. They were purchased from a range of manufacturers, with Sigma being the major source of the most chemicals and reagents.

2.1.2 Enzymes

All restriction endonucleases and buffers were purchased from New England Biolabs (NEB). Appropriate reaction buffers (either 5X or 10X) and additional supplements were supplied with all enzymes.

2.1.3 Stain and dyes

Ethidium bromide (1% solution)	Fisher BioReagents (BP1302-10)
Iodine	ThermoFisher Scientific (19656-1000)
Potassium iodide	Sigma-Aldrich (746428)

2.1.4 Antibiotics and indicators

Ampicillin Sodium Salt	Fisher Scientific (BP1760-25)
Chloramphenicol	Fisher Scientific (BP904-100)

Kanamycin Sulfate	Fisher Scientific (BP906-5)
X-Gal	G-Biosciences (RC-113)

2.1.5 Kits and assays

DNeasy Blood & Tissue Kit (50)	Qiagen (69582)
EndoFree Plasmid Maxi Kit (10)	Qiagen (12362)
QIAGEN Plasmid Mini Kit (100)	Qiagen (12125)
mMESSAGE mMACHINE® T7 ULTRA Transcription Kit	ThermoFisher Scientific (AM1345)
MEGAclear™ Transcription Clean-Up Kit	ThermoFisher Scientific (AM1908)
pENTR™/SD/SD D-TOPO® Cloning Kits	ThermoFisher Scientific (K2420-20)
QIAquick PCR Purification Kit (250)	Qiagen (28104)
Quick Ligation™ Kit	New England BioLabs (M2200S)

2.1.6 Nucleic acid molecular weight marker

GeneRuler 1 kb Plus DNA Ladder (SM1331), 123 bp DNA Ladder (15613-011) and 100 bp DNA Ladder (15628-019) all purchased from ThermoFisher Scientific.

2.1.7 Solutions and buffers

CutSmart® Buffer Components (1X)	New England BioLabs (B7204S)
EDTA (0.5M)	Sigma-Aldrich (E7889)
Ethanol (200 Proof)	Koptec (Lot: A06111505F)
UltraPure™ 0.5M EDTA, pH 8.0	ThermoFisher (15575-020)

Glutaraldehyde Solution (25% In Water)	EMD Chemicals (GX015305-1)
Trizma® hydrochloride solution (1M, pH 7.4)	Sigma-Aldrich (T2663)
IGEPAL CA-630 (Nonidet P-40):	Sigma-Aldrich
Phenol/Chloroform/Isoamyl Alcohol (25:24:1 Mixture, pH 5.2±0.3, Liq.)	Fisher Scientific (BP17531-100)
Power SYBR® Green PCR Master Mix	ThermoFisher (4367659)
Xylene (histological level)	Fisher Scientific (X3P-1GAL)

2.1.8 Cloning and expression vectors

Hsp68-LacZ-Gateway (Plasmid #37843)	Addgene
Gateway® pDONR™221 Vector	Invitrogen
pENTR™/SD/D-TOPO®	Invitrogen
pDB302 PB GWenh miRNA	Dr. David Beier lab

2.1.9 Synthetic oligonucleotides

Table 2.1.9a: Primers used to generate the *dumbo* rat downstream deletion region.

Region	**Forward Primer 5' → 3'**	**Reverse Primer 5' → 3'**	**Product Size (bp)**
Main Human Homology Region	M hum F	M hum R	589
	GGGATCGCGGCCGCGAATCCTGGCCAGTCAGTGTA	GATCGGCGCGCCGGCTTGGGGGTGGCAAACTG	
Dumbo rat deletion Region (whole)	Dum Del Whl F	Dum Del Whl R	6094
	GGGATCGCGGCCGCGTGCACCATCTTTGAGGACTTAG	GATCGGCGCGCCGTAGGGAAGCTGAGGCCAAG	
Dumbo rat deletion region (1st half)	Dum Del 1st F	Dum Del 1st R	4761
	GGGATCGCGGCCGCGCTAGAGAGAGAGCTGGGGTCT	GATCGGCGCGCCACATGAACTGTGCAAAGCTACAAGG	
Dumbo rat deletion region (2nd half)	Dum Del 2nd F	Dum Del 2nd R	1792
	GGGATCGCGGCCGCAGGAGAATGAGAGGGATCTTCTG	GATCGGCGCGCCGGCTCCAGCCTCCTTCCACCT	

The underlined regions in the forward and reverse primers show the recognition sites of the Not1 (GCGGCCGC) and Asc1 (GGCGCGCC) restriction enzymes respectively. The regions highlighted in red and blue are to balance the GC content, prevent primer dimerization and adjust the reaction temperature of the primers. The M hum R primer has 5 more bps that match with the dumbo rat deletion region sequence, hence the actual cloning size for the main human homology region is 594 bp.

Table 2.1.9b: Primers used for genotyping.

Region	**Forward Primer 5' → 3'**	**Reverse Primer 5' → 3'**	**Product Size (bp)**
Cre (created line)	Cre SYBR 5	Cre SYBR 3	65
	TGGGCCAGCTAAACATGCTT	AACAGCATTGCTGTCACTTGGT	
Turbo GFP	Turbo GFP-1 F	Turbo GFP-1 R	101
	CCGAGGACAGCGTGATCT	GGTGAAGCTGCCATCCAG	
	Turbo GFP-2 F	Turbo GFP-2 R	103
	GGGCGATAACGATCTGGA	GGCGCTCTTGAAGTGCAT	
	TurboGFP-F	TurboGFP-R	834
	AGCCTTCCAGAAGCAGAGC	AATAACATATAGACAAACGCACACC	
LacZ	LacZp1 sens	LacZp1 asens	95
	GCTGGATCAAATCTGTCGATCCTT	CGCGTACATCGGGCAAATAATATC	
	LacZp2 sens	LacZp2 asens	99
	ATAGCGATAACGAGCTCCTGCACT	ACTGTTTACCTTGTGGAGCGACATC	
Hmx1 gene WT	Common 5'	Hmx1 WT 3'	54
	GAGGACGAGGATCCGGAGC	CTGCTGTCGCCGCCGCTG	
Hmx1 gene *dumbo* mutant	Common 5'	Hmx1 dmbo 3'	54
	GAGGACGAGGATCCGGAGC	CTGCTGTCGCCGCCGCT**A**	
pDB_LTR left side	pDB_LTR_L-TTAA-F	pDB_LTR_L-TTAA-R	108
	GACGTGTTTAAAGTTTAGGTCGAG	AGAAAGAGAGAGCAATATTTCAAGAAT	
pDB_LTR right side	pDB_LTR_R-TTAA-F	pDB_LTR_R-TTAA-R	118
	CCGATAAAACACATGCGTCA	CGACAGCAGGCTGAATAATAAA	
pDB_LTR left site off (the region removed by trasposase reaction)	pDB_LTR_L-Off-F	pDB_LTR_L-Off-R	118
	ACCATGATTACGCCAAGCTC	ATTGTGGCCAAGCTGTGTG	
pDB_LTR right side off	pDB_LTR_R-Off-F	pDB_LTR_R-Off-R	102
	TTATTCAGCCTGCTGTCGTG	GTTTTCCCAGTCACGACGTT	

Table 2.1.9c: Primers used for sequencing.

Purpose of Primer Types	**Forward Primer 5' → 3'**	**Reverse Primer 5' → 3'**	**Product Size (bp)**
Checking the Att R1 site		Att R1 site R TGCCTCAAAATGTTCTTTACGA	
Checking the Att R2 site	Att R2 site forward oligo (Scott) ACTTTACCCGGTGGTGCATA	PiggyBac R GATCCTCTCCAATCGCGTTA	
Testing the Hsp70 promoter	Hsp70promTest F AGCTCCAGGAACATCCAAACT	Hsp70promTest R CTCGTCGCTCTCCATGCTA	888
Testing the Turbo GFP region	TurboGFP F AGCCTTCCAGAAGCAGAGC	TurboGFP R AATAACATATAGACAAACGCACACC	834
Testing the transposase site	TPaseTest F CTCTTTCTAAATAGCGCGAATCC	TPaseTest R CCAAGGAGGCTGTGGATG	809
Checking the Hsp68 promoter region		Hsp68-Cre-R CTTCTTGGGCATGGCGCCGCGCTCTGCTTCTGGAAG GCTG	
Checking the nls-Cre region		Hsp68-Cre-F GAAGCAGAGCGCGGCGCCATGCCCAAGAAGAAGA GGAAGGTGTCC	

2.1.10 Bacterial strains

NovaBlue singles™ competent cells	Novagen (70181-1PKG)
One Shot® TOP10 chemically competent E. coli	Invitrogen (C4040-10)
One Shot® ccdB Survival™ 2 T1R competent cells	ThermoFisher (A10460)

2.1.11 Bacterial growth media

All growth media were prepared by adding 25 g LB Broth Miller (EMD Millipore) into 1 L of distilled and deionized water, which were sterilized by autoclaving. Antibiotics, being labile chemicals, were only added after the solution had cooled to 50°C. Ampicillin (100 μg/ml), Kanamycin (50 μg/ml) or chloramphenicol (100 μg/ml) was added to maintain appropriate selective pressure.

2.1.12 Antibodies

Donkey anti-goat	ThermoFisher Scientific (Cat# A-11055)
Donkey anti-rabbit	ThermoFisher Scientific (Cat#A-21207)
Goat anti-β galactosidase	Biogenesis (cat #4600-1409)
Rabbit anti- Hmx1 protein	Turner Lab 34-1

Conjugated species-specific secondary antibodies labeled with Alexa fluorophores were obtained from ThermoFisher Scientific.

2.1.13 Miscellaneous materials

0.22 μm filtered unit	Sigma-Aldrich (F9893)
0.02 μm Whatman® Anotop® 10 syringe filter	Sigma-Aldrich (Z747653)
Agarose, Low Melting Point, Analytical Grade	Promega (PR V2111)

UltraPure™ Agarose	Invitrogen (15510-027)
Alcian Blue 8 GX	SIGMA (A5268)
Chemical Permount™ Mounting Medium	Fisher Scientific (SP15-100)
LB Broth Miller	EMD Millipore (1.10285)
Richard-Allan Scientific™ Neg-50™ Frozen Section Medium	Thermo Scientific
Potassium Ferricyanide (≥99.0%, ACS Reagent Grade)	MP Biomedicals (0215255980)
Potassium Ferrocyanide Trihydrate	MP Biomedicals (0215256080)
S.O.C. Medium	Thermo Scientific (15544-034)
Stericup-GP, 0.22 µm, polyethersulfone, 500 mL, radio-sterilized filter	EMD Millipore (SCGPU05RE)
Steriflip-GP, 0.22 µm, polyethersulfone, gamma irradiated filter	EMD Millipore (SCGP00525)

2.2 Methods used for recombinant DNA experiments

2.2.1 General molecular biology methods

General molecular biology methods described in “Current Protocols in Molecular Biology, First Edition, 1988” by Frederick M. Ausubel et al. was used a reference for the following methods: Agarose Gel Electrophoresis, Isolation, and Purification of Large DNA

Restriction Fragments from Agarose Gels, Phenol/Chloroform Extractions. Others were using the standard protocols from commercial kits.

2.2.2 Restriction enzyme digests

Restriction enzyme (RE) digests were used for analytical purposes as well as in the preparation of both vectors and inserts for ligations. Restriction enzymes were from New England BioLabs and Thermo Scientific Fermentas Molecular Biology. The CutSmart® Buffer and FastDigest Green Buffer were used for multiple enzyme digests. Generally, 1 unit of enzyme was used to digest 1 μg of DNA at 37°C for at least 1 h.

2.2.3 Preparation of Cloning Vectors

The vectors were digested with the appropriate restriction enzymes. Once digested, one tenth of the volume was electrophoresed on the agarose gel as a check to ensure complete digestion. The remaining digested vector was then electrophoresed, excised and purified from the gel by using the QIAquick gel extraction kit (QIAGEN Cat#28706).

2.2.4 Mini, Maxi Preparation of Plasmid DNA

Following overnight (O/N) growth by streaking the bacteria onto selective L-agar plates, colonies were picked, and inoculated in a culture of LB medium (2 ml or 100 ml) containing the appropriate selective antibiotic. The cultures were then incubated O/N at 37°C with vigorous

shaking. The DNA was extracted using QIAprep Spin Miniprep Kit (cat. no.27104) and QIAgen EndoFree Plasmid Maxi Kit (cat. no. 12362).

2.2.5 Polymerase Chain Reaction (PCR)

The primers used throughout this study were ordered from Eurofins Genomics and their product sizes are outlined in table 2.1.9a. The annealing temperatures for primers were determined by using the simplest equation of the Wallace rule:

Annealing temperature (Ta) = 2°C * (A+T) + 4°C * (G+C) - 5°C * (A+T) = sum of A and T residues in the primer; (C+G) = sum of C and G residues in the primer. The final reagent concentrations of each PCR reaction were: Phusion HF/GC buffer (1X), dNTP's mix (200 µM), each primer (0.5 µM), template (4 ng/µl), and Phusion® High-Fidelity DNA Polymerase (1.0 units, Thermo Scientific, M0530). PCR reaction followed 1 cycle of 98°C for 30 sec, 25 cycles (98°C, 10 sec; 65°C, 1 min per kb), 1 cycle (72°C for 5 min). PCR products were electrophoresed on 1% - 1.5% agarose gels and visualized with ethidium bromide under UV illumination.

2.2.6 Real-time PCR genotyping

The primers used throughout this study and their product sizes are outlined in table 2.1.9b. Each reaction was set up in a total volume of 25 µl. The final reagent concentrations were: 0.2 µM forward and reverse primer pair, 1x Power SYBR Green Master Mix (Life Technologies), 1%

BSA. The annealing temperature of the reaction was 65°C as previously described [40]. The MicroAmp® Optical 96-Well Reaction Plate (ThermoFisher Scientific) was used according to the manufacturer's instructions.

2.2.7 Overlap PCR

Primers commercially designed for this purpose involve two primers which share few complementary base pairs with each another as a linking point. These "end primers" are the gateway attB sites for later entry BP clonase reaction. Firstly, the “Extension” fragments were separately amplified by PCR in a reaction with a total volume of 20 µl. Then they were poured together for overlap PCR with the final concentration of the reagents at: Phusion GC buffer (1X), dNTP’s mix (200 µM), 1:1 molar ratio PCR products, and Phusion® High-Fidelity DNA Polymerase (1.0 units). This process involved a 3 min cycle at 98°C, followed by eight cycles (98°C for 10 sec, then 65°C for 15 sec), and lastly a 3 min cycle at 72°C. After the overlap PCR, we diluted the solution 100 times and used the dilution to create new extension PCR reagent with the right primers. After confirming the product by gel electrophoresis, the right-sized band was gel extracted for further cloning into the desired vector.

2.2.8 Agarose gel electrophoresis

The agarose gel was made up of 0.8%, 1%, 1.5% or 2% agarose in 1x TAE or sodium borate buffer depending on the size of the DNA products to be electrophoresed. We added ethidium

bromide (EtBr) to the agarose gel to obtain a final concentration of 0.5 µg/mL (usually about 5 µl of lab stock solution (1%) per 100 mL gel) for DNA visualization. We placed the gel in the electrophoresis tank and submerged it with the gel buffer accordingly. The DNA samples containing a suitable amount of loading buffer (at a final concentration of 1X) were then loaded into the gel slots. 60-80 V was applied to the TAE tank, while 100-120 V was applied to the sodium borate buffer tank for electrophoresis. The entire reaction was stopped when the gel loading dye (blue color) had migrated the required distance. DNA products were visualized by illumination with long or medium wave UV light.

2.2.9 Phenol/chloroform extraction of DNA

We dissolved the products into sterile dH_2O with a final volume of 50 µl. After adding an equal volume of phenol/chloroform/isoamylalcohol, the mixture was vortexed briefly and centrifuged for 5 min at 14,000 rpm. The supernatant was removed to a clean tube and gently rocked to obtain high molecular weight DNA. The sample was then EtOH precipitated as described below.

2.2.10 Ethanol precipitation of DNA

1 µl of glycogen, $1/10^{th}$ the volume of 10M LiCl (5 µl) and 3 volumes of chilled absolute (100%) EtOH (150 µl) were added to the solution containing the DNA and mixed thoroughly. Next, the tube was placed at -80°C for 30 min, then centrifuged at 14,000 rpm for 20 min and the resultant pellet was washed in 70% EtOH and air-dried before being resuspended in sterile dH_20 or TE

buffer.

2.2.11 Standard heat-shock transformation of chemically competent bacteria

Frozen competent cells were thawed on ice for approximately 20-30 min while the agar plates (containing the appropriate antibiotic) were warmed in a 37°C incubator. 1 to 5 µl of DNA (usually 10 pg to 100 ng) was then gently mixed into 20-50 µL of competent cells in a microcentrifuge or falcon tube (by flicking the bottom of the tube with a finger a few times). The competent cell/DNA mixture was placed on the ice for 20-30 min. Each transformation tube was heat-shocked by placing the lower 1/2 to 2/3 of the tube into a 42°C water bath for 30-60 sec (45 sec is usually ideal, but this varies depending on the competent cells). The tubes were returned to the ice for 2 min and then 250 µl of S.O.C medium (without antibiotic) was added to the tubes which were placed in a 37°C shaking incubator for 45 mins. Some or all of the transformed cells were plated onto a 10 cm LB agar plate containing the appropriate antibiotic. The plates were then incubated overnight at 37°C. Ultrapure DNA was prepared first using the QIAprep Spin Miniprep Kit, then the QIAGEN Plasmid Midi Kit and lastly the EndoFree Plasmid Maxi Kit. DNA preparation was performed according to the manufacturers' protocol.

2.2.12 LR/BP Clonase II reaction

This reaction was performed using the Gateway Cloning Technology (ThermoFisher Scientific). One ENTR (100 ng) with the desired sequence and one DEST (150 ng) clone were added with

TE buffer to 8 µl. pENTR™-gus was used as a positive control. 2 µl of the 5 x LR/BP-Clonase Enzyme II Mix was added to the Gateway reaction and incubated for 10 min at 37°C. 1 µl of Proteinase K solution was added subsequently and incubated for 10 min at 37°C. 1 µl of this reaction reagent was transformed into competent E. coli cells grown in the presence of the appropriate antibiotics.

2.2.13 mMessage mMachine High Yield Capped mRNA T3/T7 Transcription reaction

The commercial mMESSAGE mMACHINE® Kit (ThermoFisher Scientific) was used to generate the mRNA. Template plasmids were linearized with a restriction enzyme downstream to the insert. The reaction was assembled in 20 µl total volume of RT (1X NTP/CAP, 1 x reaction buffer, 0.1-1 µg linear template DNA, 2 µl enzyme mix) and incubated at 37°C for 1 hr. 1µl TURBO DNase was then added and the mixture was incubated at 37°C for 15 min to remove the template DNA.

2.2.14 Poly(A) tailing procedure

We added the following tailing reagents by using the mMESSAGE mMACHINE® T7 Ultra kit in the following order:

Component	**Amount**
Nuclease-free Water	36 µl
5X E-PAP Buffer	20 µl

25 mM $MnCl_2$	10 µl
ATP Solution	10 µl

We reserved 2.5 µL of the reaction mixture before adding 4 µL of E-PAP enzyme into the rest of the mixture, which was mixed gently. The final reaction volume was 100 µL, which was incubated at 37°C for 30-45 min and then placed on ice. The reaction mixture that did not contain the E-PAP enzyme was used as a control to run on a gel next to the tailed RNA at the end of the experiment.

2.2.15 Recovery of the RNA by using the MEGAclear™ Kit

The tailed RNA was further purified and recovered by removing nucleotides, short oligonucleotides, proteins, and salts using the MEGAclear Kit (ThermoFisher Scientific). All steps included gentle mixing. Elution solution was added into the RNA sample to reach a total volume of 100 µL. After gentle mixing, another 350 µL of Binding Solution Concentrate was added. We applied the sample to the filter cartridge which was inserted into the collection and elution tube, and centrifuged at 12,000X g for 1 min. The centrifuged sample was then washed with 2X 500 µL Wash Solution and RNA was eluted from the filter with microinjection buffer, and incubated closed cap in a 65°C heat block for 10 min. By centrifuging for 1 min at room temperature (12,000X g), the eluted RNA was recovered.

2.3 Methods used for animal study

2.3.1 Maintenance of the mice

The *Hmx1*$^{dm/dm}$ mice used for the tomographic study were obtained from heterozygote x heterozygote crosses in colonies maintained at the Seattle Children's Research Institute. Animals were housed in the Thoren#1 small mouse cage. The vivarium was maintained at 23±1°C on a 12-h light, 12-h dark cycle (0700-1900 h light). All animals were raised in group housing with their siblings until they were weaned at postnatal (P) 21 days old. All studies were conducted according to the National Institutes of Health (NIH) Guide for the Care and Use of Laboratory Animals and were approved by the Institutional Animal Care and Use Committee at Seattle Children's Research Institute.

2.3.2 Microtomography (MicoCT) analysis of the adult mice skulls

The adult mice skulls were imaged at P28 days by using a SkyScan 1076 micro-computed tomographic (microCT) scanner (SkyScan, Antwerp, Belgium) in the Small Animal Tomographic Analysis (SANTA) facility located within Seattle Children's Research Institute, Seattle, WA. Scans were performed at an isotropic resolution of 17.21 μm using the following settings: 55 kV, 180 μA, 1.0 mm aluminum filter, 360-millisecond exposure, rotation step of 0.7°, 180° scan, and 3-frame averaging. Raw data was reconstructed using the NRecon V1.6.2 software (SkyScan, Belgium) and the images were resliced in the coronal plane to simplify subsequent delineation of regions of interest. Reconstructed data was imported into Analyze 10.0

(Mayo Clinic) for segmentation of the mandibles and skull. Comprehensive shape analysis of the skull and hemi-mandibles were performed as previously described [41]. The 3-dimensional rendered images of each data set were generated using Drishti V2 Volume Exploration software (http://sf.anu.edu.au/Vizlab/drishti) [42].

2.3.3 Contrast-enhanced MicoCT analysis of the adult mice muscles

The P28 days *Hmx1*$^{dm/dm}$ and *Hmx1*$^{wt/wt}$ mice heads were fixed overnight in phosphate buffered formal saline (PBFS) solution (PFA made in 1X PBS, dissolved by heating to 65°C and cooled to room temperature, PBFS should be used fresh or stored at -20°C.) upon retrieval from prolonged storage at -20°C. The heads were cut off ventrally around the anterior edge where the fore limbs attach to the body, and dorsally around the first thoracic vertebrae. The detached heads were further immersed in a 2% solution of iodine potassium iodide (IKI made in 1X PBS) for 4 days. It had previously been demonstrated the 2% concentration of IKI can obtain the best microCT muscle image with minimal shrinkage in adult mice heads [43]. Scanning and image-related processes are described in the preliminary results section. Attachment sites of the masseter, temporalis, lateral pterygoid, and digastric (both bellies) muscles were carefully segmented by using DrishtiPaint V2.6 and later registered in Drishti software for photographic and volumetric analysis. The spatial information of the muscles was also examined by 3D registration with the original microCT scan of the skull.

2.3.4 Embryo collection

Embryos were obtained from timed mating. Female mice were separated into a single cage and weight gain was used to confirm pregnancy. Assuming fertilization took place around midnight during a 7 PM to 5 AM dark cycle, embryos were deemed of age E0.5 (0.5 dpc) at noon of the day on which the vaginal plug presence was detected. The embryos were E1.5 at noon on the next day, and so on. The critical time points for external ear development were used to determine time points for sample collection and embryos were further staged according to a published method [44].

2.3.5 Optical projection tomography (OPT)

Fixed embryo samples were embedded in 1.1% low-melting-point agarose, trimmed, and mounted on stubs, then dehydrated in methanol and cleared in benzyl alcohol: benzyl benzoate (1:2). After three rounds of clearing, they were imaged under ultraviolet light (for anatomic detail) by using a Bioptonics 3001M Optical Projection Tomography scanner with data acquired for each specimen in 400 rotational positions. NRecon Version 1.6.2 reconstruction software (Skyscan, Belgium) was used to process the raw scans. Finally, Drishti software was used to render volumes and to take photos for the embryos as mentioned above.

2.3.6 Post-OPT de-embedding:

We used a single-edged blade to remove as much agarose plug from around the specimen as

possible. The sample was then washed with 100% methanol for many changes, to completely remove the BABB from the agarose and specimen. Complete removal of BABB was determined by the clarity of the water containing the residual methanol wash. The agarose was then rehydrated in 70%, 50%, 30% and 10% ethanol with a minimum of 60 min gentle shaking at RT for each step. Samples were further incubated in 0.29 M sucrose for at least 60 min at RT to remove the excess agarose. The samples were additionally washed twice in fresh 57°C sucrose for the next procedure.

2.3.7 X-gal staining:

Embryos with *LacZ* transgene were dissected in ice-cold PBS (1X) and fixed in 4% PBFS solution for 20 min. After fixation, embryos were transferred into a 30 min detergent buffer wash (0.01% sodium deoxycholate, 0.02% NP-40 and 2mM $MgCl_2$) for three times at RT. Following that, embryos were stained overnight in staining solution (5 mM $K_4[Fe(CN)_6]\cdot 3H_2O$, 5 mM $K_3[Fe(CN)_6]$ and 40 mg/mL X-gal in detergent buffer solution) at 37°C.

2.3.8 Microinjection buffer:

10 mM Tris pH 8.0 and 0.2 mM EDTA pH 8.0 were prepared in high-quality water from 1 M Tris-HCl stock (Sigma T2663) and 0.5 M EDTA pH 8.0 (ThermoFisher 15575), respectively. We made 200 ml of filtered solution by running the mixture through a 0.22 µm filtered unit (Sigma-Aldrich F9893). The first 500 ml used to wash the filter was discarded, and the next 200

ml was kept in the provided sterile container. This mixture was then filtered through a 0.02 μm Whatman® Anotop® 10 syringe filter (Sigma-Aldrich Z747653) prior to diluting the DNA for microinjection. The pH of the injection buffer was 7.8 in our experiments.

2.3.9 Pronuclear injection for creating the transgenic mice

Different transgenic lines were generated at Lawrence Berkeley National Laboratory, University of Washington preclinical research and transgenic services (UW-PRTS) or Cyagen Biosciences for screening or line-keeping purposes. Pronuclear injections were carried out as previously described [45]. Transgenic mice were identified by real time-PCR with the appropriately designed primers (see **Table 2.1.9b**).

Using Cyagen Biosciences which generated the Hmx1 enhancer Cre line as an example, the pBS2SKP-Palmiter-Hmx1-HHR-Cre (5,910 bp) vector was prepared by growth in E.Coli. After the plasmid preparation, Not1 and Apal1 restriction enzymes were used in the plasmid linearization process to produce 2,949/1,246/987/728 bp fragments. The 2,949 bp fragment containing the transgenic cassette (Hmx1-HHR-Cre sequence) was purified and injected into the pronucleus of fertilized eggs (C57BL/6N strain), followed by implanting the injected eggs into surrogate mothers to obtain transgenic pups. Genotyping of transgenic pups was carried out by using the transgene PCR primer F: ATATGGCCCGCGCTGGAGTT and transgene PCR primer R: CAACTAGAAGGCACAGTCGAGGC (Product size: 209 bp).

2.3.10 Histology (H&E staining)

The mice head samples were fixed overnight in 4% PBFS solution (pH=7.4, 4°C). We detached the left ear from the skill at the root of the ear lobe. The left ear and the remaining skull were washed in 1X PBS several times. The left ear was then transferred into the tissue embedding cassette and dehydrated with a series of 50% ethanol and 70% ethanol washes. The rest of the head sample was submerged in 14% EDTA (pH=7.4) for three weeks. The solution was discarded and replaced every day for the first week, then every other day for the remaining two weeks. A pin test combined with a quick microCT scout scan was performed at the end of three weeks to confirm complete decalcification. Samples were dehydrated with a series of 50% ethanol and 70% ethanol washes followed by processing and paraffin embedding. 8-10 μm sections horizontal to the cutting plane of the ear, and sections coronal to the mouse head were obtained and mounted on slides. Slides were deparaffinized and stained for hematoxylin and eosin.

2.3.11 Immunofluorescence

Embryos for immunofluorescence were fixed in 4% paraformaldehyde in phosphate-buffered saline, equilibrated in 15% then 30% sucrose, embedded in OCT medium and cryo-sectioned at 18-20 μm, as previously described [25]. The Hmx1 antiserum shows no reactivity to CM in *Hmx1*$^{dm/dm}$ mice. The antisera were then washed thrice with 1X PBS for a total of 30 min then incubated with Alexa-Fluor-conjugated species-specific secondary antibodies (Life Technologies,

Grand Island, NY) at RT for 1 hr. The antisera were washed thrice in the dark with 1X PBS for 10 min per wash and was finally mounted with Vectashield Mounting Medium, and sealed with nail polish (optional).

2.3.12 Sex genotyping of the embryos

DNA was extracted from 2 mm mouse tail tissue using 500 µl of 50 mM NaOH for 30-45 min followed by 50 µl Tris-HCl neutralization. The remaining body tissues were stored frozen for future analysis as needed. The KAPA mouse genotyping kit (KK7352, Standard kit) was used for sex genotyping of the embryos. 1 µl of the DNA extraction was added directly to a 25 µl reaction (1X KAPA mix, 0.48 µM each primer), and ran for one 3 min cycle at 95°C, thirty 30 sec cycles (each cycle consisting 15 sec at 95°C and 15 sec at 57°C), and one 42 sec at 72°C. Primers used were specific for amplifying the male-specific Sry gene [46]:

Sry-F primer: 5'-TTGTCTAGAGAGCATGGAGGGCCATGTCAA-3' and

Sry-R primer: 5'-CCACTCCTCTGTGACACTTTAGCCCTCCGA-3'.

PCR products were separated by electrophoresis on 1% Sodium Borate agarose gels and visualized with ethidium bromide under UV illumination, with a predicted 300 bp fragment.

2.3.13 Behavioral analysis (air puff test)

The air puff test has been used as a measure of craniofacial sensory-motor response [47]. In this test, puffs of air are blown into the face of the subject. The stereotypical reflex to the puff test

includes backward movement of the ears. The test itself is benign, but the mice in this study were monitored for interference with respiration, and for self-injurious behavior during and 5 min after the test. A uniquely designed apparatus, comprising two clear plastic plates 4 cm apart from each other, was used to restrain the mice in a passive position. The mice were held by their tails and held facing front in the middle air with only their forelimbs resting on a 1.7 mm diameter metal bar. Mice were acclimated to the restraint device for 5 min, a day before the testing, to lessen the effect of restraint anxiety. A polyethylene foam sheet covered the bottom of apparatus, and protected the mice from falling off. A ruler was set at the right side of the apparatus as a scale reference. The air puff was generated by a commercial foot pump (Intex Giant Bellows Foot Pump) and directly delivered from a fixed nozzle to the mice with their faces were in the direction of the air flow. Five puffs were delivered at 15 sec intervals. The responses of the mice were recorded by continuous video. We reviewed the video to determine the frames in which the subjects exhibited the maximum response (a rotation of the ears away from the air flow while holding the metal bar). iMovie (Version 2.2.1) photo capture function was used to obtain the original frame photos. Images were further analyzed by using the ImageJ (Version 1.49) linear measurement function. Tips of the ear were used as landmark points. The distance change in the left and right ear tips with the air puff reflex was scored and compared between the experimental and control groups.

2.3.14 Statistical analysis

Quantitative results for linear measurements of the skull size, mRNA transcript levels, and behavioral tests are represented by mean scores +/- S.E.M. and were analyzed by two-tailed independent t-tests using Prism 3 for Windows (GraphPad Software, La Jolla, CA).

CHAPTER THREE: ANOMALIES OF THE HMX1 MUTANT MICE

3.1 History of *Hmx1* mutant *dumbo* mice

The expanding repertoire of genetic technologies in the past few years helped us to gain a better understanding of human biology and disease. Among these technologies, random mutagenesis-phenotype screening in animal models is a program that can uncover novel genes without bias or assumptions. The mouse, with a high similarity in physiology, tissue structure, and organization to humans, has become the premier genetic model organism for such studies. Mutagens such as UV radiation or mutagenic chemicals can induce DNA mutations in cells or organisms. Mutants sharing a similar phenotype can point to an underlying network of genes that potentially affect the same genetic pathway or biological process. Different severity in phenotypes may help to identify key players in a pathway.

The *Hmx1*$^{dm/dm}$ *dumbo* mouse model was generated by Jackson laboratory through their N-Ethyl-N-Nitrosourea (ENU) mutagenesis program [26]. The *Hmx1*^{dm} allele mutation was identified as a nonsense point mutation in the coding region of exon one spanned by the rump-white (*Rw*) inversion of chromosome 5 in mice of C57BL/6 genetic background [48]. *Rw* is a radiation-induced mutation on chromosome 5 which causes depigmentation of the posterior and ventral abdomen. It was used as a balancer to identify recessive mutations within the ~50 megabases spanned by *Rw* [49]. The first report of the *dumbo* mice was based on this mixed background with 9 *dumbo* mutants and 6 controls. The laterally protruding ear phenotype engendered the animal's name "*dumbo*". It was noted that the middle ear structures and hearing are normal in the *dumbo* mice [26], but they have hypertrophy of the gonial bone and partly penetrant exencephaly [26].

Much of the early research on the Hmx gene family focused on the neuronal/retinal function of various members of these genes in the mouse, *Drosophila,* and zebrafish [17, 23,

38]. *Hmx1*'s function in lateral craniofacial development which contributes to the distinct ear phenotype is poorly understood. Furthermore, the restricted phenotype associated with loss of *Hmx1* is distinct from all other known syndromes which have more extensive craniofacial malformations, suggesting a more specific and distinct role in the development of the lateral facial region. By obtaining a clear understanding of the *dumbo* phenotype in a mouse model with or without loss of *Hmx1*, I aimed to build up a solid foundation for directing further mechanistic and gene regulation studies.

3.2 Perinatal lethality, similarity to OAS, and novel ear phenotype found in *dumbo* mice

Mice bearing the *dumbo* allele (*Hmx1*^{dm}), strain B6;C3Fe-*Hmx1*$^{dm/Rw/JcsJKjn}$, were obtained from Jackson Laboratories (Stock #008677). These mice were crossed with pure C57BL/6N mice (Charles River) for more than ten additional generations prior to the experiments described below. Genotyping of the *Hmx1*^{dm} and wild-type *Hmx1* (*Hmx1*^{wt}) alleles was performed by real-time PCR using specially designed oligonucleotide primers (see **Table 2.1.9b**) [25]. Mendelian transmission of the *dumbo* allele was observed between E10.5 and E14.5 with 42 *Hmx1*$^{wt/wt}$, 105 *Hmx1*$^{wt/dm}$ and 37 *Hmx1*$^{dm/dm}$ embryos (22.8%, 57.1% and 20.1%, respectively; chi-square $p = 0.1391$). 26 pairs of heterozygous x heterozygous mating were set up to obtain 156 animals at mature age. The characteristic low-set protruding ears, microphthalmia, and cataracts of the *Hmx1* mutant mice were still observed after moving the *Hmx1*^{dm} allele onto this pure genetic background (see **Fig. 3 A-D**). Both genders of *dumbo* mutant mice are fertile. Non-Mendelian transmission was observed for the *Hmx1*^{dm} allele in post-weaning animals with 49 *Hmx1*$^{wt/wt}$, 86 *Hmx1*$^{wt/dm}$ and 21 *Hmx1*$^{dm/dm}$ mice (31.4%, 55.1% and 13.5%, respectively; chi-square $p = 0.0029$, see **Fig. 4**), corresponding to approximately ~57% perinatal lethality. Hence the breeding data in this project confirm the qualitative findings of Wilson et al [50] that the *dumbo* allele is semi-lethal at the perinatal

stage. Typically mice that die in the perinatal period are consumed by the mothers and are only occasionally found by investigators. In two of nine E14.5 *Hmx1*$^{dm/dm}$ OPT imaged embryos, both males, an anterior head malformation overlying the anlage of the pre-tectum, caudal to the epiphysis and pineal recess, at the junction between the diencephalon and the mesencephalon was noted (see **Fig. 5 A-B'**). Also two male *Hmx1*$^{dm/dm}$ mutants at postnatal day 28 (P28), but no female mutants or controls of either sex, presented with a frontal bone and posterior frontal suture anomaly (see **Fig. 5 C-D**), which could be related to the anterior head malformation shown in the embryos. This partially penetrant anomaly could represent a mild neural tube defect related to the exencephaly previously documented [26] and explain the observed non-Mendelian ratio/perinatal lethality. It should be noted that exencephaly was a common finding in the first report [26], which may have resulted from other alleles that co-segregated with *Hmx1*^{dm} in the *Hmx1*$^{dm/Rw}$ mice. Amongst the *Hmx1*$^{dm/dm}$ mice generated in this study, there were 11 females and 10 males with no sex bias.

In the careful examination of the *dumbo* mature mice performed as part of this thesis study, an extra tag at the lower edge of the external ear in all the *dumbo* mutant mice was noted (see **Fig. 6 A-B**). This observation suggested a significant role for *Hmx1* in the ear development in both normal and *dumbo* mutant mice. Hence *Hmx1*'s role was further investigated in early embryo ear development.

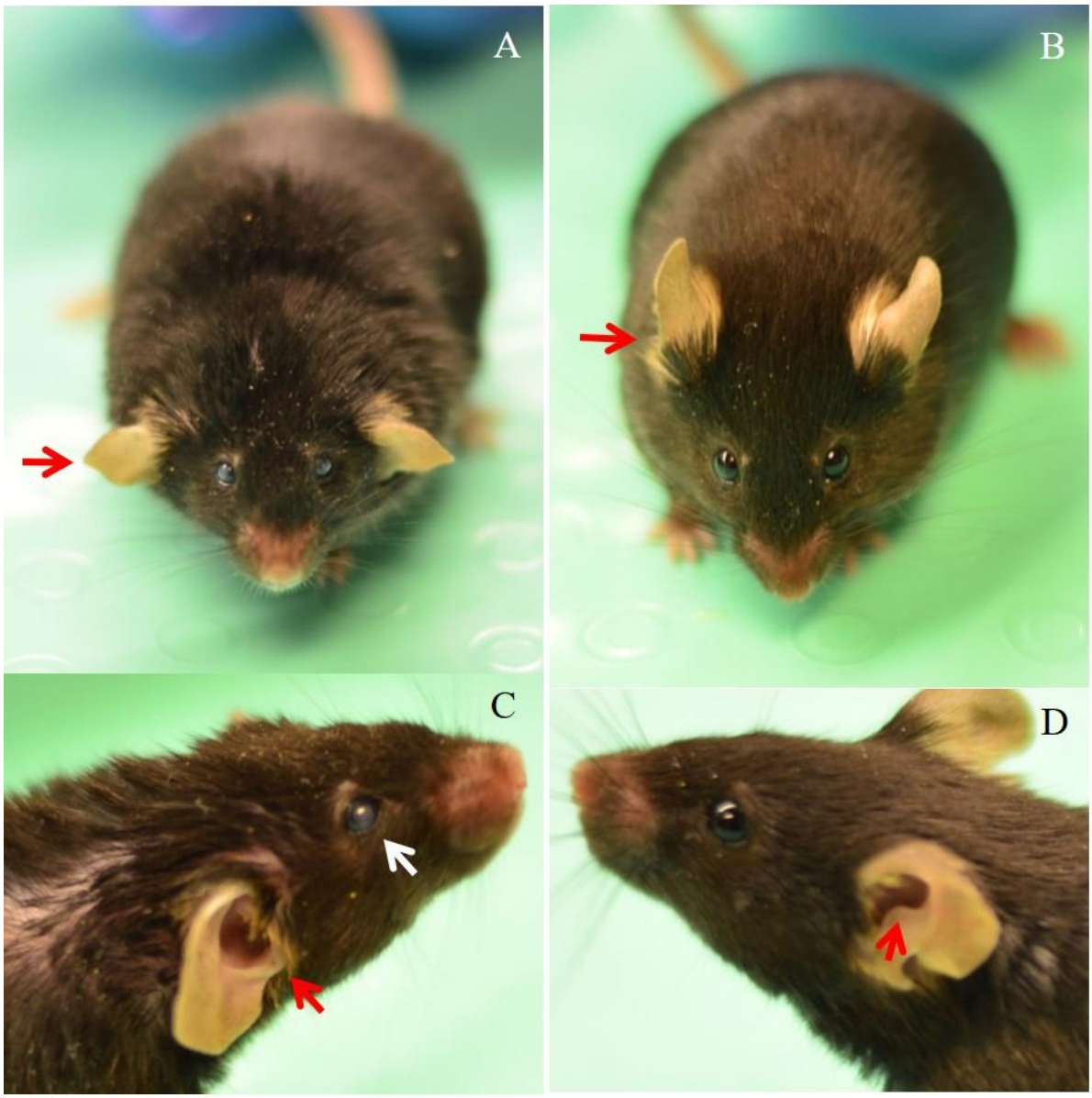

Figure 3. The ear and eye defects in *Hmx1*$^{dm/dm}$ mutant animals. Dorsal and lateral view of a P28 *Hmx1*$^{dm/dm}$ (A, C) and control (B, D). Note the ventrolateral displacement of the pinna in the *Hmx1*$^{dm/dm}$ mutant mouse (compare A to B, red arrow), microphthalmia and cataracts [26] in the *Hmx1*$^{dm/dm}$ mutant mouse (compare C to D, white arrow) and flat anti-tragus in *Hmx1*$^{dm/dm}$ mutant mouse (compare C to D, red arrow).

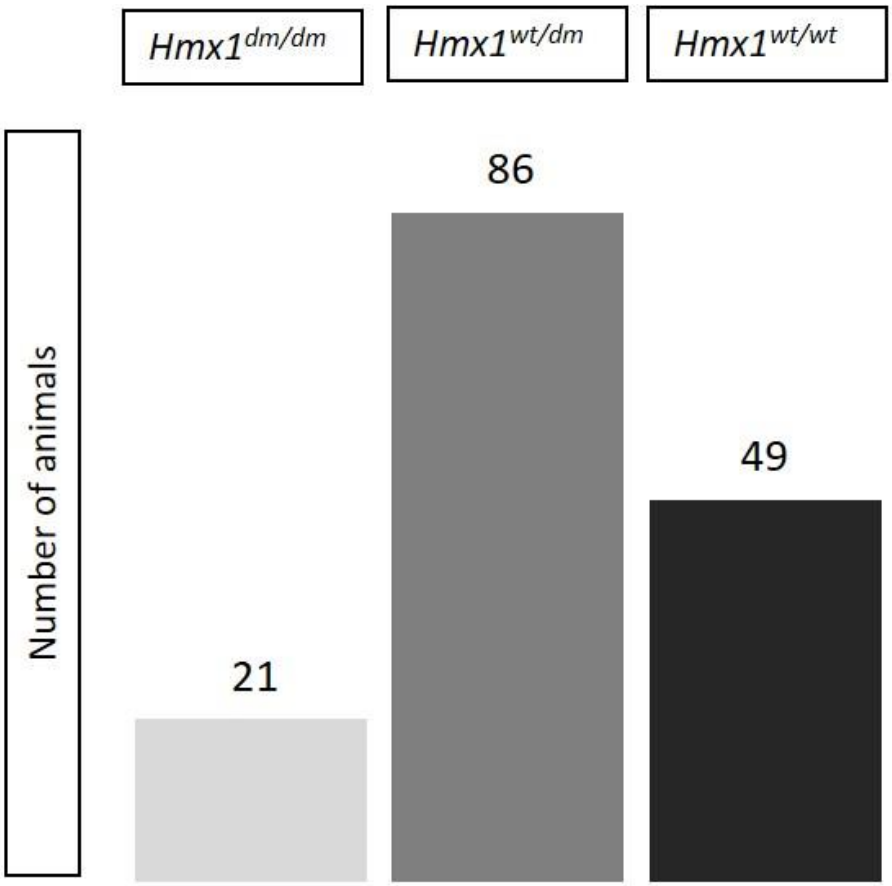

Figure 4. The number of each genotype from 26 heterozygous x heterozygous mating events. Non-Mendelian transmission of the *Hmx1*^{dm} allele in post-weaning animal, suggesting perinatal lethality.

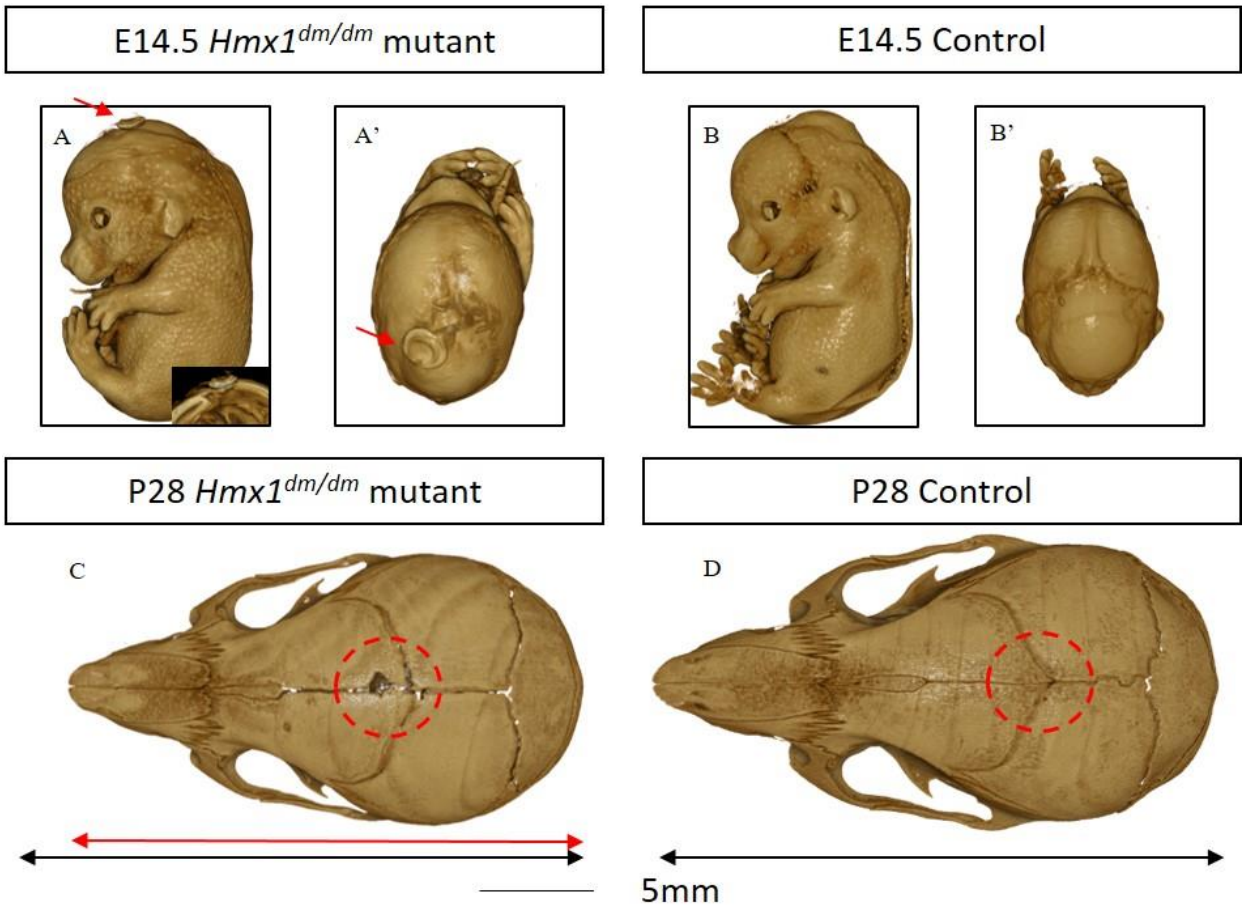

Figure 5. Craniofacial defects in *Hmx1*$^{dm/dm}$ mutant animals. (A-B') OPT of E14.5 *Hmx1*$^{dm/dm}$ mutant (A, A') and control (B, B') embryos shows the anterior head malformation present in 2 male *Hmx1*$^{dm/dm}$ embryos (compare A to B, arrow; compare A' to B', red arrow; *Hmx1*$^{dm/dm}$ n = 9, control n = 12). Inset in A is an OPT slice through the malformation (red arrow). (C-D) MicroCT analysis of P28 animals reveals abnormalities in 2 male *Hmx1*$^{dm/dm}$ (C) skulls (red dashed circle) but not controls (D) (*Hmx1*$^{dm/dm}$ n = 17, control n = 28).

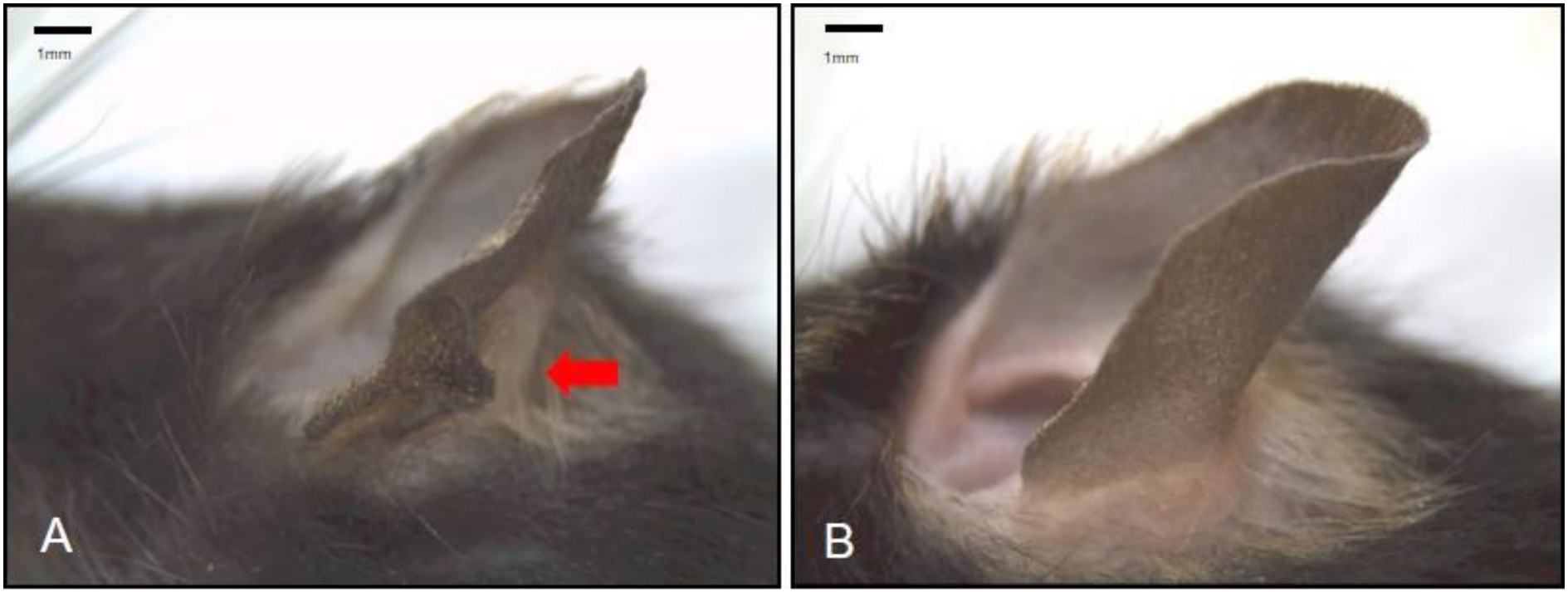

Figure 6. Ear malformation in mature *Hmx1*$^{dm/dm}$ mutant mice. Representative posterior view of a P28 *Hmx1*$^{dm/dm}$ (A) and control (B) ear.

The red arrow in (A) highlights the extra ear tag.

3.3 Hmx1 is involved in the development of lateral facial structures

The structural study of the Hmx1 mice at key embryonic stages could set a benchmark for understanding craniofacial development in both the control and *dumbo* mutant animals. The critical time points for external ear development (E11.5 - E18.5) were chosen to collect the *dumbo* mutant and control embryos following standard methods (see **Methods 2.3.4**). Samples were further treated for OPT-based morphology analysis [51, 52]. Image capture and analysis were done by using the Drishti software package (see **Methods 2.3.5**). The exact stage of each embryo was further confirmed according to a published method [44]. There was no statistical difference between the size of five E14.5 *dumbo* (11.316±0.718 mm) and ten heterozygous control embryos (11.760±0.5932 mm, Student's t-test, $p = 0.223$).

Representative embryo photos are lined up with the P28 mature mouse ear for a clear understanding of the ear development in the embryo as a whole (see **Fig. 7, 8**), with the detailed differences of the ear structures noted in **Fig. 8**. Like humans, the normal ear development in mice (control group) moves laterally and cranially during the development process to attain its adult location and overall configuration [53]. At E11.5, the six low tubercules which will form the pinna can be discerned. From E12.5, the lateral ear shows rapid development and becomes protruded, and by E13.5 the pinna forms a crest at right angles to the head. At E14.5, the growing pinna turns forward and covers about one-half of the external auditory meatus. At E15.5 the pinna covers more than half of the external auditory meatus, and the external auditory meatus is almost completely covered by the pinna at E16.5. Even though considerable ear growth will happen later, the E18.5 ear closes up the auditory meatus and reaches its final position which is maintained throughout life. In contrast, the low-set of the ear position and the extra fold of the pinna in the P28 *dumbo* mutant mice can be traced back to E11.5 and through embryonic development. At age E11.5, the appearance of the ventral BA2 hillocks, particularly the central and to a lesser extent the

ventral-most hillocks, are abnormal. In humans, these structures contribute mostly to the antitragus, the lobe, and caudal aspects of the helix [15]. By E12.5, mutants could be recognized by variable failure or delay in rotating the developing auricle (see **Fig. 8 C-D**). By E13.5, a distinct furcation at the lower edge of the developing lobe could be seen (see **Fig. 8 E-F**). It's striking that the E11.5 *dumbo* mutant embryo's BA2 enlarged region could potentially give rise to the novel finding of the extra fold in the ear of mature *dumbo* mice (see **Fig. 8 K-L**). H&E staining of the adult mice showed the extra ear tag's cartilaginous component (see **Fig. 9**).

Homeobox family genes are known to have control over region-specific differentiation and boundary expressions of tissue specification and cell fate [54]. Loss of *Hmx1* function may diminish the boundary restriction to the cartilaginous cells in this region which could lead to the extra fold at the lower back of the pinna. Mechanical force might also play a role in this process. Since the pinna's movement is restricted from going upward and backward, the outgrowth of the pinna could also force a group of cartilaginous cells to fold back to form the extra fold. While this novel finding of the extra ear tag needs further investigation, I moved on to investigate the cranium, skeletal, and muscular structures underneath the surface of the low-set ear at the adult stage to test the phenotypic correlation.

Figure 7. Characterization of the embryonic development observed in *Hmx1*$^{dm/dm}$ animals from E11.5 to E18.5. Representative lateral view of *Hmx1*$^{dm/dm}$ mutant and control from embryonic day E11.5 to E18.5. The low-set, malformed *dumbo* ears present in *Hmx1*$^{dm/dm}$ mutant embryos (see red dashed circles and lines). Scale bars = 1 mm. Abbreviations: BA1, branchial arch1; BA2, branchial arch 2.

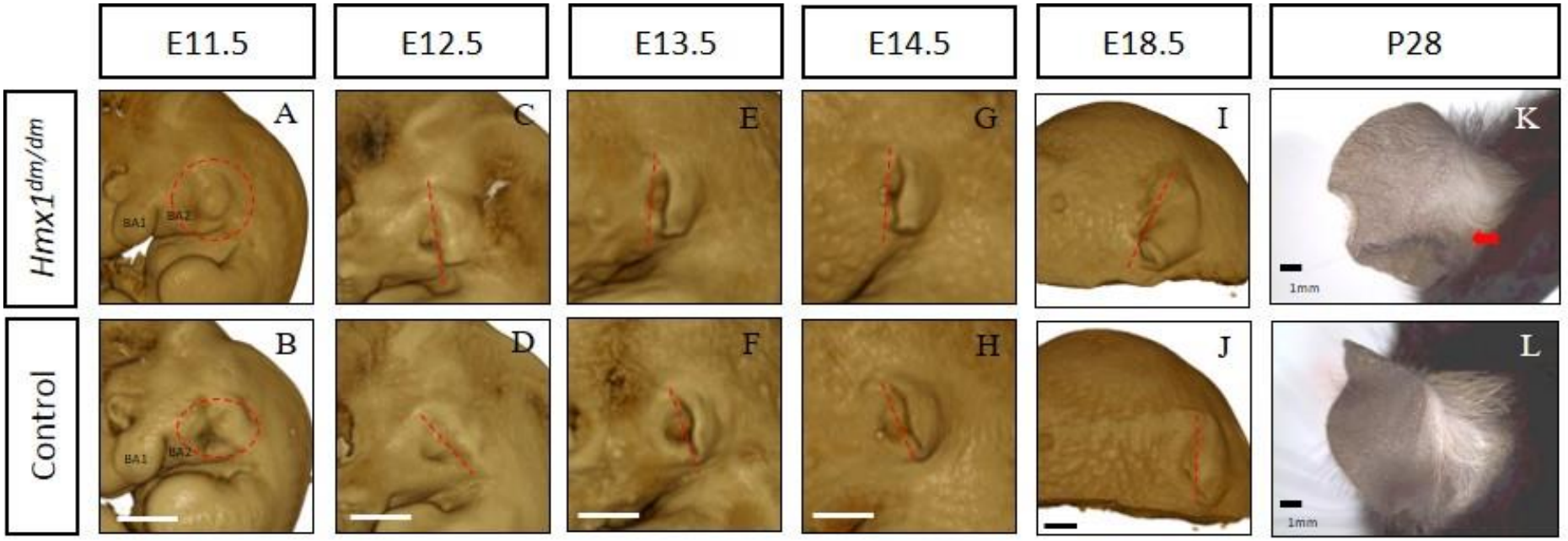

Figure 8. Characterization of the embryonic and postnatal ear phenotype observed in *Hmx1*$^{dm/dm}$ animals from E11.5 to P28. *Hmx1*$^{dm/dm}$ mutant (A, C, E, G, I) and Control (B, D, F, H, J) embryos show morphological differences in the external ear (pinna). (A-J) Optical projection tomography of E11.5 (A-B; *Hmx1*$^{dm/dm}$ mutant n = 5, control n = 7), E12.5 (C-D; *Hmx1*$^{dm/dm}$ mutant n = 5, control n = 3), E13.5 (E-F; *Hmx1*$^{dm/dm}$ mutant n = 5, control n = 4), E14.5 (G-H; *Hmx1*$^{dm/dm}$ mutant n = 9, control n = 12) and E18.5 (I-J; *Hmx1*$^{dm/dm}$ mutant n = 2, control n = 2). (K, L) Representative dorsal view of a P28 *Hmx1*$^{dm/dm}$ mutant (K) and control (L) ear highlight the malformation present in *Hmx1*$^{dm/dm}$ mutant mice (see K, red arrow; *Hmx1*$^{dm/dm}$ mutant n = 17, control n = 28). Scale bars = 1 mm. Abbreviations: BA1, branchial arch1; BA2, branchial arch 2.

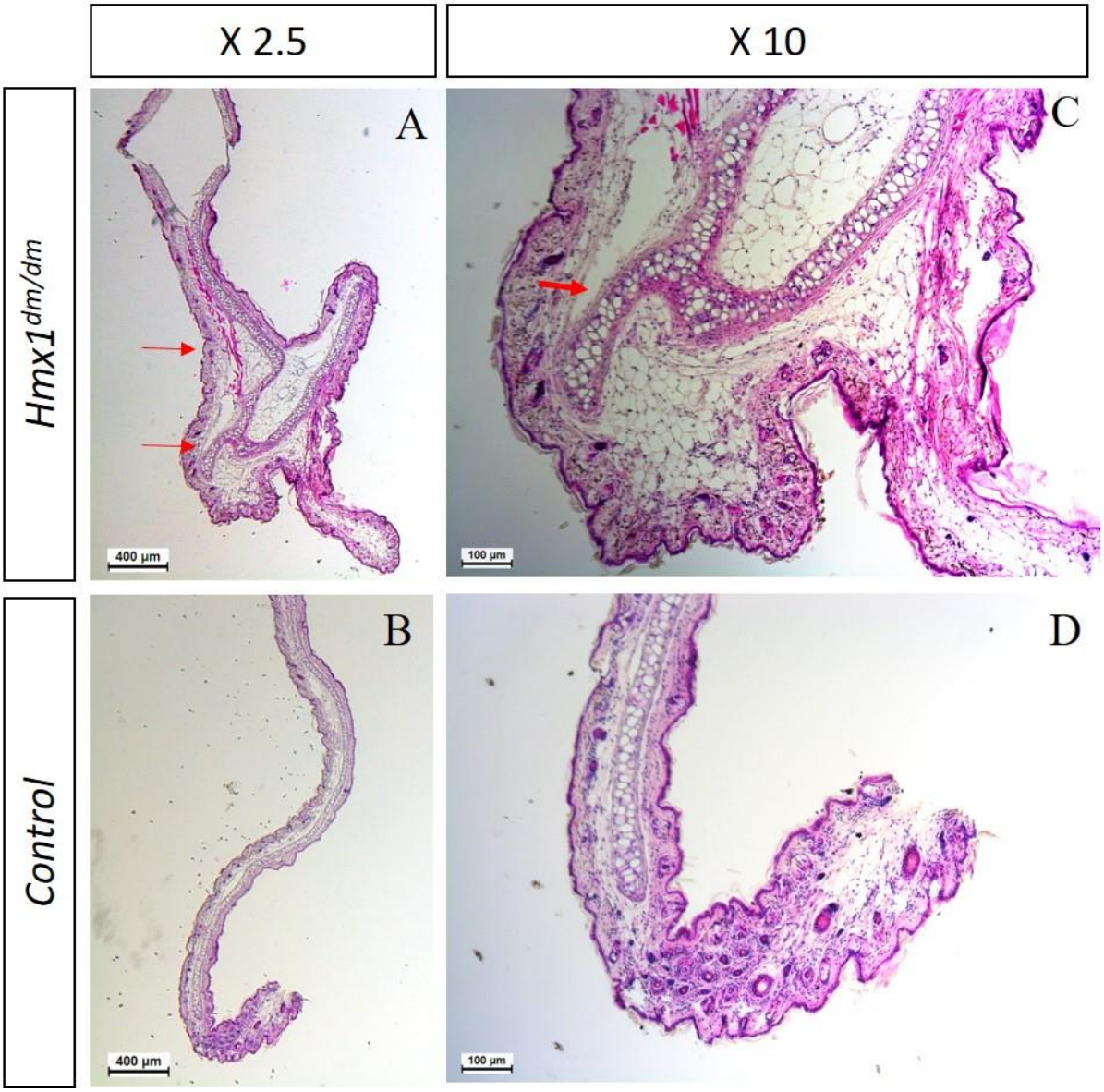

Figure 9. Histological analysis of external ear observed in *Hmx1*$^{dm/dm}$ and control at P28 stage. H&E cross sections of *Hmx1*$^{dm/dm}$ (A, C) and control (B, D) mouse ear tag. The red arrows point to areas showing muscle attachment and extra folding of the cartilaginous content in the *Hmx1*$^{dm/dm}$ mutant mouse.

3.4 Cranio-skeletal anomalies and weight loss of *Hmx1*$^{dm/dm}$ mutant mice

3.4.1 Visual inspection of the bony structural changes in *Hmx1*$^{dm/dm}$ mutant mice

High-resolution microCT imaging was used (see **Methods 2.3.2)** to examine the skulls of P28 *Hmx1*$^{dm/dm}$ and control *Hmx1*$^{wt/wt}$ mice, which were obtained from 16 heterozygote x heterozygote crosses. After carefully examining the bony supporting structures in the lateral facial region where the prominent "*dumbo*" ear is located, hypoplasia of the left and right paraoccipital processes was identified in all the *Hmx1*$^{dm/dm}$ mutant mice (see **Fig. 10 A**). The paraoccipital process is part of the occipital bone and immediately adjacent to the auditory bulla. It is functionally equivalent to the human mastoid process which is a major attachment site for muscles of head and mandibular movement (the digastric posterior belly, longissimus capitis, splenius captis, and the sternocleidomastoid muscles). Notably, adult *dumbo* rats show a similar defect (see **Fig 10 B**). What's more, all mutants (both sexes) but no controls had premature fusion of the squamosal and parietomastoid sutures (see **Fig. 11 A-B**).

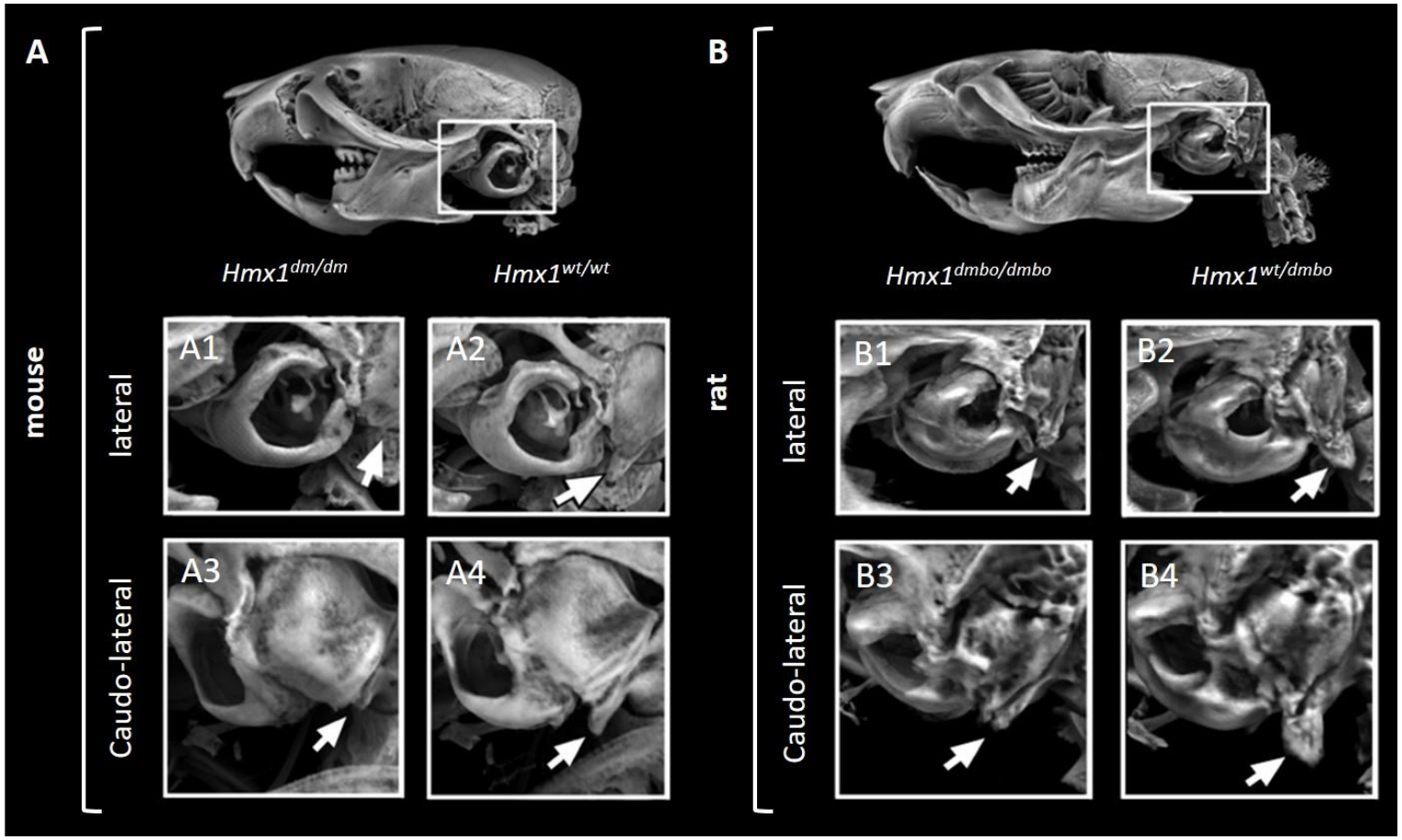

Figure 10. MicroCT reveals hypoplasia of the paraoccipital processes in the *Hmx1*$^{dm/dm}$ mutant mice and *dmbo* rat (photos took by Dr. Timothy Cox)**.** (A) MicroCT analysis of *Hmx1*$^{dm/dm}$ mutant (A1, A3) and control (A2, A4) mouse skulls (compare A1 to A2, arrows- lateral view; compare A3 to A4 arrows- caudo-lateral view; *Hmx1*$^{dm/dm}$ mutant n = 17, control n = 28). (B) MicroCT analysis of *Hmx1*$^{dmbo/dmbo}$ (B1, B3) and control mutant (B2, B4) rat skulls (compare B1 to B2, arrows- lateral view; compare B3 to B4 arrows- caudo-lateral view; *Hmx1*$^{dmbo/dmbo}$ mutant, n = 2; control, n = 2).

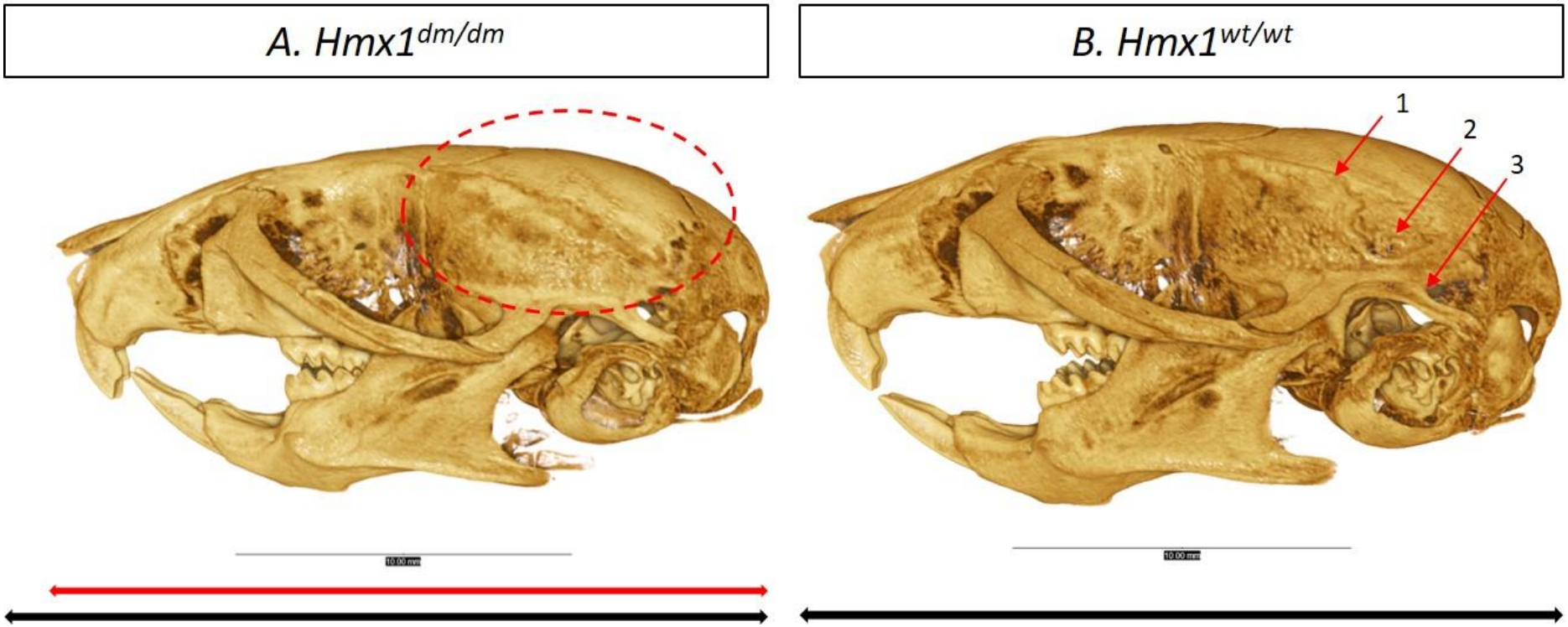

Figure 11. Fusion of the lateral sutures in *Hmx1*$^{dm/dm}$ mutant mice. (A) Fusion of the squamosal and parietomastoid sutures can be observed in all the *Hmx1*$^{dm/dm}$ mutant mice. The temporal bone seems to have more growth at the root of the postglenoid process (B3) which evens out a linearized suture (red dashed circle). (B) Control animals have the clear squamosal (B1) and parietomastoid sutures (B2). The parietal bone is inserted into the temporal bone at the root of the postglenoid process, which forms a curved suture line.

3.4.2 Landmark based linear measurement study of the *Hmx1*$^{dm/dm}$ mutant mice skulls

A landmark-based method was first used to quantitatively validate the size and some other differences noticed from the visual inspection. 18 points on the cranium and 6 points on the mandible were selected (see **Fig. 12, Table 2**) to compare the linear differences between the control and *Hmx1*$^{dm/dm}$ mutant mice.

The results showed that *Hmx1*$^{dm/dm}$ mice have smaller skulls (see **Table 3**) compared to controls. The shape differences were noted at the maxillary and tympanic regions. Even though the length of the *Hmx1*$^{dm/dm}$ mouse mandible was reduced, the posterior height of the left and right mandible from condyle to the tip of the angular process had no statistical difference between the two groups. The significant difference between the left-to-right angular process width, but not the condyle width, showed that *Hmx1*$^{dm/dm}$ mice's left and right mandibles lean closer to each other at the angular level. The left and right mandibles are symmetrical in both the *Hmx1*$^{dm/dm}$ mutant (M-Cdi length, $p = 0.489$; Cdi-angular process length, $p = 0.690$; M-G length, $p = 0.528$) and wild-type control mice (M-Cdi length, $p = 0.463$; Cdi-angular process length, $p = 0.704$; M-G length, $p = 0.768$).

Since the *Hmx1*$^{dm/dm}$ skulls were generally smaller in size, ratios between the full cranium length (AP length, anterior nasal spine to ophistion), cranium width (distance between posterior zygomatic roots), and the cranium height (bregma and basisphenoid-occipital junction) were further compared between the *Hmx1*$^{dm/dm}$ and the control group (see **Fig. 13**). This showed that even with a smaller skull size, the *Hmx1*$^{dm/dm}$ mice had a relatively wider cranium (see **Table 4**). These observations could relate to the human OAS report that patient VII 9 has flattening of the cranial base and short mandibular rami [12].

Figure 12. Schematic of one representative WT skull with landmarks. Description of 24 points for linear measurements, in which 18 points on cranium and 6 points on mandible (showing in blue).

#	Ref	Point	Type	Description
			DORSAL + LATERAL	
1	ans	anterior nasal spine	Mid	most anterior point of interpermaxillary suture at base of nasal aperture
2	na-r	nasale - right	Mid	Most anterior point of nasal bones
3	n	nasion	Mid	Point between nasal and fronal bones (on frontal,right)
4	flac-r	intersection of frontal process of maxilla with frontal and lacrimal bones- right	R	
5	flac-l	intersection of frontal process of maxilla with frontal and lacrimal bones - left	L	
6	zps-r	anterior-superior point on zygmatic process of maxilla - right	R	lateral to infra orbital fissure
7	zps-l	anterior-superior point on zygmatic process of maxilla - left	L	"
8	zrp-r	zygomatic root posteior - right	R	posterior point on base of zygomatic process of temporal bone - right
9	zrp-l	zygomatic root posteior - left	L	"
10	br	bregma	Mid	Intersection of coronal and sagittal suture (Parietal and frontal suture)
11	la	lamda	Mid	Intersection of coronal and lambdoid suture (interpatietal)
12	op	Ophistion	Mid	Posterior aspect of foramen magnum
13	tys-r	most postero-inferior point on superior part of tympanic ring - right	R	
14	tys-l	most postero-inferior point on superior part of tympanic ring - left	L	
			VENTRAL	
15	pmm	midline point on premaxillary - maxillary suture	Mid	
16	pns	posterior nasal spine	Mid	Posterior most point on hard palate (right)
			CRANIAL BASE + VAULT	
17	ISS	presphenoid-basispheniod junction	Mid	on basisphenoid
18	SOS	basisphenoid-occipital junction	Mid	on basisphenoid
			MANDIBLE (right and left)	
19	cdi-r	Posterior inferior condyle point	Mid	
20	g-r	Tip of angular process	Mid	
21	m-r	Anterior inferior point on mental process	Mid	on midline of each half
22	cdi-l	Posterior inferior condyle point	Mid	
23	g-l	Tip of angular process	Mid	
24	m-l	Anterior inferior point on mental process	Mid	on midline of each half

Table 2. Description of 24 landmark points used for linear measurement (designed with Dr. Siddharth Rajiv Vora and Dr. Timothy Cox**).** The first 18 points were on the cranium, they were also used for 3D shape analysis. The last 6 points were on the mandibles (3 on each side) for linear measurement only.

Distance (mm)	Description	*Hmx1*$^{dm/dm}$ (n=17)		*Hmx1*$^{wt/wt}$ (n=24)		t-test	
		M	SD	M	SD		
AP length	ans --- op	19.22	0.19	19.94	0.15	0.007	**
Cranium width	zrp-r ---- zrp-l	10.11	0.06	10.30	0.03	0.007	**
Cranium height	br ---- SOS	6.05	0.03	6.29	0.04	0.0001	***
Basisphenoid length	ISS --- SOS	2.76	0.04	2.90	0.02	0.010	*
Full maxillary length	ans --- pns	9.76	0.11	10.24	0.08	0.001	***
Back of skull length	pns --- op	9.70	0.08	9.89	0.07	0.08	
Tympanic width	tys-r --- tys-l	9.16	0.06	9.42	0.04	0.002	**
Mandible condyle width	cdi-r --- cdi-l	9.71	0.08	9.86	0.06	0.158	
Mandible angular process width	g-r --- g-l	8.05	0.10	8.68	0.10	0.00007	***
Right M-Cdi length	m-r --- cdi-r	9.01	0.09	9.48	0.08	0.0002	***
Right Cdi-angular length	cdi-r --- g-r	3.03	0.05	3.07	0.04	0.485	
Right M-G length	m-r --- g-r	7.74	0.07	8.24	0.07	0.00001	***
Left M-Cdi length	m-l --- cdi-l	8.92	0.10	9.41	0.07	0.0003	***
Left Cdi-angular length	cdi-l --- g-r	3.01	0.04	3.05	0.04	0.391	
Left M-G length	m-r --- g-r	7.67	0.08	8.21	0.07	0.00001	***

Table 3. Representative linear measurements of the *Hmx1*$^{dm/dm}$ mice and *Hmx1*$^{wt/wt}$ control mice. *P*-value in red means significant statistical difference was observed between the two groups ($p < 0.05$,*; $p < 0.01$, **; $p < 0.001$, ***). P-value in black means no statistical difference was seen between the two groups.

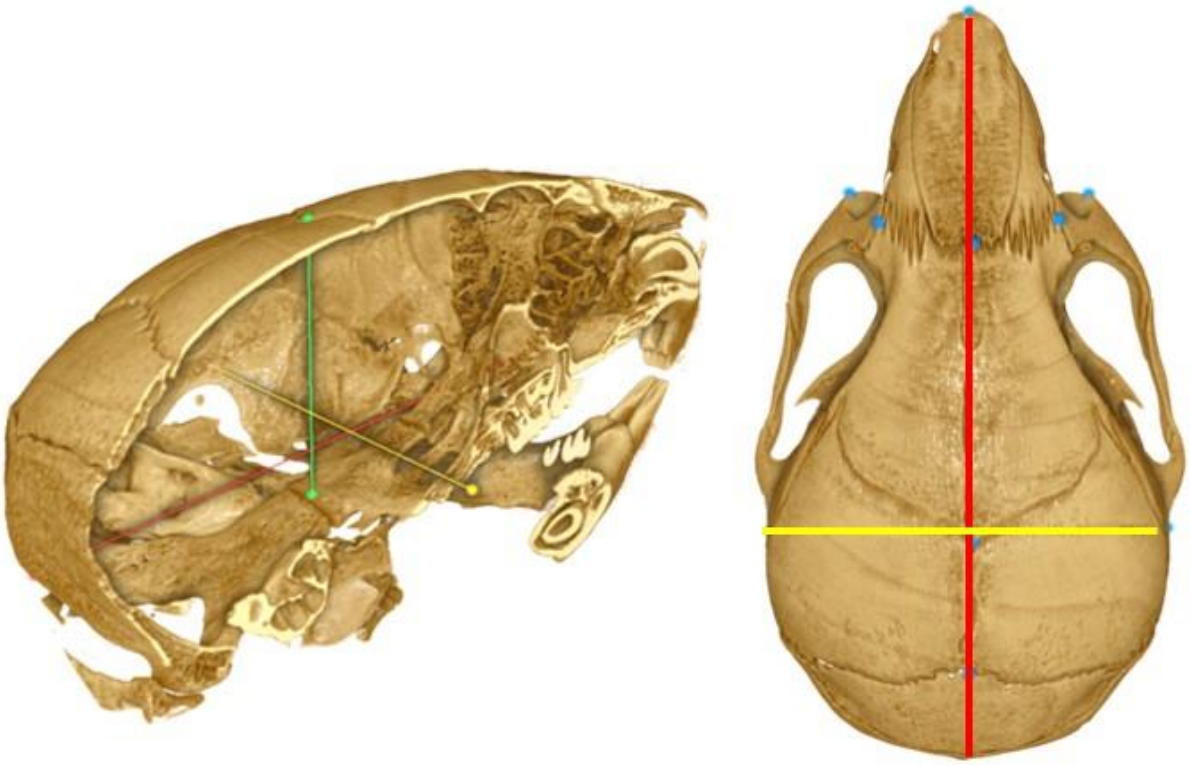

Figure 13. Representative linear measurements on one of the control mice skulls. Red line, AP length; yellow line, cranium width; green line, cranium height.

ratio	*Hmx1*$^{dm/dm}$ (n=17)		*Hmx1*$^{wt/wt}$ (n=24)		*t*-test	
	M	SD	M	SD		
AP length/Cranium width	1.900	0.009	1.935	0.010	0.0130	*
AP length/Cranium height	3.177	0.025	3.170	0.011	0.6776	
Cranium width/height	1.672	0.007	1.639	0.006	0.0009	***

Table 4. The linear measurement's ratio comparison of the *Hmx1*$^{dm/dm}$ mice and *Hmx1*$^{wt/wt}$ control mice. Significant differences were found in the AP length/Cranium width and Cranium width/height ($p < 0.05$), but not the AP length/Cranium height ($p < 0.05$,*; $p < 0.01$, **; $p < 0.001$, ***).

3.4.3 Weight loss in the postnatal day 28 *Hmx1*$^{dm/dm}$ mutant mice

By obtaining the overall weight from each individual mouse at postnatal day 28 (P28), the *Hmx1*$^{dm/dm}$ group (13.1924±0.5490 g, *n = 17*) exhibited reduced body mass when compared to heterozygous (15.8408±0.3198 g, *n* = 49, *p = 0.007*) and wild-type (15.5643±0.5591 g, *n = 28, p = 0.0001*) littermates (see **Fig. 14**). The *Hmx1*$^{dm/dm}$ male mice (13.12875±1.1015 g, *n = 8,*) weighed on average ~21% less than heterozygous (16.9167±0.4512 g, *n* = 24, *p = 0.0011*), and ~23% less than wild-type controls (17.2753±0.4943 g, *n* = 15, *p = 0.0011*) (see **Fig. 15**), while *Hmx1*$^{dm/dm}$ female mice (13.1078±0.4395 g, *n* = 9) were slightly less (~11%) than heterozygous controls (14.8080±0.3507 g, *n* = 25, *p = 0.0126*) but comparable in weight to wild-type controls (13.5900±0.7615 g, *n* = 13, *p = 0.6317*). The heterozygous and wild-type controls had no statistical weight difference (*p = 0.1041*) (see **Fig. 16**).

Thus I conclude that the *Hmx1*^{dm} allele influences the overall body size in the mutant animals, but male *dumbo* mice are especially affected since they were significantly smaller than their sex and age-matched controls. Size and weight differences between genotypes were not detectable in late-gestation embryos, suggesting this is likely a postnatal event.

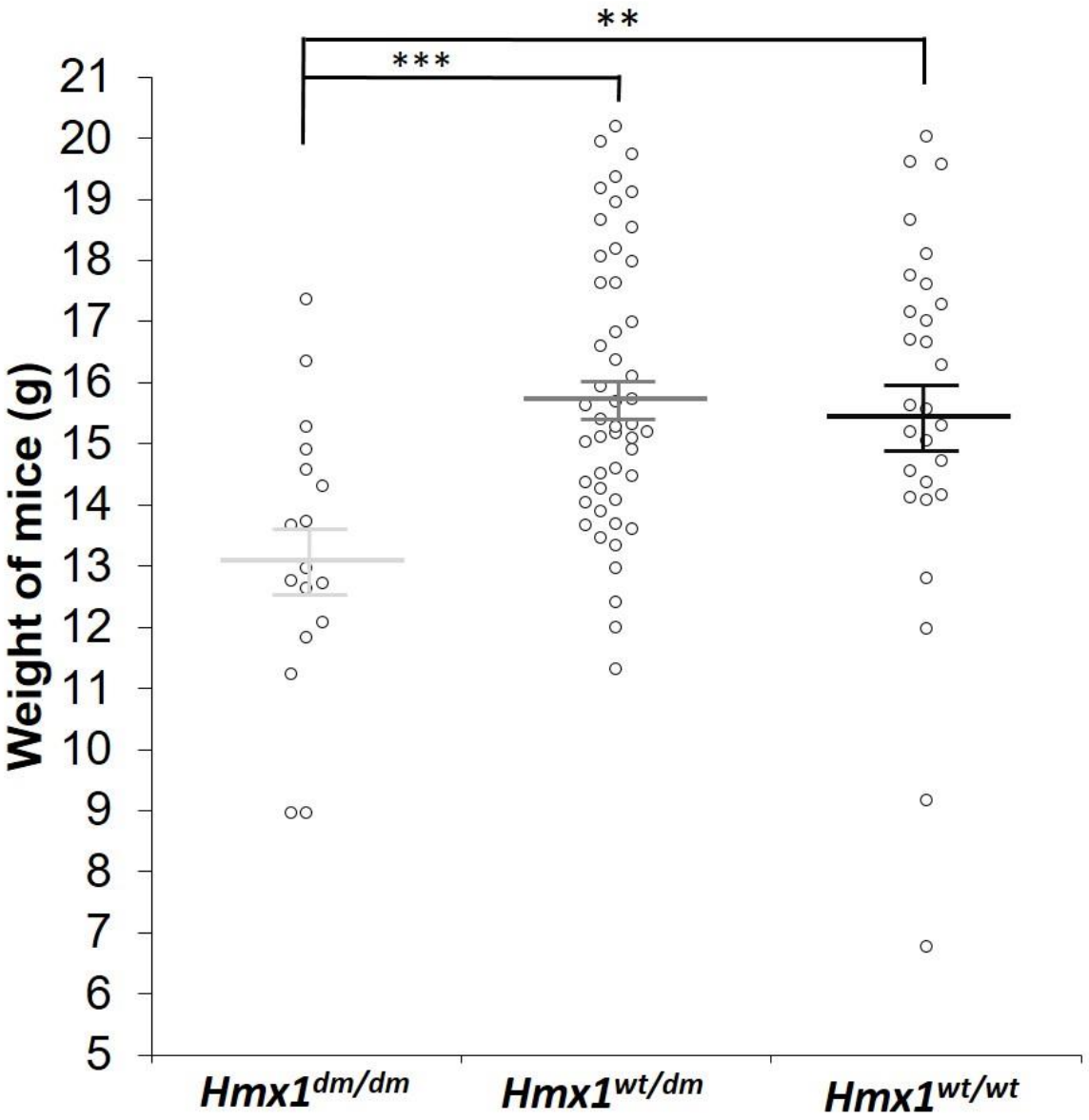

Figure 14. Postnatal body weight loss in *Hmx1*$^{dm/dm}$ mutant animals. Comparison between *Hmx1*$^{dm/dm}$ mutant animals (n = 17) to *Hmx1*$^{wt/dm}$ (n = 49, $p = 0.0001$) and *Hmx1*$^{wt/wt}$ (n = 28, $p = 0.007$) at P28.

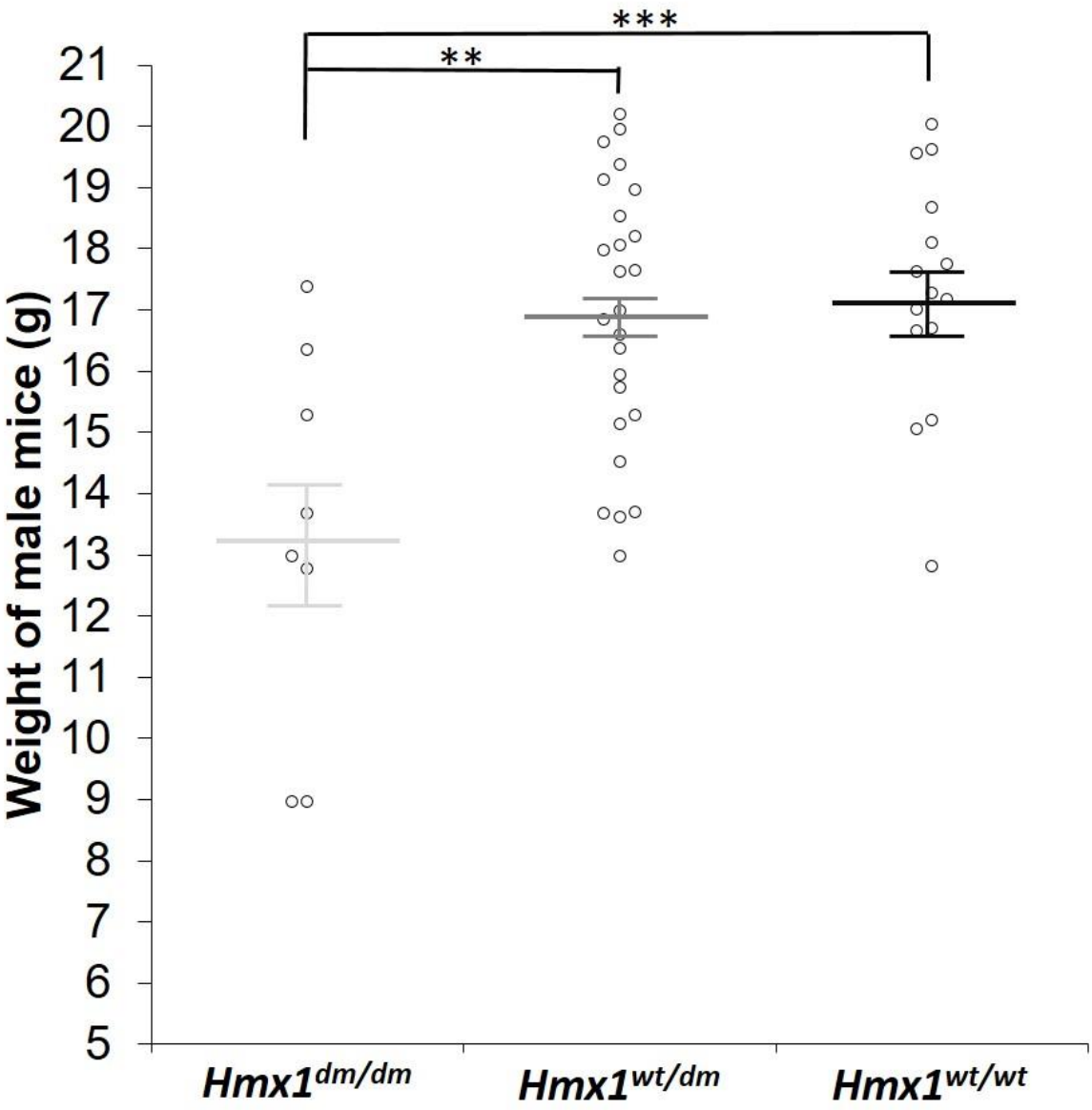

Figure 15. Significant weight reduction in male *Hmx1$^{dm/dm}$* mutant mice. Comparison between *Hmx1$^{dm/dm}$* mutant male animals (*n* = 8) to *Hmx1$^{wt/dm}$* (*n* = 24, *p = 0.0011*) and *Hmx1$^{wt/wt}$* (*n* = 15, *p = 0.001*) at P28, a subset of the same mice in **Fig. 14**.

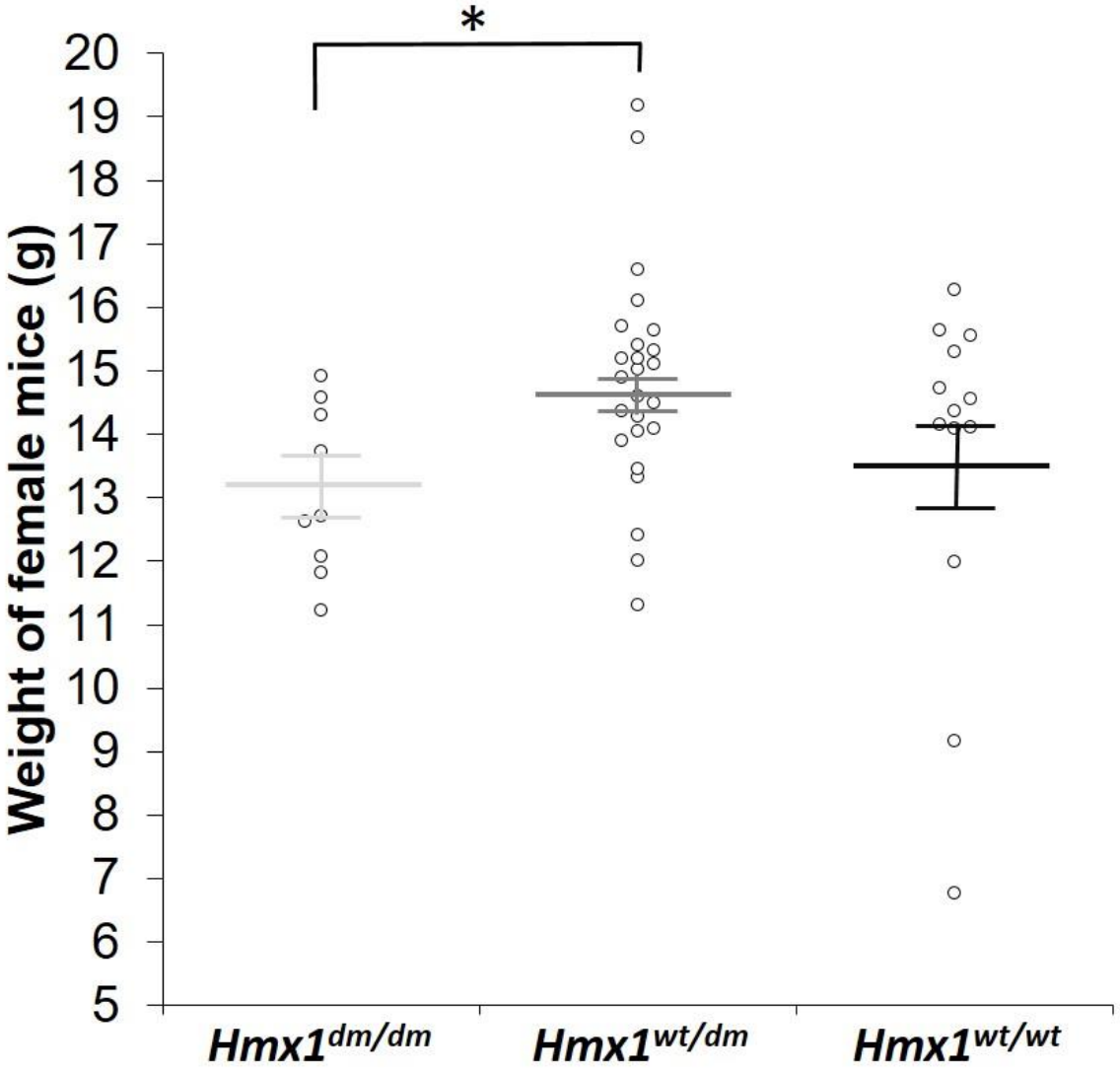

Figure 16. Comparable weight of *Hmx1*$^{dm/dm}$ mutant female mice to the wild-type control. Comparison between *Hmx1*$^{dm/dm}$ mutant female animals (*n* = 9) to *Hmx1*$^{wt/dm}$ (*n* = 25, *p = 0.0126*) and *Hmx1*$^{wt/wt}$ (*n* =13, *p = 0.6317*) at P28, a subset of the same mice in **Fig. 14**.

Description (mm/g)	*Hmx1*$^{dm/dm}$ (n=17)		*Hmx1*$^{wt/wt}$ (n=24)		t-test
	M	SD	M	SD	
AP length/ weight	1.492	0.054	1.360	0.067	0.134
Cranium width/ weight	0.472	0.021	0.430	0.023	0.124
Cranium height/ weight	0.787	0.032	0.707	0.040	0.186
Basisphenoid length/ weight	0.213	0.006	0.198	0.009	0.174
Full maxillary length/ weight	0.757	0.026	0.698	0.034	0.176
Back of skull length/ weight	0.754	0.029	0.675	0.034	0.083
Tympanic width/ weight	0.713	0.028	0.646	0.035	0.146

Table 5. Comparison of the linear measurement corrected by weight showed no difference between the *Hmx1*$^{dm/dm}$ mutant and *Hmx1*$^{wt/wt}$ control group.

After correction for the size by using the weight of the animals, the differences between *Hmx1*$^{dm/dm}$ mutant and *Hmx1*$^{wt/wt}$ control were not significant (see **Table 5**). The weight correction analyses imply that the *Hmx1*$^{dm/dm}$ mutant mice skull size linear measurement is proportionally reduced with the weight.

The craniofacial and long bones of the skeleton have different origins during development: the former originate from the cranial neural crest cells while the latter are contributed by the lateral plate mesoderm. I sought to find out *Hmx1*^{dm} allele's influence on long bone development. Accessible in the skull scan, ulna bones from the forelimbs were selected to represent long bone growth. The straight shape of ulna by comparison with the radius also makes it preferable. Most importantly, a previous study found that mouse radius has a different allometric pattern during growth than other long bones [55]. Hence, the distance between most posterior and most prominent anterior points of ulna were used to represent long bone growth (see **Fig. 17**). Since the male *Hmx1*$^{dm/dm}$ mutant mice were mostly affected in size. I selected 7 male *Hmx1*$^{dm/dm}$ mutants with 7 male wild-type controls for this study.

The results showed that the *Hmx1*$^{dm/dm}$ mutant mice's ulna bone is also shorter in length, but after adjusting for weight difference (ulna/weight), the *Hmx1*$^{dm/dm}$ group (0.868±0.057 g, $n = 7$) exhibited no statistical difference when compared to wild-type (0.716±0.032 g, $n = 7$, $p = 0.007$). AP length, cranium width, cranium height, and full maxillary length can be corrected by ulna length, but not for basisphenoid distance nor back of skull length (see **Table 6**). With the direct measurement of the back skull length in **Table 3** which showed no statistical difference between the two groups, I predicted that a shortened maxilla causes the longitudinal change in the cranium of *Hmx1*$^{dm/dm}$ mutant mice. With growth potential even at the P56 stage [56], the basisphenoid may also contribute to the anterior-posterior dimension change in the *Hmx1*$^{dm/dm}$ mutant mice.

Figure 17. Representative linear measurement of the ulna bone on a wild-type control mouse. The red line represents the length of the ulna bone.

Description	*Hmx1*$^{dm/dm}$ male mice (n=7)		*Hmx1*$^{wt/wt}$ male mice (n=7)		t-test	
	M	SD	M	SD		
Average of left and right ulna (mm)	10.664	0.288	11.475	0.084	0.031	*
Ulna/ AP length	0.564	0.005	0.570	0.002	0.297	
Ulna/ Cranium width	1.065	0.018	1.111	0.007	0.052	
Ulna/ Cranium height	1.781	0.045	1.818	0.012	0.448	
Ulna/ Basisphenoid length	3.983	0.037	3.881	0.019	0.038	*
Ulna/ Full maxillary length	1.116	0.008	1.110	0.003	0.504	
Ulna/ Back of skull length	1.113	0.013	1.150	0.004	0.031	*
Ulna/ Tympanic width	1.181	0.017	1.217	0.008	0.089	

Table 6. Comparison of the linear measurement corrected by ulna between the *Hmx1*$^{dm/dm}$ mutant and *Hmx1*$^{wt/wt}$ control group ($p < 0.05$ is in red, showing the statistical difference).

3.4.4 3D shape analysis of the *Hmx1*$^{dm/dm}$ mutant mouse skulls

The linear measurements provided insights into the general structural change in the *Hmx1*$^{dm/dm}$ mutant mouse skull, but the most accurate shape analysis is to look at the quantified spatial information in 3D. *Analyze 10.0* software was used for virtual segmentation. Five landmarks were placed onto the mandible surface (see **Fig. 18**). The cranium had 18 landmarks (see **Fig. 12**) which were consistently used for the 3D morphometric alignment. Each dataset was reduced to 35 microns for simplifying data handling and reducing computation time. The external contour of each structure (hemi-mandible and cranium) was extracted from the image. Then the 3D morphometric analysis was done by using the deformable registration-based tool created by Dr. Sara Rolfe and Dr. Timothy Cox [41]. Differences were compared in the cranium, left and right hemi-mandibles within each animal, and the left hemi-mandibles between the mutant and control groups. Scan noise was removed from the images, borders were clarified between the object and the background, gaps and holes were filled based on geodesic active contours [57]. Once the contours were extracted, the left hemi-mandibles were first mirrored to permit comparison to the right sides for shape differences. An affine transformation was applied to align the images and to remove pose differences. Comparisons were done between left and right mandibles for each individual *Hmx1*$^{dm/dm}$ (n = 17) and no statistical difference was observed in the *dumbo* mutant group, as expected in wild-type mice [58]. Then I compared the mandible and skull shape differences between the *dumbo* and control groups by using a template sample (the left mandible and skull of one one representative *Hmx1*$^{wt/wt}$ mouse) and compared all the left side mandibles and skulls with this template. The temporal, incisor, angular process, masseteric ridge, back of the zygomatic arch of the *Hmx1*$^{dm/dm}$ mice showed the most significant differences (see **Fig. 19 A, E** average of magnitude feature, showing red; noted in arrows). There was little variance in the wild-type group's skull and mandible (standard deviation of magnitude

feature, shown in teal), but high variance in the *Hmx1*$^{dm/dm}$ group's crania, angular process, and incisor region of the mandible (**Fig. 19 I**).

Hmx1 expression in the craniofacial mesenchyme can be detected at E10.5 in the dorsal part of the branchial arch (BA)1, the caudal half of BA2, peripheral nervous system, and the eye [12]. These early events lead to changes in the ear morphology. However, the subtle structural changes muscle attachment sites of dumbo mice reveal potential secondary effects due to the loss of Hmx1 function. The mandible has been reported to have a large number of higher resorptive osteoclasts [59], hence the high remodeling flexibility. Influenced by mechanical force, temporal pattern of loading and other factors, the remodeling of bone happens throughout the whole ontogenesis process [60]. The superficial and deep layer of masseter attach to the lateral side of the angular process and the masseteric ridge separately; internal pterygoid attaches to the medial side of the angular process; and the masseter posterior deep belly and internal pterygoid muscles attach to the zygomatic arch. All of these areas may thus be subject to remodeling by biomechanical forces.

In conclusion, this complete characterization of the *dumbo* ear and its supporting structures through the developing process helped to visualize Hmx1's contribution to the morphogenesis of the skull. Because Hmx1 is expressed in the precursors of nerves and soft tissues, it is likely that some of the minor defects in the craniofacial structures are secondary changes related to neuromuscular defects. All of this information directs our etiological investigation.

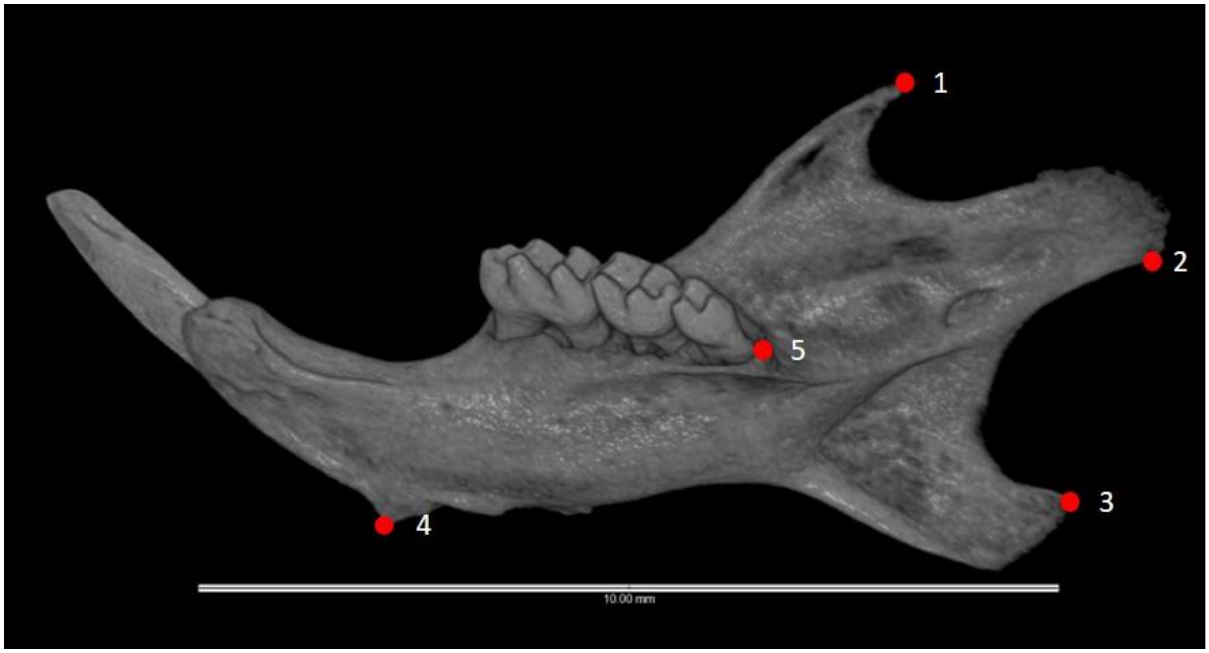

Figure 18. Schematic of a right side wild-type mandible with shape analysis landmarks. Point 1, tip of coronoid process; point 2, posterior inferior condyle point; point 3, tip of angular process; point 4, anterior inferior point on mental process; point 5, most posterior tip of the alveolar bone of third molar.

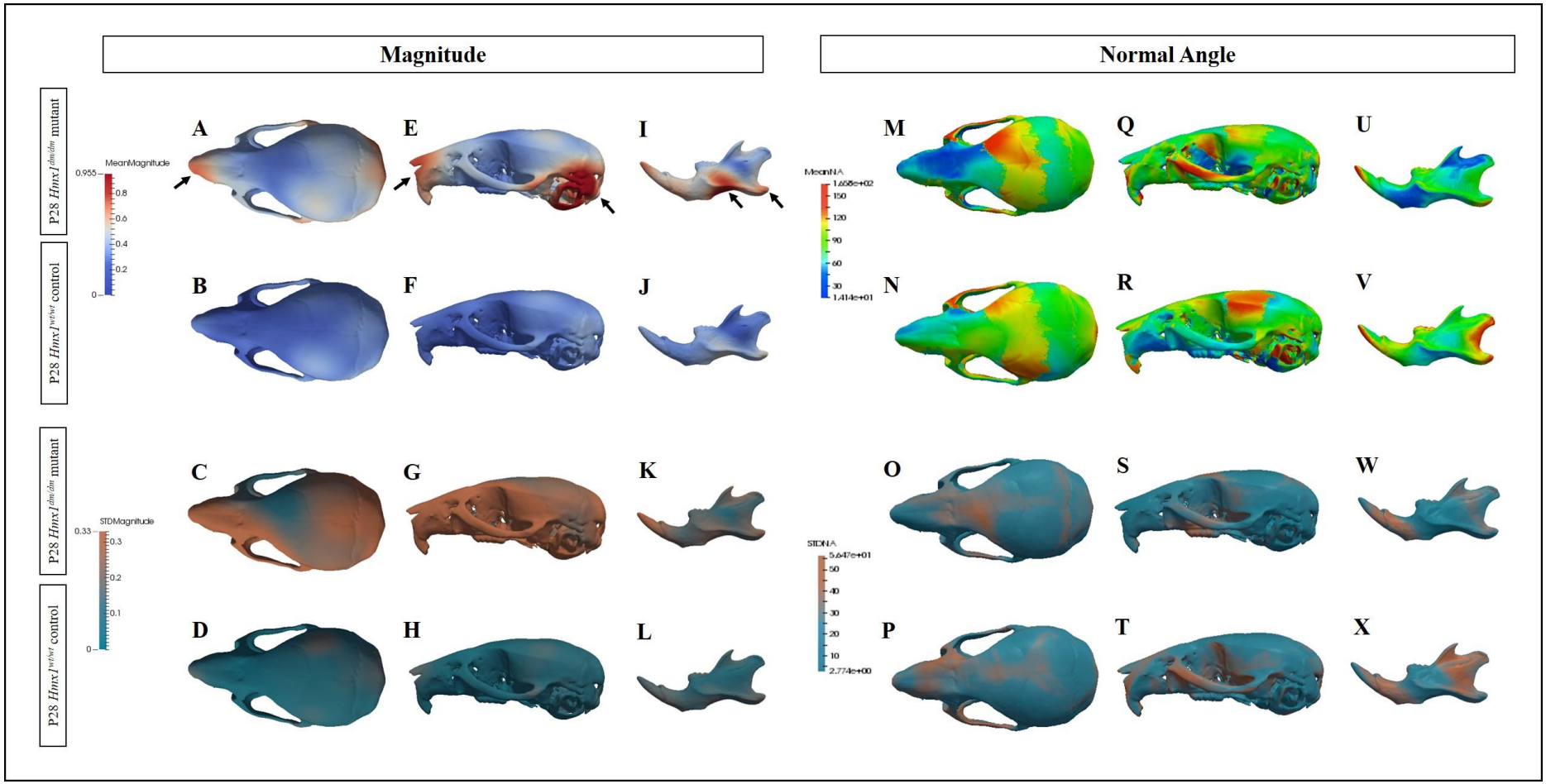

Figure 19. *Hmx1*$^{dm/dm}$ mutant animals exhibit shape changes in both the cranium and mandible (photos generated by Dr. Sara Rolfe**).** Deformational analysis of P28 *Hmx1*$^{dm/dm}$ mutant and *Hmx1*$^{wt/wt}$ control skulls. Heat maps are projected onto a standard control skull and highlight the relative mean (A-B, E-F, I-J, M-N, Q-R, U-V) and standard deviation (C-D, G-H, K-L, O-P, S-T, W-X) shape differences (A-L) or normal angle differences (M-X) apparent in *Hmx1*$^{dm/dm}$ (A, C, E, G, I, K, M, O, Q, S, U, W) mutants compared to controls (B, D, F, H, J, L, N, P, R, T, V, X) animals (*Hmx1*$^{dm/dm}$ n = 17, *Hmx1*$^{wt/wt}$ control n = 24). Arrows highlight the highest magnitude of shape differences present in the skull (A, E) and mandible (I) of *Hmx1*$^{dm/dm}$ animals.

3.5 Abnormal ear reflex response of the *Hmx1*$^{dm/dm}$ mutant mice

Defects in nerve or muscle function could lead to an abnormal neuromuscular outcome. *Hmx1* expression in the peripheral nervous system is restricted to the mandibular lobe of trigeminal ganglion (TG), general somatosensory neurons in the geniculate ganglion, some neurons of statoacoustic (vestibulocochlear, VIII) and the dorsal root ganglia at E10.5 [25]. A previous report showed Hmx1 is a requirement for the normal somatosensory neuron development in geniculate ganglion, which innervates the ear [25]. The musculoskeletal defects in *dumbo* mice are discussed above. In order to test integrated neuromuscular function in these mice, I applied the forced air reflex test to adult (P60+) *Hmx1*$^{dm/dm}$ and littermate control mice in a controlled environment (see **Methods 2.4.13**). Videos were made to record the response of mice before, during and after they were exposed to a 10-second constant-pressure air puff in their face. It was repeated 3 times for each animal and the mice were expected to have a normal response of closing their eyes and tucking their ears back against the skull.

In controls, a consistent response that included eye closure and ears retracting back to the head was observed. Although *Hmx1*$^{dm/dm}$ mutant mice could close their eyes, their ears remained perpendicular to the head (see **Fig. 20 C**). Quantitative measure the change of the ear tips distance with and without air puff showed a significant difference (p = 0.00025) between the *Hmx1*$^{dm/dm}$ mutant mice (0.27±0.60 mm, n = 5) and the control group (6.49±1.27 mm, n = 4).

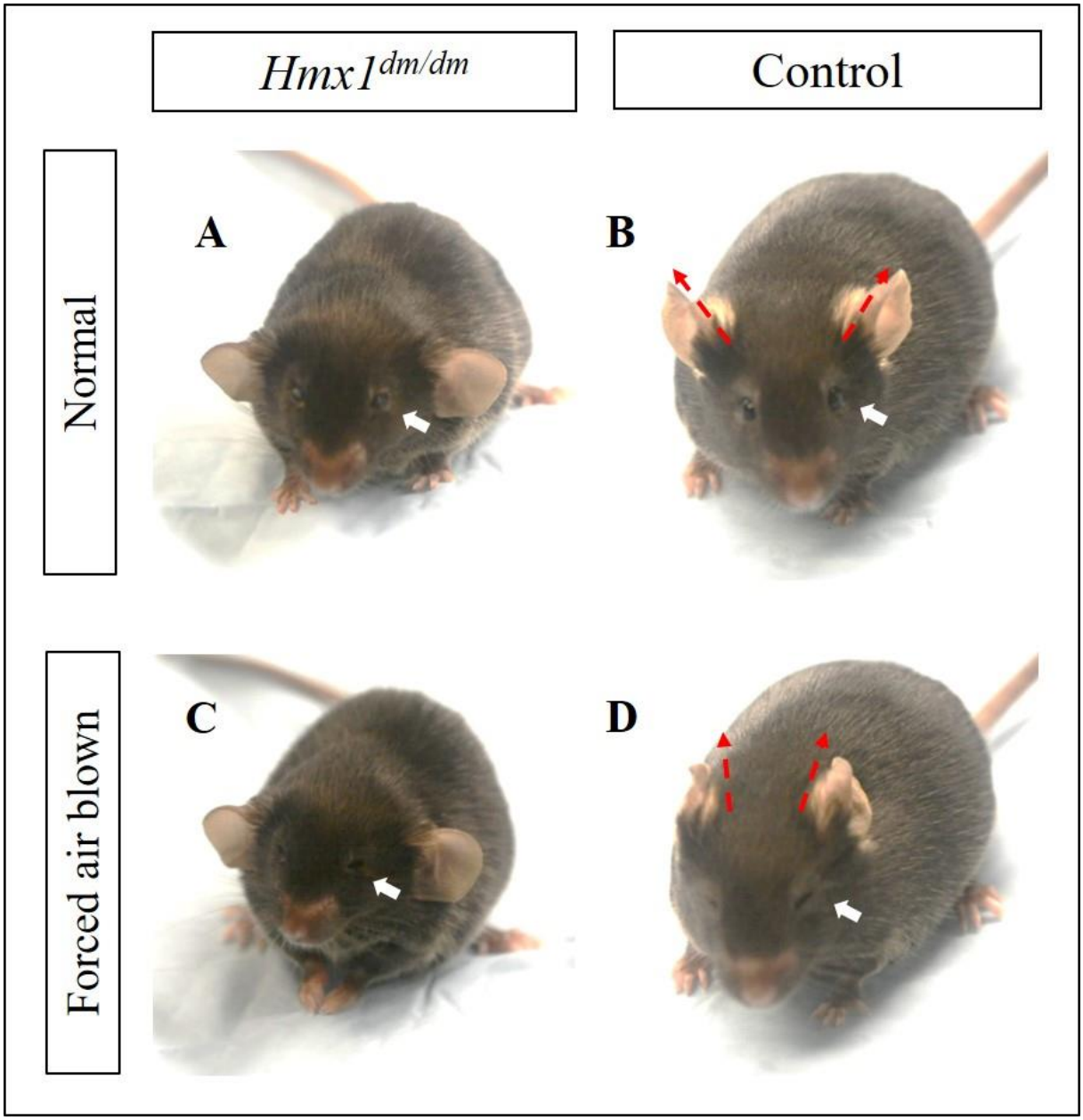

Figure 20. Response to air puff reflex test in *Hmx1*$^{dm/dm}$ mutant and control mice. Representative images of adult (P60+) *Hmx1*$^{dm/dm}$ (A, C) and littermate control (B, D) mice before (A, B) and during the air puff test (C, D) demonstrate that *Hmx1*$^{dm/dm}$ mutant mice, in contrast to controls, do not fold their ears flat to the skull in response to having air blown on their face (compare red dashed-arrows in B, D; *Hmx1*$^{dm/dm}$ n = 5, control n = 4), although *Hmx1*$^{dm/dm}$ mice can effectively close their eyes (compare white arrow in A to C and B to D).

3.6 Discussion

As mentioned before, the *dumbo* mice used in the study were generated in a pure C57Bl/6N background. By eliminating the interference of other unknown factors, the investigation of *dumbo* allele in our study supports the hypothesis that Hmx1 plays a central role in cranioskeletal development, especially of the lateral facial region.

Novel findings of the previously unappreciated *dumbo* phenotype helped us to understand Hmx1's function more precisely. First, the bifurcated caudal aspect of the developing pinnae at embryonic stages, especially the ectopic cartilaginous flap at the lower back of the adult ear pinna associated with loss of Hmx1, is distinct from other genes like Hoxa2 [33, 61], PLCB4 and GNAI3 [62] which affect ear development more extensively. The loss of Hmx1 may represent a restricted homeotic transformation. Second, the morphological changes in the craniofacial sutures are influenced by the mechanical loading [63], mechanical strain from mastication is known to affect the development of the mandible [64–66]. Third, postnatal cranioskeletal anomalies at the muscle attachment site of lateral-temporal region reflect a potential muscular function defect: the paired bony paraoccipital processes which are functionally equivalent to the mastoid processes in humans attaching with muscles of the head and neck movement (digastric posterior belly, longissimus capitis, splenius captis and the sternocleidomastoid); the masseteric ridge and angular process of the mandible attach by muscles of the mastication (masseter, internal pterygoid). Further investigations about the neuromuscular circuit by Dr. Jessica Rosin helped to determine Hmx1 was not present in muscle precursor cells, reductions were found in the great auricular nerve which penetrates the caudal of the pinna and the somatosensory auriculotemporal nerve from the mandibular nerve at E12.5 and E13.5 embryos (see **Fig. 21**). Thus the functional deficit in *dumbo* ear movement could be the result of musculoskeletal defects, sensory defects, or a combination of both. Future tissue-specific disruption of Hmx1 should help resolve the

cellular contributions to the *dumbo* phenotype.

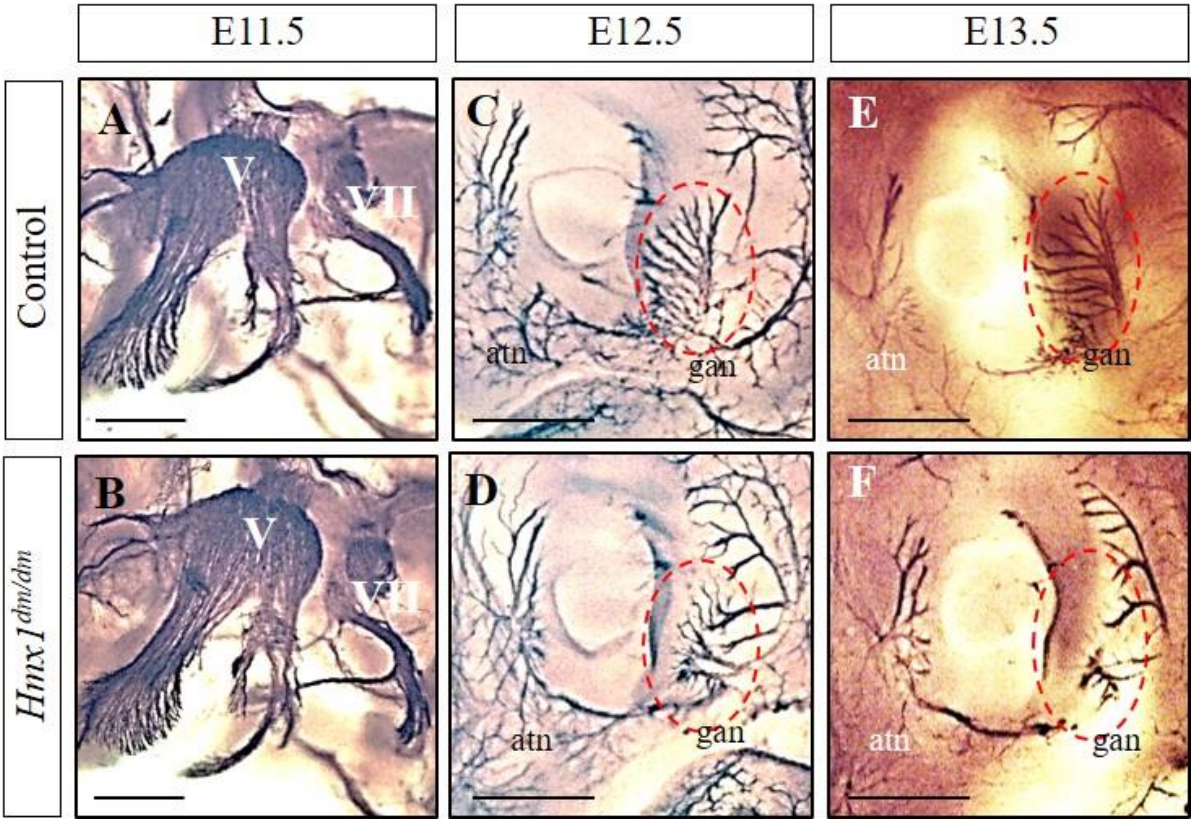

Figure 21. *Hmx1*$^{dm/dm}$ animals show defects in sensory nerve branches (courtesy of Dr. Jessica Rosin**).** Figure A-F: Neurofilament staining using a 2H3 antibody in control (A, C, E) and *Hmx1*$^{dm/dm}$ mutant (B, D, F) embryos at of E11.5 (A, B; control n = 6, *Hmx1*$^{dm/dm}$ mutant n = 5), E12.5 (C, D; control n = 6, *Hmx1*$^{dm/dm}$ n = 4) and E13.5 (E, F; control n = 8, *Hmx1*$^{dm/dm}$ n = 2) shows the trigeminal (V) ganglion is intact in E11.5 *Hmx1*$^{dm/dm}$ embryos, noticeable defects can be seen in the great auricular nerve (gan) and the auriculotemporal nerve (atn) that surround and innervate the pinna of *Hmx1*$^{dm/dm}$ mutant embryos at both E12.5 and E13.5 (red dashed-circle;). Scale bars = 500 μm.

CHAPTER FOUR: DELETED REGION IN DUMBO RAT CONTAINS AN EVOLUTIONARILY CONSERVED REGION (ECR) TO DRIVE HMX1 EXPRESSION IN CRANIOFACIAL TISSUES

4.1 The *dumbo* rat Hmx1 downstream deletion region contains an ECR

The transcription regulation ability of the noncoding component in the genome has received much attention from biologists in the past decades. Comparison of genomic sequences among diverse vertebrate species can help identify these highly conserved regions, which can play important roles in transcriptional regulation. Transgenic models have demonstrated that these conserved non-coding elements regulate gene expression within specific tissues [67]. However, the functional components of non-coding elements that specifically contribute to the craniofacial development and related disorders remain largely unclear, and important regulatory regions do not necessarily show a high degree of sequence conservation [68]. Thus major challenges still exist in determining the pathogenicity of newly discovered enhancer variants.

Recent work from our group showed that the *Hmx1* coding sequence is normal in *dumbo* rats. However, expression of the Hmx1 protein was lost in the craniofacial mesenchyme (CM) of the first and second branchial arches (BA1 and BA2), while the peripheral nervous system expression was unaffected [28]. By sequencing the entire *Hmx1* locus in *dumbo* rats, our collaborator Dr. Takashi Serikawa identified a 5,777 bp deletion in the distal conserved region (DCR) residing ~80 Kb downstream of the

Hmx1 transcription unit (see **Fig. 22**). In this deletion region, a core evolutionarily conserved region (ECR) of 594 bp was found to be highly conserved in vertebrate classes (see **Fig. 23**). Remarkably, a 76 bp duplication within this core ECR was also identified by another group in the bovine crop ear allele [31]. Hence, I hypothesized that this ECR is a tissue-specific enhancer, which contributes to the auricular development by regulating *Hmx1* expression in the lateral facial mesenchyme. To test this hypothesis, the transgenic mouse reporter assay, one of the most widely used mammalian *in vivo* enhancer activity testing tools, was used to study the Hmx1 ECR's function. By understanding this ECR and clarifying *Hmx1's* function, we could analyze the gene regulation network that correlated with lateral facial development.

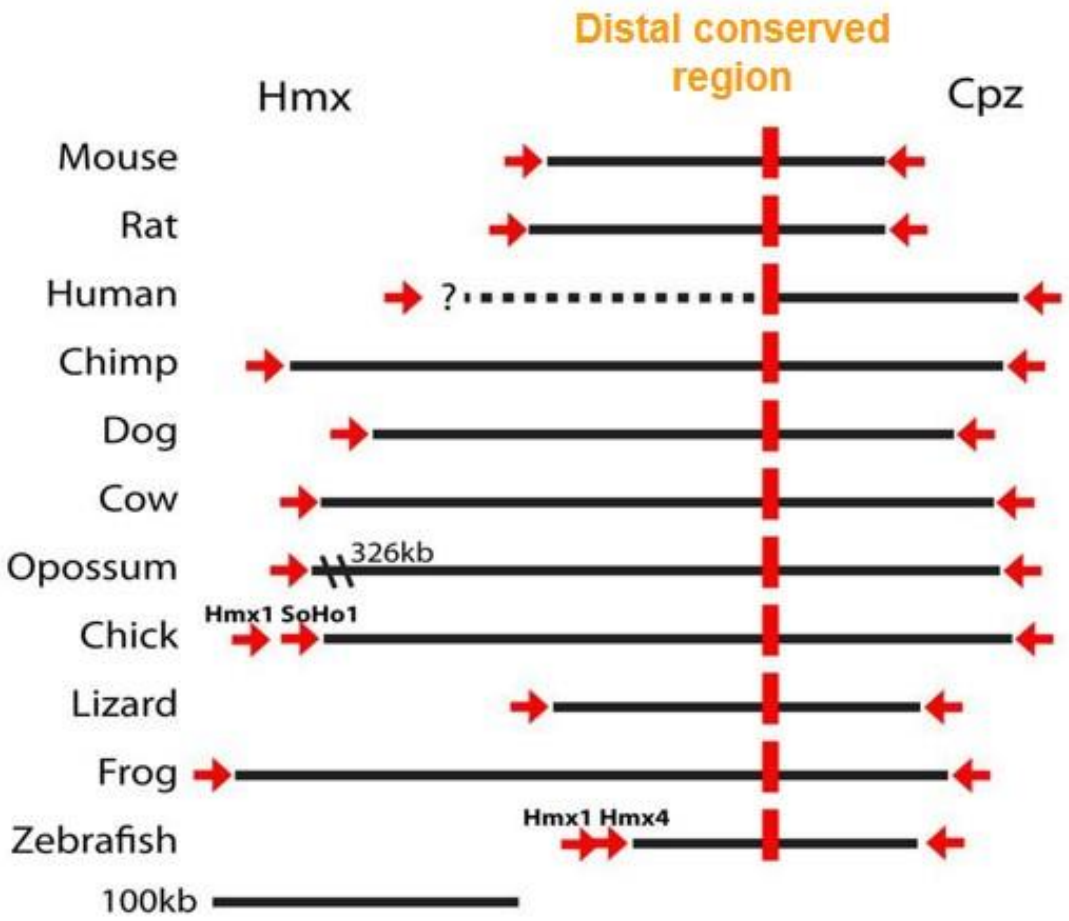

Figure 22. Comparative genomics of the Hmx1 downstream deletion region (adapted from Quina et al [28])**.** Red arrows indicate the 3' end of the actual or predicted Hmx1 and Cpz transcripts, and the direction of transcription. The red dash line represents the distal conserved region (DCR) is highly conserved across all vertebrate classes.

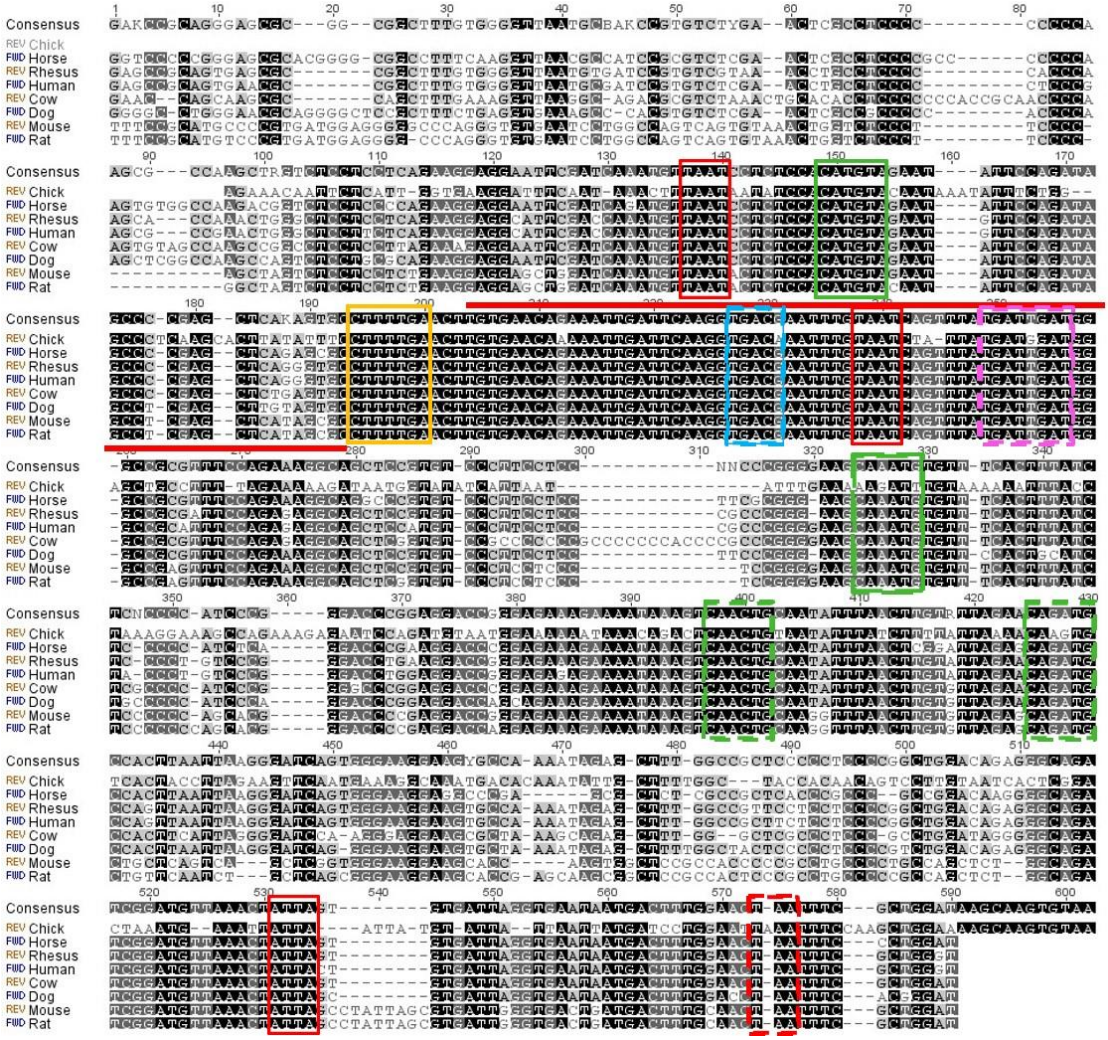

Figure 23. The sequence of the core 594 bp sequence of the ECR in seven different species. Residues completely conserved across all seven species are highlighted in black. Residues with a lighter shade of grey depicting a lower level of conservation. Predicted transcription factor binding sites are shown in color-coded boxes {**Hox**, **Ebox**, **Tef/Lef2**, **Meis/half Creb site**, **Pbx/Hox**}. The 76 bp duplication within this core ECR that was identified in the bovine crop ear allele is lined in red.

4.2 Generation of the *dumbo* rat Hmx1 downstream deletion region

In order to obtain mouse genomic sequences, we took advantage of the bacterial artificial chromosome (BAC) mapping of the mouse genome. According to the UCSC Genome Browser mouse July 2007 (NCBI37/mm9) assembly, two BAC clones (RP23-30C19 and RP23-26P10, see **Fig. 24**) that cover the whole *dumbo* rat deletion region, were obtained from a repository at the Children's Hospital Oakland Research Institute. These BAC clones were then used as templates to subclone the desired genomic regions (see **Methods 2.2.9**). I began with the goal of generating PCR products for the entire rat *dumbo* deletion region (dmWhole), the proximal and distal halves of this region, and the specific *dumbo* ECR (dmECR, see **Fig. 25**). The primer pairs used to amplify the desired region were designed based on the Primer3: WWW primer tool (http://biotools.umassmed.edu/bioapps/primer3_www.cgi).

The RP23-30C19 BAC clone was used as the template for all the fragments generated (see **Methods 2.2.5**). Not1 (GCGGCCGC) and Asc1 (GGCGCGCC) restriction enzyme recognition sites were designed into the forward and reverse primers respectively for inserting (ligating) the fragments into the entry clone. The DNA products were confirmed in size by using gel electrophoresis (see **Methods 2.2.9, 2.2.10**). All the primer pairs gave the right size products except the Dum Del 2nd F/R primer pair (see **Fig. 26 lane 3**). This could because the Dum Del 2nd F/R primer pair forms primer dimers that prevented the primers from binding to the template. According to the ~2000 bp light lower band that emerged in the Del Whl F/R primer pair reaction (see **Fig. 26 lane 6**, white arrow), a non-specific Dum Del Whl F or R

primer binding site existed inside the *dumbo* rat whole deletion region. By trying different primer combinations, specific bands were obtained for the Dum Del 1st F/R primer combinations and the Dum Del Whl F/ Dum Del 1st R primer combination (see **Fig. 27 lane 3 and 5**). It indicated that the Dum Del Whl R primer is the one with a non-specific binding site that contributes to the non-specific band. Unfortunately, I was not able to generate the 2nd half of the deletion region by trying out additional combination: the Dum Del 2nd F/ Dum Del Whl R primers combination also did not give any product (see **Fig. 27 lane 6**). Since the Dum Del Whl R primer could give the right-sized product, it is the Dum Del 2nd F primer that contributed to the failure of the *dumbo* rat second half deletion region product.

All three fragments with the right sizes were digested by Not1 and Asc1 restriction enzymes (see **Methods 2.2.2**) and further ligated with the linearized pENTR/SD/D-TOPO entry vector separately. Successful insertions were confirmed with Not1 and Asc1 double digestions as well as sequencing.

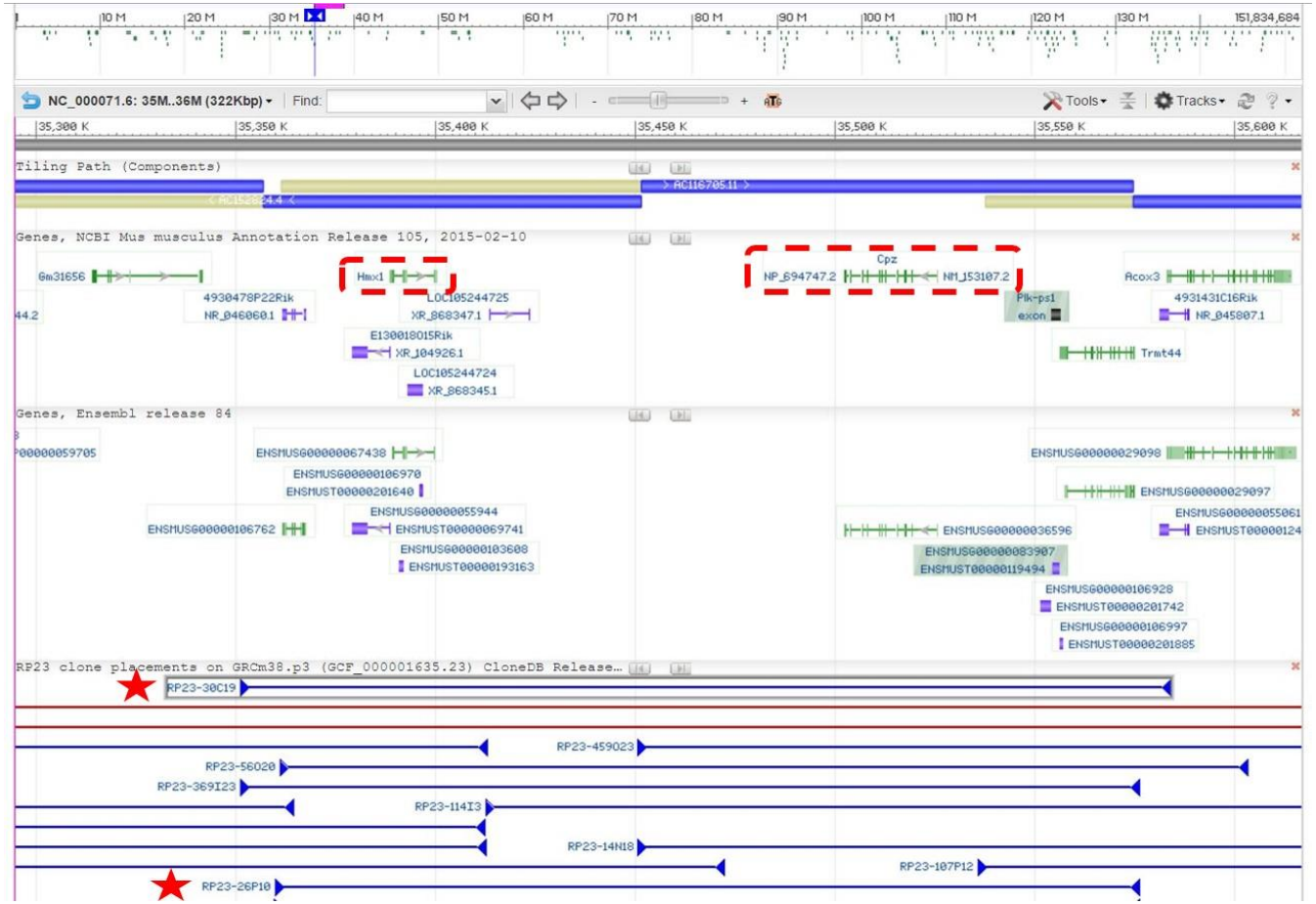

Figure 24. The NCBI-Clone website showing the two BAC clones (RP23-30C19 and RP23-26P10) and their positions relative to the Hmx1 gene. The coding regions of Hmx1 and Cpz genes are shown in boxes with red dashed lines. The two red stars indicate the two BAC clones (http://www.ncbi.nlm.nih.gov/clone/609011/).

Figure 25. The fragments generated for the *dumbo* rat downstream deletion region and the design of the primer pairs. The arrows with different numbers and directions represent the primers designed for generating the fragments. The **evolutionarily conserved region** (dmECR, 594 bp) was generated by 1. M hum F and 2. M hum R primers. The **Dumbo rat first half deletion region** (4,761 bp) was generated by the 3. Dum Del 1st F and 4. Dum Del 1st R primers; the **Dumbo rat whole deletion region** (dmWhole, 6,094 bp) was generated by the 5. Dum Del Whl F and 6. Dum Del Whl R primers; the **Dumbo rat second half deletion region** (1,792 bp) was generated by a combination of 7. Dum Del 2nd F and 8. Dum Del 2nd R primers. The exact sequences of the primers can be found in **Table 2.1.9a**.

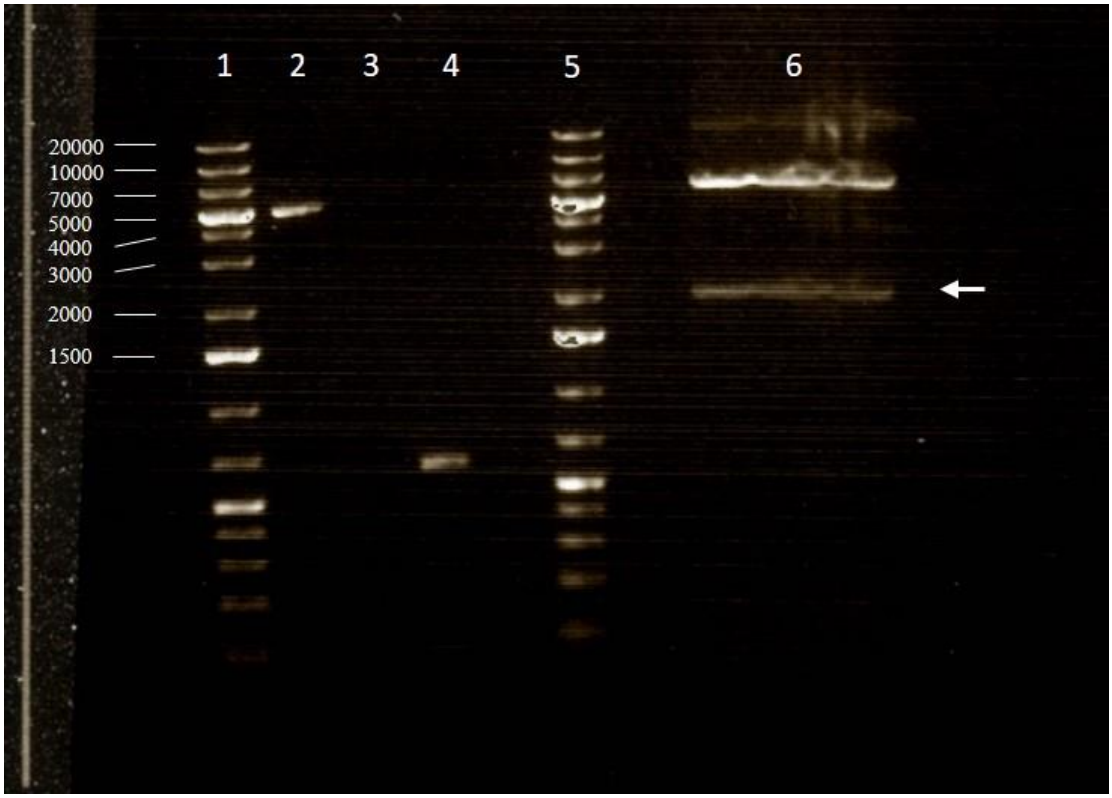

Figure 26. *Dumbo* rat downstream deletion region PCR fragments. GeneRuler 1kb Plus DNA Ladder (lane 1, 5); dumbo rat first half deletion region fragment (lane 2, Dum Del 1st F/R primers, size 4,761 bp); dumbo rat second half deletion region fragment (lane 3, Dum Del 2nd F/R primers, expected size 1,792 bp); evolutionarily conserved region fragment (lane 4, M hum F/R primers, size 594 bp); dumbo rat whole deletion region fragment with a nonspecific lower band noted in white arrow (lane 6, Dum Del Whl F/R primers, size 6,094 bp).

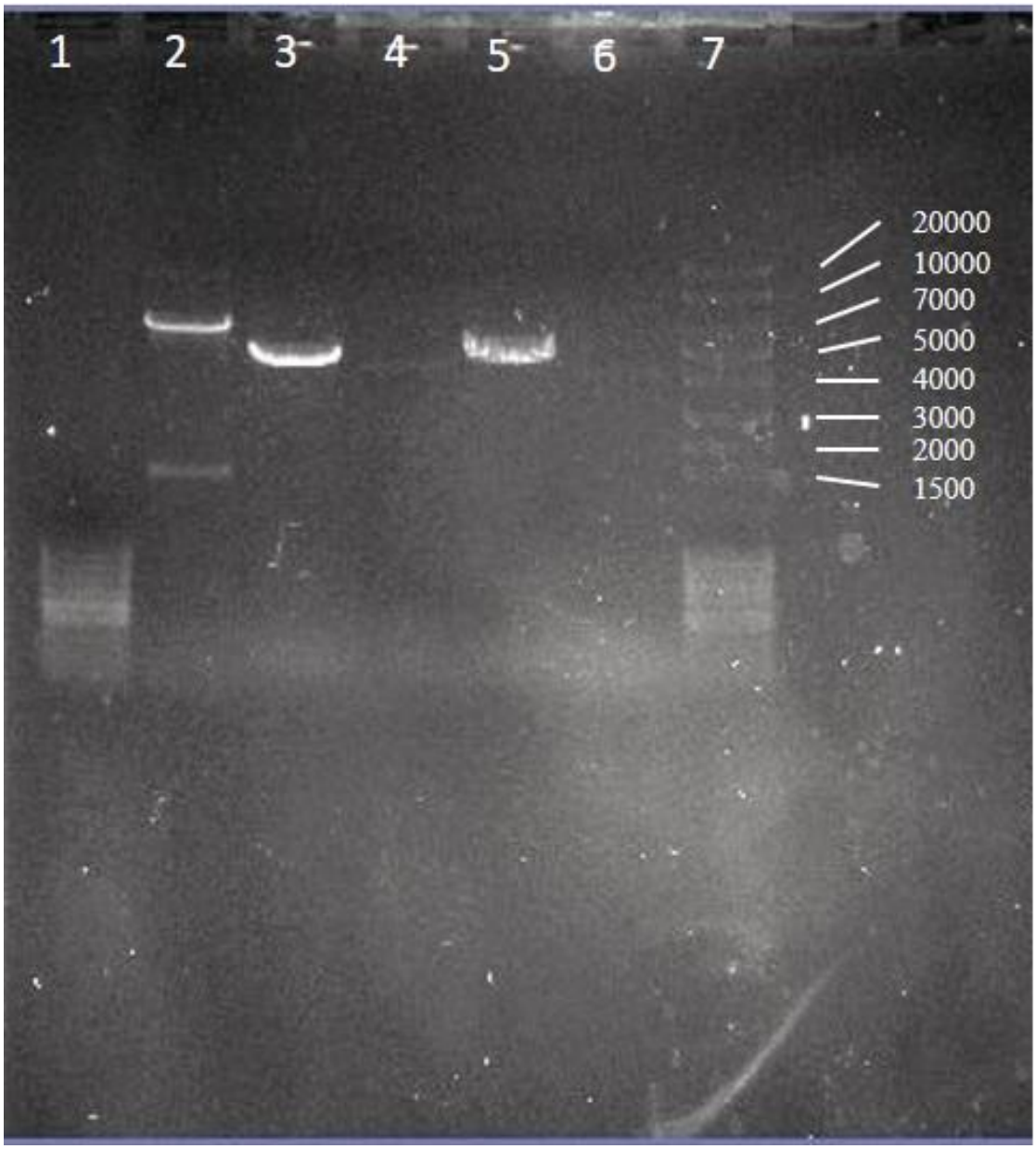

Figure 27. *Dumbo* rat downstream deletion region PCR fragments. 100 bp ladder (lane 1); dumbo rat whole deletion region fragment (lane 2, Dum Del Whl F/R primers, size 6,094 bp); dumbo rat first half deletion region fragment (lane 3, Dum Del 1st F/R primers, size 4,761 bp); dumbo rat second half deletion region fragment (lane 4, Dum Del 2nd F/R primers, size 1,792 bp); dumbo rat first half deletion region fragment using combined primers (lane 5, Dum Del Whl F/ Dum Del 1st R primers, size 4,827 bp); dumbo rat second half deletion region fragment using combined primers (lane 6, Dum Del 2nd F/ Dum Del Whl R, size 1,859 bp); GeneRuler 1kb Plus DNA Ladder (lane 7).

4.3 Transient transgenic testing of the *dumbo* rat deletion region using the PiggyBac (PB) system

The transgenic mouse reporter assay is a popular qualitative *in vivo* method to measure enhancer activity. Its strength lies in assessing the tissue-specific enhancer activity within the whole organism. For this assay, the testing sequence of potential enhancer activity is linked to a reporter gene (for example, *LacZ*) and then delivered into mouse zygotes through pronuclear injection [69]. The reporter gene expression patterns are scored visually, such as by GFP fluorescence, or enzymatic staining for β-galactosidase.

One problem in transient transgenic assays is the relatively low rate of incorporation in the injected embryos, which typically is around 10-15%. Transposon-mediated transgenesis is a strategy for overcoming this low incorporation rate. DNA transposons are genetic elements that efficiently transpose between vectors and chromosomes via a "cut and paste" mechanism. Transposable elements have been routinely used for insertional mutagenesis in transgenic animals. The PiggyBac (PB) transposon was named as a single family for its unique tetranucleotide TTAA target-site. The PB elements are ~2.4 kb transposons with 13 bp inverted terminal repeats (ITRs) and an amino acid transposase [70, 71]. It is a highly useful transposon for genetic engineering in a wide variety of species [72–75]. Compared to the *Sleeping Beauty* system (the first functional transponson in mammalian cells) [76], the PB system overcomes the local hopping phenomenon with a high efficiency in integrating the transgene. It can also carry up to ~10 kb of foreign sequences without

a significant reduction in integration efficiency [74]. The classical pronuclear injection of linear DNA results in the formation of transgene concatamers, where multiple copies of the transgene are inserted into the genome [77]. The PB system produces single copies of integrated transgenes, which helps to obtain a normal physiological level expression of the transgenes without leaving a footprint [74]. The insulator ends of the vector also protect the transgene against position effects.

The transposon vector pDB302 GWenh miRNA (see **Fig. 28**), pBB201 pcMC *PBase* (normal transposase), and pBB294 pcMV hyper *PBase* (hyperactive transposase) were generously provided by Dr. David Beier. First, the AvrII restriction enzyme was used to remove the region from IRESaa to WPREaaa off the pDB302 GWenh miRNA, and this new plasmid was named as pDB305 (8,937 bp). The plasmid construct was verified by PvuII digestion and sequencing. LR clonase reactions were set up separately between the pDB305 and the pENTR/SD/D-TOPO entry vectors with the three different deletion region inserts. The successful integration of the three dumbo rat fragments into the pDB305 plasmid was confirmed by restriction enzyme digestion: dumbo rat whole deletion region (dmWhole) into pDB305 plasmid (see **Fig. 29**); dumbo rat first half deletion region into pDB305 plasmid (not shown); and dmECR deletion region into pDB305 plasmid (see **Fig. 30**). The NheI and KpnI restriction enzyme digestion information can be found in **Table 7**.

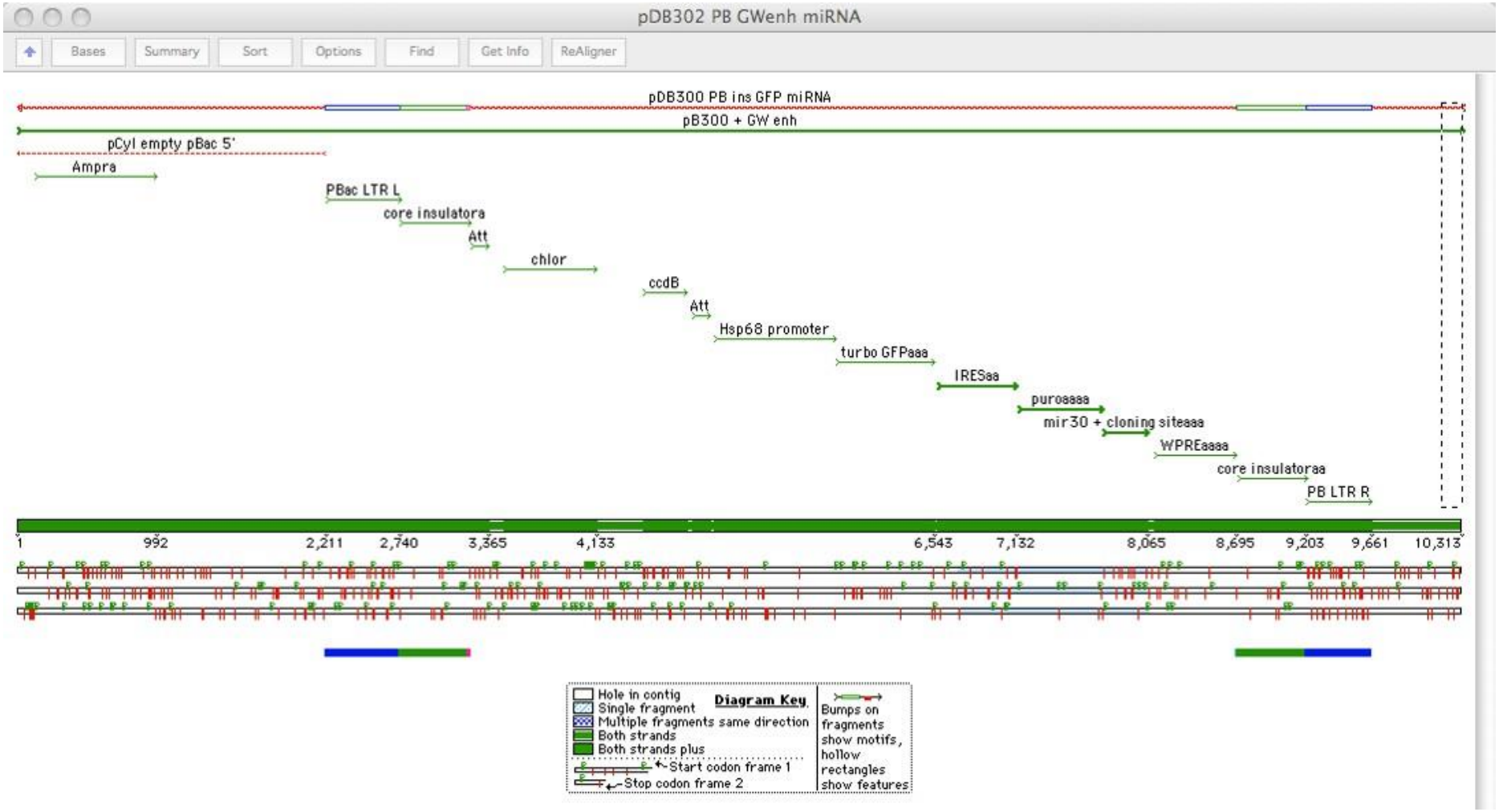

Figure 28. The PiggyBac turbo GFP destination vector for transgenic analysis (vector generously provided by Dr. David Beier)**.**

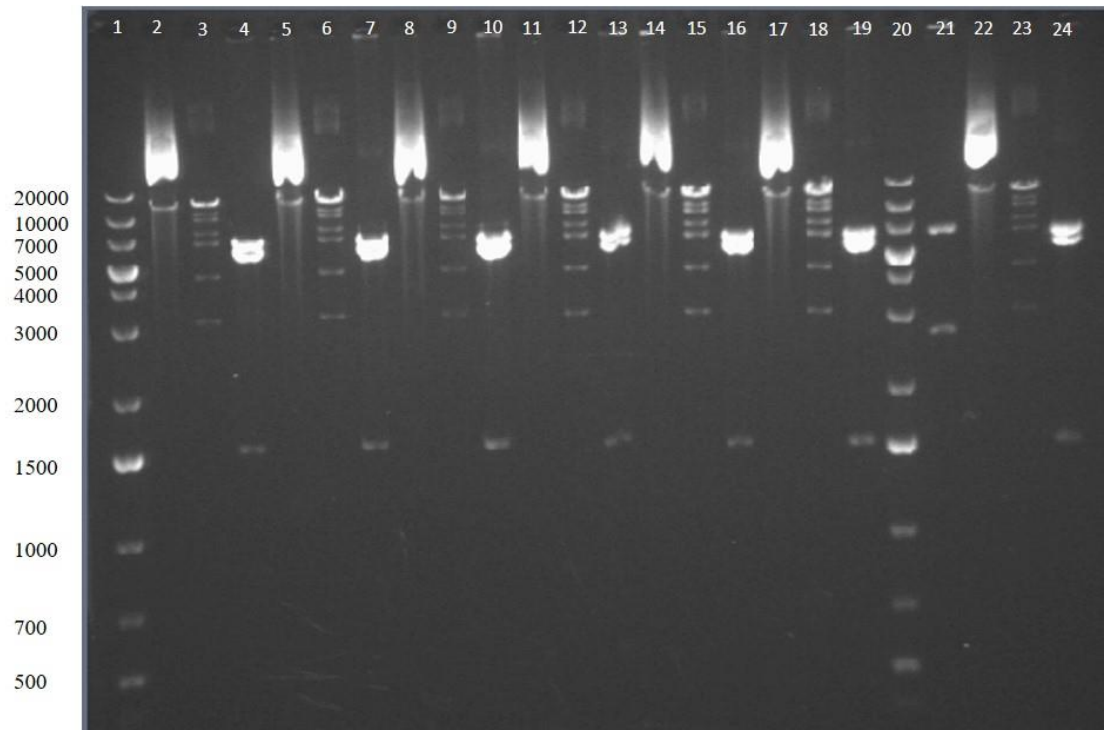

Figure 29. The successful insertion of the dumbo rat whole deletion region (dmWhole) into pDB305 plasmids. Three adjacent lanes are from a single colony. For example from left to right, lanes 2, 3, 4 are the same plasmid at uncut, KpnI digested and NheI digested stages. GeneRuler 1kb Plus DNA Ladder (lanes 1, 20); uncut plasmids with the dmWhole (lanes 2, 5, 8, 11, 14, 17, 22); plasmids with the KpnI-digested dmWhole (lanes 3, 6, 9, 12, 15, 18, 23); plasmids with the NheI-digested dmWhole (lanes 4, 7, 10, 13, 16, 19, 24); NheI digested pDB305 plasmid (lane 21). The NheI digestions were showing the right-sized bands, but not the KpnI digestions. With a size of 8,937 bp, the pDB305 plasmid can be digested by NheI into 2,612 bp and 6,325 bp fragments, and by KpnI into 2,760 bp and 6,177 bp fragments. With a size of 13,396 bp, the pDB305 plasmid with dmWhole can be digested by NheI into 1,504 bp, 5,567 bp, and 6,325 bp three fragments, and by KpnI into 2,947 bp, 4,245 bp and 6,177 bp fragments.

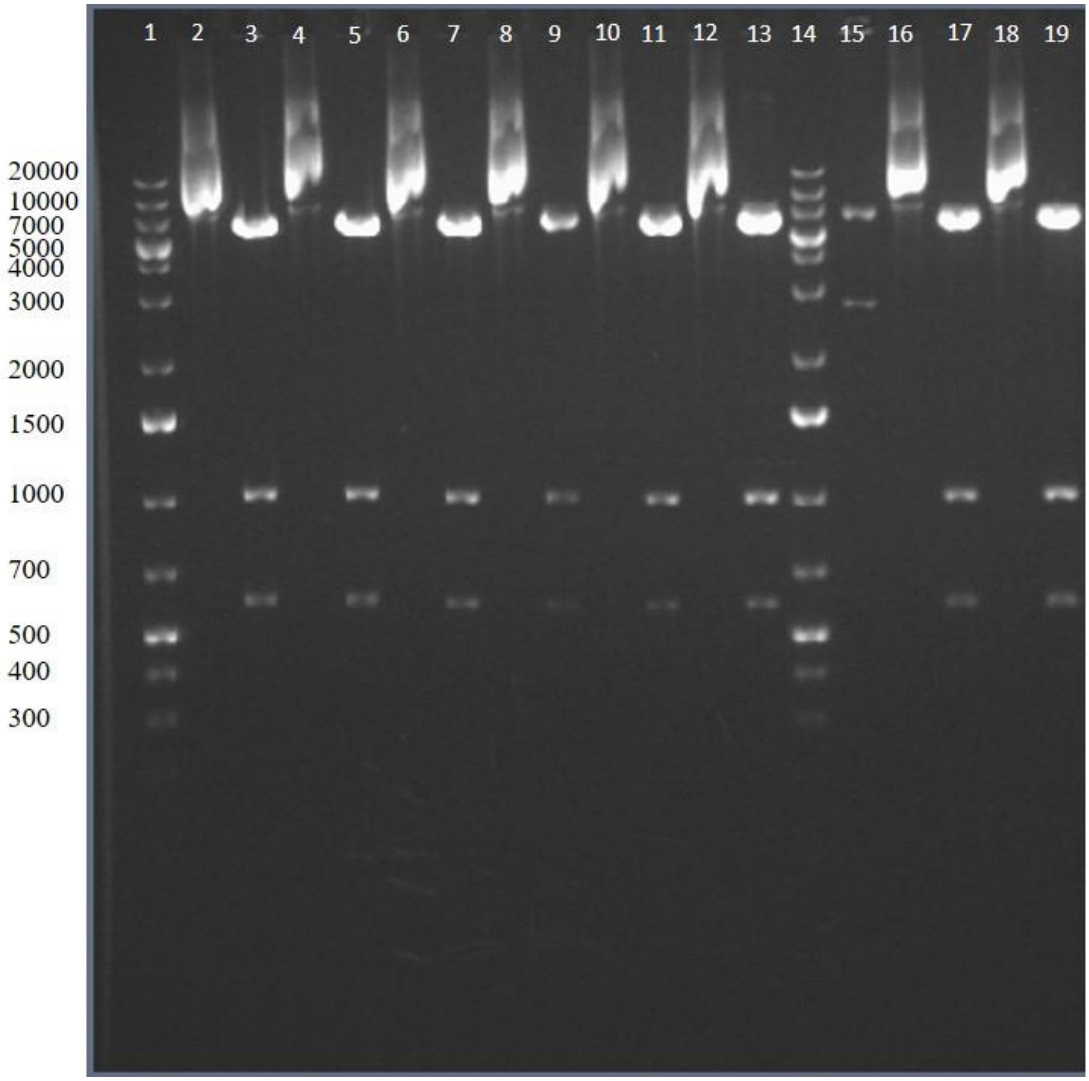

Figure 30. The successful insertion of the ECR deletion region into pDB305 plasmids. Two adjacent lanes come from a single colony. For example, lanes 2 and 3 are the same plasmid at uncut and NheI digested stages. GeneRuler 1kb Plus DNA Ladder (lanes 1, 14); the dmECR deletion region inserted uncut plasmids (lane 2, 4, 6, 8, 10, 12, 16, 18); NheI digested the dmECR deletion region inserted plasmids (lane 3, 5, 7, 9, 11, 13, 17, 19); NheI digested pDB305 plasmid (lane 15). With a size of 8,937 bp, the pDB305 plasmid can be digested by NheI into two fragments of sizes 2,612 bp and 6,325 bp. With a size of 7,893 bp, the pDB305 plasmid with the dmECR can be digested by NheI into three fragments of 581 bp, 987 bp, and 6,325 bp.

	Size (bp)	NheI digestion (bp)	KpnI digestion (bp)	BspHI digestion (bp)
pDB305	8937	2612, 6325	2760, 6177	1008, 7929
pDB305 + ECR region insert	7893	581, 987, 6325	1716, 6177	1008, 6885
pDB305 + dumbo rat first half deletion region insert	12066	1438, 4303, 6325	1709, 4180, 6177	1008, 11058
pDB305 + dumbo rat whole deletion region insert	13396	1504, 5567, 6325	2974, 4245, 6177	1008, 12388

Table 7. The sizes of the pDB305 plasmid with and without different deletion region insertions and the fragment sizes after NheI, KpnI or BspHI restriction enzyme digestions.

After sequencing all the fragments, we collaborated with the preclinical research and transgenic services (PRTS) at the University of Washington for the transgenic assay. The pDB305 dmWhole and pDB305 dmECR plasmids were used. The transposase mRNA was generated from the pBB294 pcMV hyper *PBase* plasmid (hyper active transposase) using the standard kits (see **Methods 2.2.13 – 2.2.15**). All preparation procedures strictly followed the PRTS pronuclear microinjection protocol (see **Methods 2.3.8 and 2.3.9**). Quality and effective polyadenylation of mRNA was checked using 1% agarose gel electrophoresis. 2.0 µg/ml PB transposon DNA and 20 µg/ml *PBase* mRNA were mixed together in the injection buffer, as they were suggested to result in the highest transgenic efficiency [78].

A total of 39 dmWhole and 29 injected dmECR deletion region transposon embryos were implanted into four different pseudopregnant females. Embryos were collected at day E12.5. In the dmWhole transposon injection group, 4 embryos (with 3 underdeveloped) and 6 embryos (with 2 underdeveloped) were obtained from two separate female mice. In the dmECR transposon injection group, only one in two pseudopregnant female mice gave 6 embryos. The tail tissues were collected from the embryos before fixing them in cold 2% PFBS for 30 mins. No GFP signal could be detected under the fluorescence microscopy. The Turbo GFP primer pair was used for genotyping successful transgenic embryos (see **Table 2.1.9b**). Positive controls for genotyping were generated by mixing 1 µl of 0.1ng dmECR inserted pDB305 plasmid separately into 9 µl and 99 µl of a wild-type mouse tail DNA prep (11.7 ng/µl). In all 16 embryos, only one successful dmWhole transposon embryo was found.

A second transgenic attempt was made by using the pT3Ts-*PBase* mRNA from pBB232 plasmids [78] with all other conditions identical to the first attempt. A total of 44 fertilized eggs with the dmWhole insert were implanted into three pseudopregnant females. 4 out of the 13, 4 out of the 15, and 3 out of the 16 implanted embryos were collected at E12.5. 29 fertilized eggs with the dmECR transposon insert were implanted into two pseudopregnant females, 6 out of the 14 and 6 out of the 15 implanted embryos were collected at E12.5 from each female. Tail DNA was extracted from all embryos before fixing the embryos in 2% PFBS for 30 minutes. Genotyping results showed no transgene positive embryos this time (see **Table 8**).

The PB transposase reaction is a footprint-free, reversible process, and a correctly located insertion could be translocated/re-excised under conditions of excessive transposase expression. The optimal DNA and mRNA concentrations are important to guarantee and maintain a successful insertion. Other facts like the chromatin structure which could also influence the stability of the transgene: if the insertion was inside an open configuration region of the chromosome, the transposase could have easily been removed. With all this information in mind, much effort would be needed to investigate the right system, injection concentrations and supporting techniques for creating the transgenic mice. In light of our limited resources, we turned to a more conventional transgenic method in further analysis of the enhancer function of the ECR.

Injection essay	pDB305 transposon vector with	Implanted embryos	Pseudo female	E12.5 embryos
First round	Dumbo rat whole deletion region	39	A	4
			B	6 (1 positive)
	ECR region	29 with albino	C	no embryo
			D	6 (with 4 albino)
Second round	Dumbo rat whole deletion region	13	E	4
		15	F	4
		16	G	3
	ECR region	14	H	6
		15	I	6
Total		**141**		**39 (1 positive)**

Table 8. Summary of embryos used for two co-injection events of the PB transposon DNA with the *PBase* mRNA. In a total of 39 embryos, only 1 genotyped positive embryo was found from the pseudo-female B (highlighted in yellow).

4.4 The ECR is a craniofacial tissue-specific enhancer of Hmx1 gene

Having abandoned the transposase-mediated strategy, we collaborated with Dr. Axel Visel's group at Lawrence Berkeley National Laboratory, who routinely uses a mouse heat-shock gene (Hsp68) regulated β-galactosidase gene reporter system (LacZ system) for transient transgenic analysis [67, 79]. pENTR/SD/D-TOPO vectors with the two deletion fragments (dmWhole and dmECR) were sent to the Visel laboratory, and these fragments were transferred into the Hsp68-LacZ-Gateway plasmid (Addgene, Plasmid #37843) by LR clonase reaction. The conventional mouse transgenesis assay protocol was followed (see **Methods 2.3.9**) to create the transient transgenic dmWhole-Hsp68-LacZ and dmECR-Hsp68-LacZ embryos. The presence of enhancer activity was determined by positive LacZ staining for both the dmWhole and dmECR embryos. Five embryos were obtained from the dmWhole group and eight embryos were obtained from the dmECR group (shown in **Fig. 31)**. All five dmWhole transgenic embryos showed β-galactosidase staining in BA2 at E11.5 (see **Fig. 31 A-E**). Three out of five embryos also exhibited staining in a band of mesenchyme across the frontonasal region, the dorsal aspect of the eye and the dorsal BA1 mesenchyme (see **Fig. 31 B-D**). Variable levels of staining were noted in restricted regions of the developing neural tube (see **Fig. 31 A-E**). The single dmWhole embryo with ectopic blue staining (see **Fig. 31 A**) could have resulted from the position effects of the randomly integrated transgene. This might occur if the transgene in the dark blue embryos located adjacent to a strong genomic enhancer, leading to its expression during early embryonic development.

Even with the variable β-galactosidase staining patterns in the embryos, it should be noted that the expression was consistent in the BA2, the dorsal part of BA1, and the band in the frontonasal region for most dmWhole embryos. This restricted pattern coordinated with the staining in dmECR embryos (see **Fig. 31 F-M**), which was remarkably consistent. One representative dmECR embryo (see **Fig. 31 H**) was selected and processed for optical projection tomography (OPT) imaging. The 3D virtual dissection showed the LacZ signal was restricted to the lateral facial mesenchyme, which matched with the endogenous Hmx1 protein expression in the E12.5 mouse embryo (see **Fig. 32**).

These investigations verified that the ECR of the dumbo rat deletion region functions as a facial mesenchyme-specific enhancer at the frontonasal, dorsal BA1 and BA2 areas. Since the dmWhole embryos demonstrated similar expression patterns as the dmECR embryos, enhancers that target other areas of Hmx1 expression, such as the eye or the sensory ganglia, must lie outside the dumbo rat deletion region examined in this study. Species-homology alignment for the entire Hmx1 genomic region would give a clue as to the location of these other enhancers.

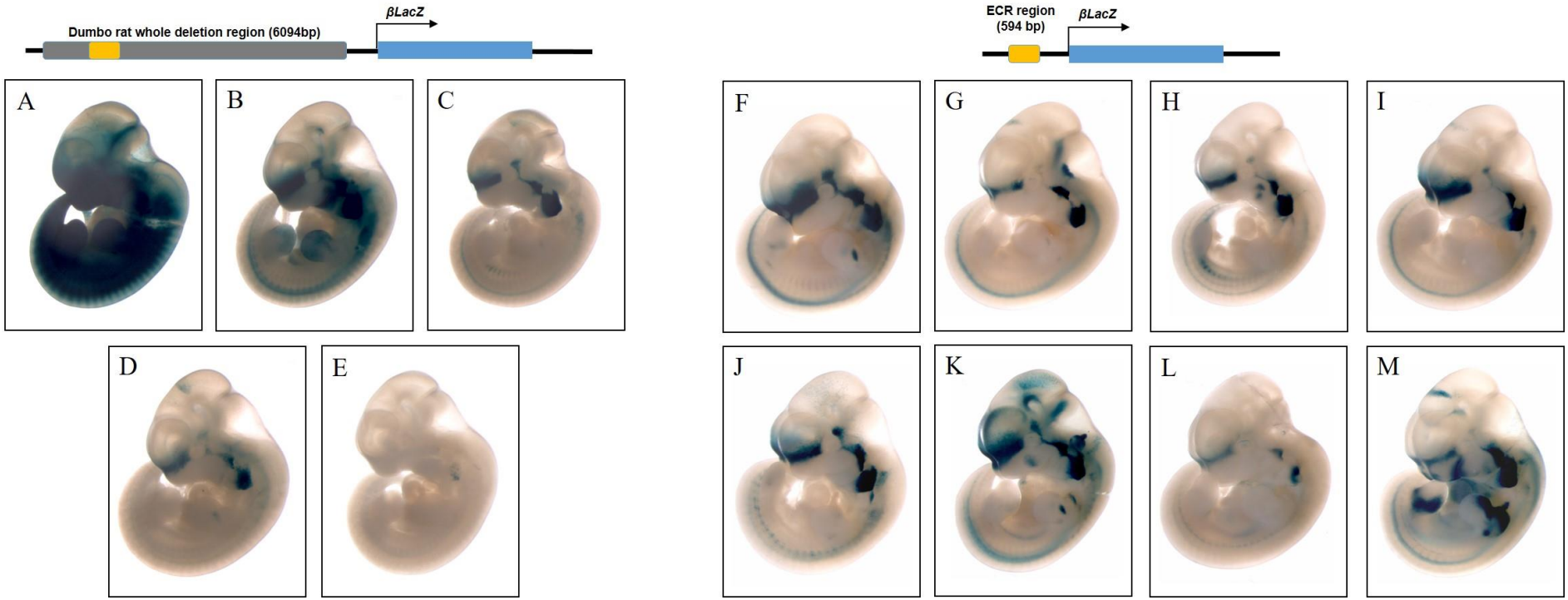

Figure 31. Transient transgenic analysis of the dumbo rat deletion region identified the specific facial regions which ECR regulates during development (photos took by Dr. Jennifer A. Akiyama)**.** A-E: E11.5 dmWhole (6,094 bp) transient transgenic embryos showed staining in BA2 at E11.5. F-M: E11.5 transient transgenic embryos with the dmECR (594 bp) fragment showed strongly staining bands in the frontonasal region, craniofacial mesenchyme of dorsal BA1 and the entire BA2 regions.

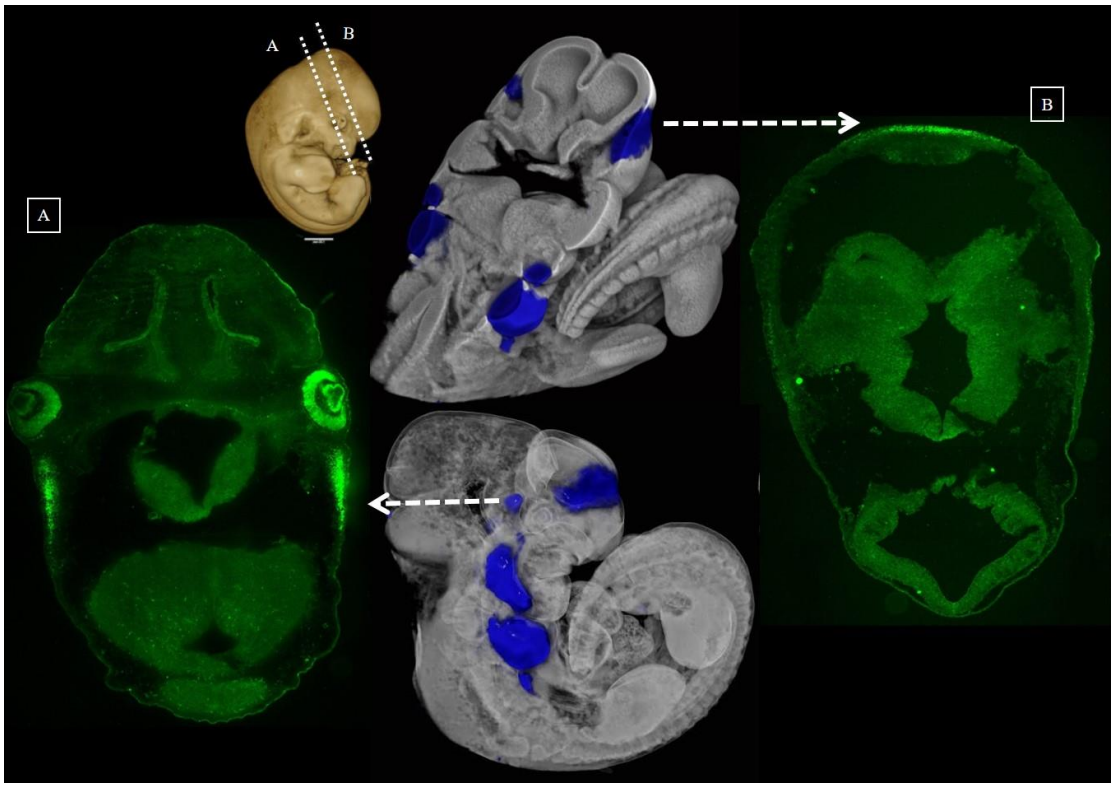

Figure 32. OPT virtual dissection of the E11.5 dmECR LacZ stained embryo (embryo Fig. 31 H) demonstrated the restricted signal within the mesenchyme. The white dotted lines on the yellow E12.5 embryo represent the immunofluorescence sectioning planes for the two cross sections, A and B. The highlighted green signal represents endogenous Hmx1 protein expression which correlates with the LacZ signal (white dotted arrows).

4.5 Generation of stable Hmx1-enhancer transgenic lines

The transient transgenic study only investigated the dmECR LacZ expression at a single time point (E11.5) during embryonic development, and by itself could not show the structures to which these enhancer-expressing regions give rise to. In collaboration with the UW transgenic core, I next generated the permanent dmECR LacZ lines by using the same Hmx1 dmECR-Hsp68-LacZ construct from the transient assay. 123 transgenic embryos were implanted and 42 pups were born. 3 male (CH-5791, CH-5820 and CH-5821) and 1 female (CH-5831) mice were further genotyped to be LacZ positive (see **Table 2.1.9b** for primers), with a transgenic rate of 3.25%. The E11.5 embryos harvested and stained from these four independent founder lines showed a pattern consistent with the transient transgenetic experiments. The activity of the dmECR-LacZ transgene was then analyzed at developmental stages ranging from E9.5 to E16.5 using the CH-5791 line. This assessment showed minimal activity at E9.5 (data not shown). By E10.5, activation of dmECR was readily observed in the frontonasal region and throughout BA2 (see **Fig. 33 A-A'**). At E11.5, the dmECR continued to drive expression in the frontonasal region and throughout BA2, in addition to the dorsal region of BA1 (see **Fig. 33 B-B'**). From E12.5 to E13.5, the dmECR drove transgene expression in the frontonasal and lateral facial regions, including tissues surrounding the eye and in a band of tissue at the back of the head that included the posterior region of the developing pinna (see **Fig. 33 C-D'**). Between E14.5 to E16.5, the dmECR-LacZ transgene continued to drive expression in two broader domains that became more regionally-restricted and

separate from one another (see **Fig. 33 E, F, G**); specifically, the rostral face, including the frontonasal region and tissue surrounding the eye, and a separate expression domain in the caudal region of the head, extending from the posterior limit of the stain in the pinna to the back of the head (see **Fig. 33 E-G'**). This particular transgenic line also showed expression in the developing neural tube, midbrain, hindbrain, zeugopod, both the fore- and hind-limb digits, and ribs. Since this expression was not observed in all four lines, it may or may not be related to dmECR function.

This *LacZ* reporter system demonstrated that the dmECR sequence functions as a distal enhancer which regulates endogenous Hmx1 expression in lateral facial areas (dorsal aspect of BA1, BA2, frontonasal and region caudal to the eye). Fortunately, the β-galactosidase marker was still present at the late embryonic developmental stage (E16.5), which helped to confirm the dmECR enhancer-expressing cells give rise to lateral facial structures like the ear pinna. Yet, there is still a chance that the LacZ-expressing cells do not fully represent the original Hmx1 precursors, since Hmx1 may be transiently expressed in some cells and LacZ protein could persist in some cells for a longer duration than Hmx1 protein, but is not a permanent lineage marker.

In order to accurately track cell migration, I attempted to use the classic Cre-recombinase technology fate-mapping system (Cre/LoxP system) [80]. Cre-recombinase is a recombinase enzyme derived from the P1 Bacteriophage that will excise genomic sequences flanked by LoxP recognition sites. Reporter mice have

been designed in which Cre-excision of a transcriptional stop flanked by LoxP sites will activate an enzymatic or fluorescent reporter. These reporters are often constructed in the mouse Rosa(26) gene locus, which has the potential to express in any cell type. Since the transient transgenic experiment confirmed the dmECR is a tissue specific enhancer in the craniofacial region, attempts were made to generate dmECR Cre line mice. These mice were created at the UW PRTS and Cyagen Biosciences by using pCDNA3.2-Hmx1-ECR-Hsp68-nlsCre-IRES-mCherry (generated by myself) and pBS2SKP-Palmiter-Hmx1-HHR-Cre (assembled by Dr. Jessica Rosin) constructs respectively. Even though we successfully generated the dmECR Cre reporter lines, after crossing the Cre line male mice with the RosaLacZ reporter female mice, we obtained fully stained embryos for both of the constructs in different transgenic mouse lines.

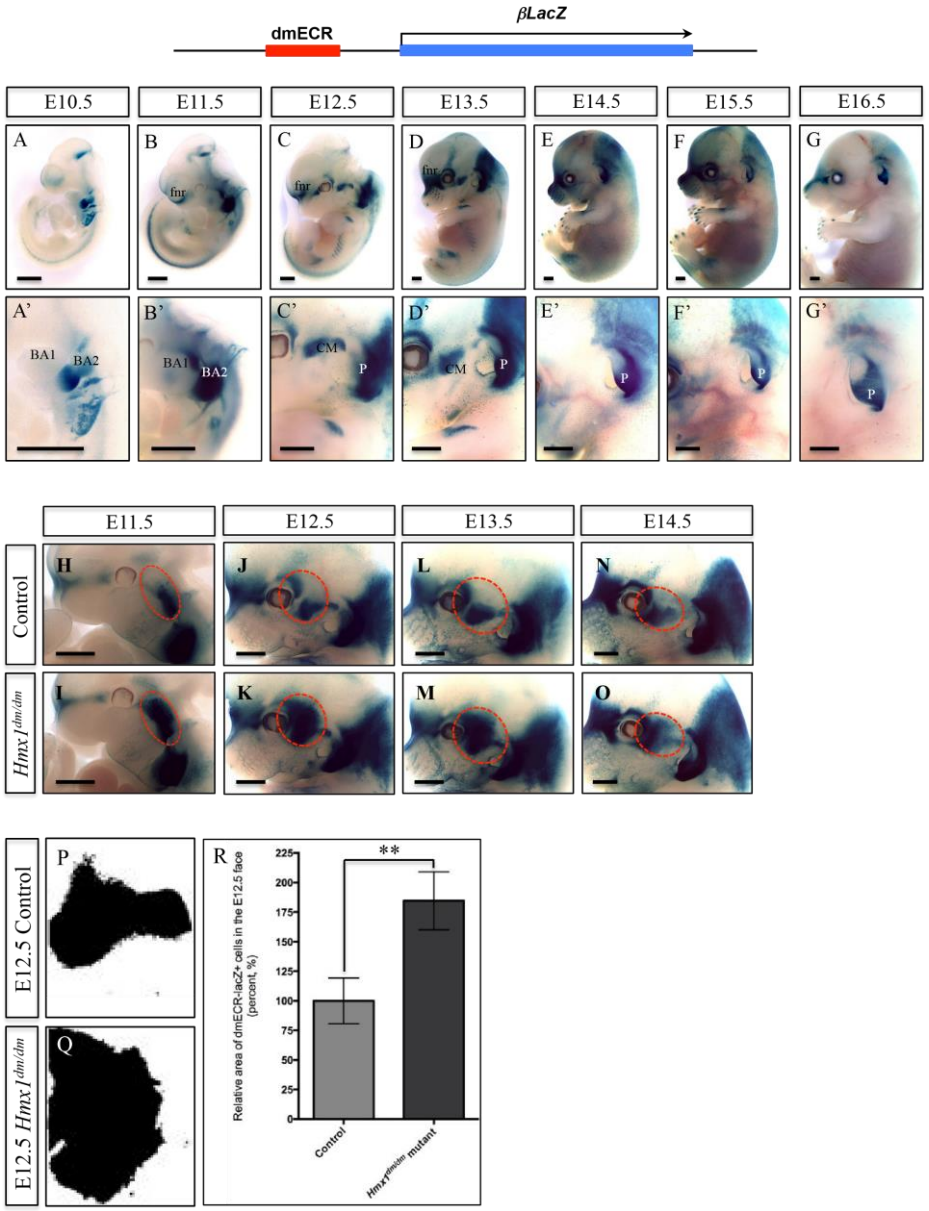

Figure 33. The developmental activity of the dmECR enhancer is expanded in *Hmx1*$^{dm/dm}$ mutants (courtesy of Dr. Jessica Rosin**).** Figures A-G': Embryos at different developmental stages. Staining of E10.5 (A, A'), E11.5 (B, B'), E12.5 (C, C'), E13.5 (D, D'), E14.5 (E, E'), E15.5 (F, F') and E16.5 (G, G') embryos from the 594bp dmECR transgenic line shown in Fig. Q. Figures H-O: dmECR staining in control (H, J, L, N) and *Hmx1*$^{dm/dm}$ mutant (I, K, M, O) embryos at E11.5 (H, I; control n = 4, *Hmx1*$^{dm/dm}$ mutant n = 1), E12.5 (J, K; control n = 4, *Hmx1*$^{dm/dm}$ mutant n = 4), E13.5 (L, M; control n = 3, *Hmx1*$^{dm/dm}$ mutant n = 2) and E14.5 (N, O; control n = 9, *Hmx1*$^{dm/dm}$ mutant n = 4) shows an expansion of the dmECR staining pattern in *Hmx1*$^{dm/dm}$ mutants (red dashed-circle). Figures P & Q: Representative binary particle area diagrams from ImageJ displaying dmECR-LacZ+ cells present in the faces of controls (P) and *Hmx1*$^{dm/dm}$ mutant (Q) embryos at E12.5. Figure R: Quantification of the area displayed in P and Q for E12.5 controls (n = 4) and *Hmx1*$^{dm/dm}$ mutant (n = 4) embryos (plotted values are the mean +/- S.E.M., p = 0.0016). Abbreviations: fnr, frontal nasal region; CM, craniofacial mesenchyme; P, pinna. Scale bars = 1 mm.

4.6 Discussion

A conventional transgenic strategy has yielded a great deal of information regarding the tissue-specific enhancer function of the *dumbo* ECR. On the other hand, two advanced transgenic strategies did not succeed.

The PiggyBac transposase-mediated transgenesis failed after two attempts. A review of the literature did not reveal a specific reason for the failure in these experiments, but this is a new technique with relatively few published reports [74, 78]. The previous studies reported the survival rate between 70 to 80% of embryos after microinjection [81, 82]. In traditional pronuclear injection, DNA concentration was reported to influence the transgenic efficiency. 1 ng/µl DNA seemed to have the most efficient transgenic rate of 13.2% with a 30% survival rate after embryo implantation [82]. Reports also showed variabilities in survival rate due to differences in DNA and *PBase* mRNA concentrations. Sumiyama et al showed DNA at 20 ng/µl and mRNA at 30 ng/µl concentrations could improve the overall outcome by achieving approximately 40% survival rate and around 66% integration frequency [83]. Bjork et al found 1.4 -2.0 ng/µl PB transposon DNA and 17-23 ng/µl *PBase* mRNA resulted in 46% transgenic efficiency [78]. Strictly following the Bjork's protocol, the low 27.67% survival rate after implantation and a 0.71% transgenic rate in our study suggested potential defects with the constructs or technique drawbacks in the transgenic core. Sequencing primers were designed to test the Hsp70 promoter, Turbo GFP and transposase site in the construct (see **Table 2.1.9c**). The DNA from the one successful integrated transgenic embryo was used as a template for analysis. The PCR

products of the Hsp70 promoter and Turbo-GFP region gave the correct sizes and sequencing result. A 2 bp mismatch in the Hsp70 promoter was noted based on the expected vector sequence (see **Fig. 34**). Their location near the start of the promoter made it hard to define if they could impact the promoter's function. However, the poor sequencing quality of the transposase region, the mismatch with the template, and change in PCR product size (see **Fig. 35**) all pointed to the transposase region defect. This could explain the low integration rate of the transgenics.

Unlike the PiggyBac system which integrates the transgene into the host genome at a specific "TTAA" site. The conventional transgenic method is randomly inserted the transgene into the genome. The genomic environment at the integration site has a substantial influence on the expression of the transgenes. It is quite common that some of the transgenic lines do not express the transgene at all or at a very low level. Transgenes could also influence by a strong promoter/enhancer/repressor near the integration site and have different expression patterns from that expected. If a portion of the cells expresses the transgene, there will be a mosaic transgene expression pattern. The progressive extinction could be the worst case as the expression decreases or even completely stops after multiple generations of breeding [84]. Because transgene expression can be influenced by chromosomal position effects, we tested all permanent dmECR LacZ lines after establishing them. The LacZ expression was monitored for more than five generations in four different permanent lines and consistent expression pattern was found. This demonstrated that the dmECR sequence

functions as a distal enhancer which regulates endogenous Hmx1 expression in lateral facial areas (dorsal aspect of BA1, BA2, frontonasal and region caudal to the eye).

I also attempted to move one step forward from the LacZ reporter system to the Cre/LoxP recombination system to permanently label Hmx1-expressing cells. This would facilitate the sorting of *Hmx1* expressing cells, and allow us to investigate Hmx1 tissue-specific transcriptional targets. However, some non-specific expression of the X-gal staining over the entire embryo for both dmECR-Cre lines was observed. This could have occurred because the dmECR's enhancer function was turned on at an earlier developmental stage than E9.5 when tissue-specific Hmx1 expression in the trigeminal ganglion was first seen [24].

If early embryonic expression is a characteristic of the dmECR, an alternative approach, an inducible CreER(T2)/LoxP system could be considered for future experiments [85]. In the CreER(T2)/LoxP system, the transgenic mice contain a transgene that expresses a modified form of Cre recombinase that is non-functional until it interacts with an inducing agent (tamoxifen). Once this system has been successfully established, a clear gene expression profile can be accurately obtained at critical developmental time points. Identification of downstream targets of Hmx1 can then be achieved by performing RNA-seq analysis on Hmx1 cells specific to the region of interest.

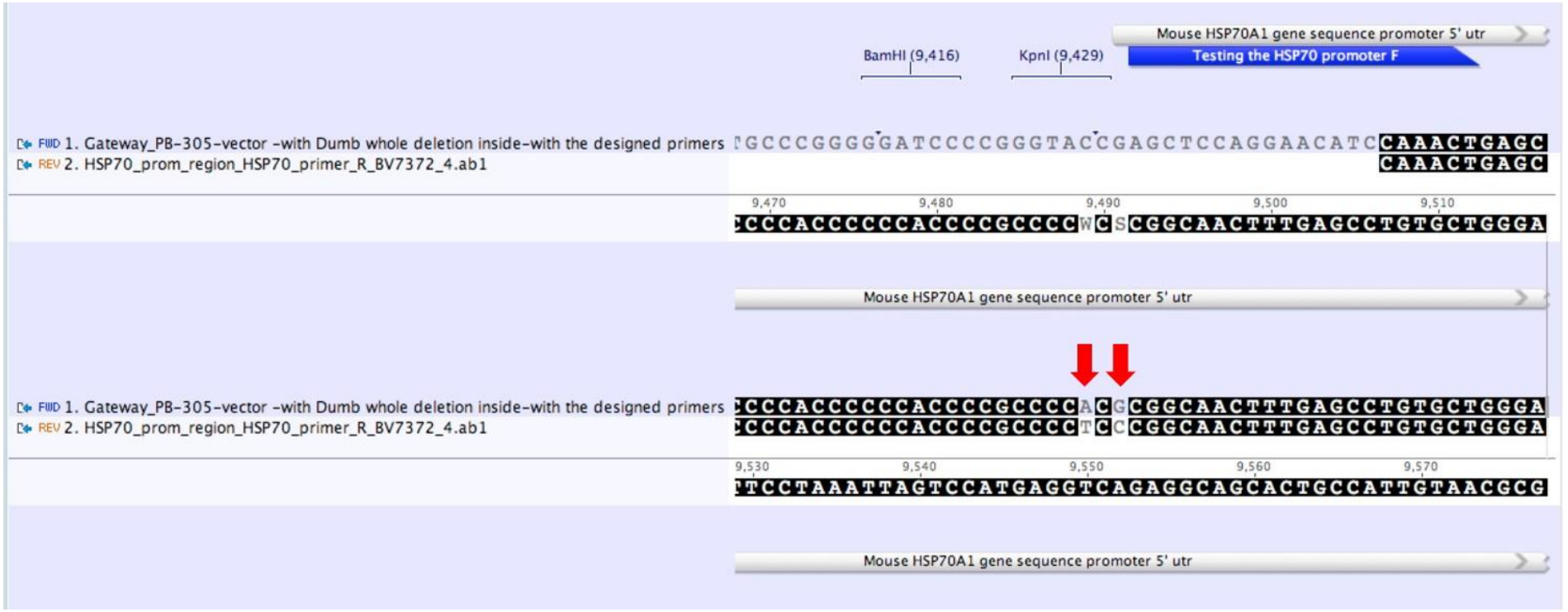

Figure 34. The 2 bp mismatch of the Hsp70 promoter sequence compared with the expected promoter sequence. The red arrows point to the 2 bp mismatch.

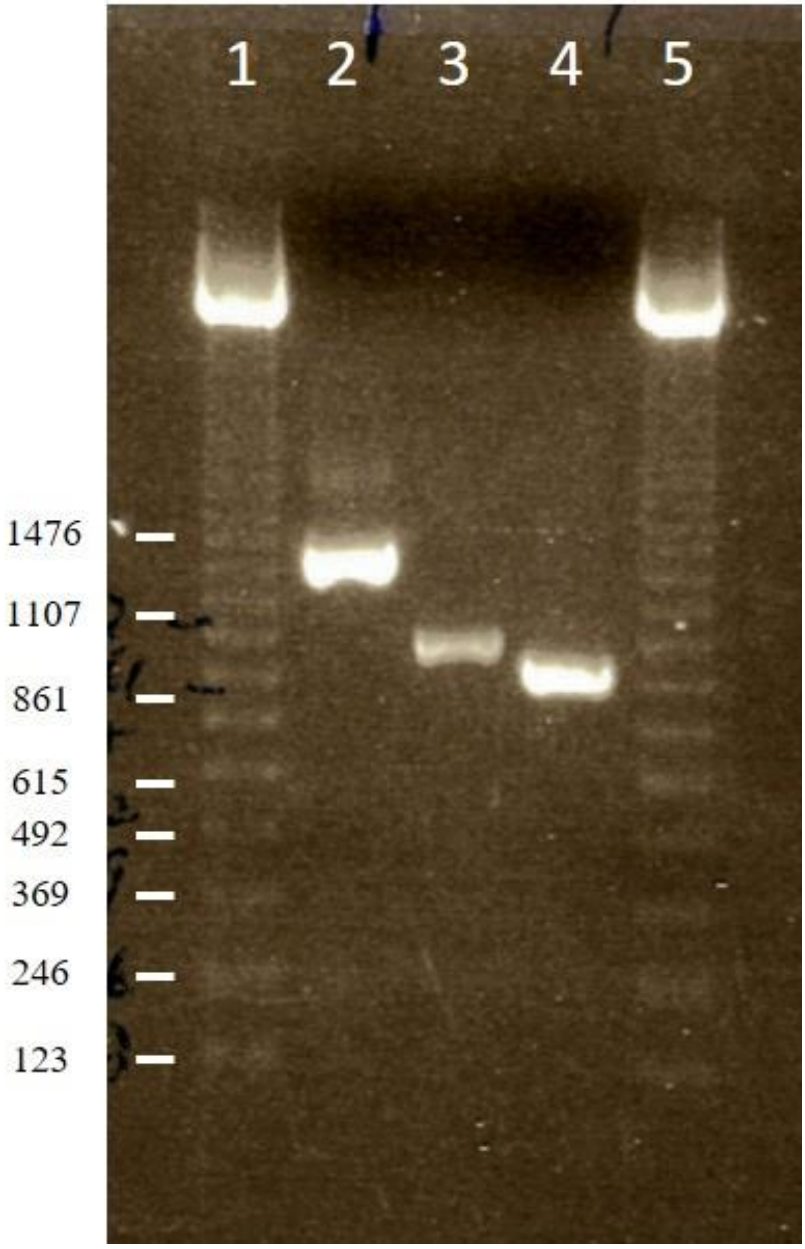

Figure 35. The PCR products of the transposon in the only successfully integrated dumbo rat whole deletion region embryo. Life technology 123 bp DNA Ladder (lanes 1, 5); Transposase site testing failed to show the right product (lane 2, optimal product size is 809 bp); Hsp70 promoter testing showed the right product with a size of 888 bp (lane 3); Turbo GFP region testing also showed the optimal product with a size of 834 bp (lane 4).

CHAPTER FIVE: SUMMARY AND FUTURE DIRECTIONS

In this study, I characterized craniofacial development in the *Hmx1* loss of function *dumbo* mouse model and identified the Hmx1 tissue-specific enhancer responsible for the development of craniofacial structures, particularly in the lateral facial regions. In this discussion section, I have also incorporated some findings by my colleagues which help to interpret the findings I have presented. By enhancing our understanding of the Hmx1 regulatory network, these studies could have a significant translational impact given the paucity of research on lateral facial birth defects.

Mechanisms of partial lethality, growth retardation, and craniofacial structure abnormalities in *dumbo* mice. The *dumbo* allele showed non-Mendelian transmission and approximately 57% perinatal lethality in a C57Bl/6N genetic background, slightly higher than the 40% observed in the previous report on the *Rw* genetic background [26]. On the C57Bl/6N pure background, only male *dumbo* mice were significantly smaller than their sex and age-matched controls. Unreported lateral cranioskeletal anomalies such as hypoplastic paraoccipital processes and premature fusion of the squamosal and parietomastoid sutures were described for the first time. By using the morphometric analysis of skull phenotypes, we found large differences in magnitude between $Hmx1^{dm/dm}$ and control mice over the masseteric ridge and angular process of the mandible as well as over the snout and temporo-occipital regions of the skull. It has been shown in published literature that mechanical loading influences the cranial suture morphology [63]: the internasal sutures of rats with a reduced masticatory function could

thus demonstrate synostosis by obliterative osteogenesis [86]. Specifically, the neuromuscular circuit defect (confirmed by air puff tests) observed here in the *dumbo* mutant mice could reduce the muscle function around the squamosal and parietomastoid sutures, contributing to the premature fusion of the sutures. Mechanical strain from mastication is also known to affect the development of the mandible [65]. These subtle defects in the mandibles of *dumbo* mutant mice, especially the masseter ridges and angular processes, also suggest the existence of a nerve and/or muscle defect in the *dumbo* mutant mice. Reduced mechanical function of the neuromuscular circuit could also explain the reduced postnatal weight gain in the *dumbo* mutant mice, as the mice might have experienced difficulty in food consumption. At this point, we do not have a clear model for why the weight loss differentially affects male *dumbo* mice.

We considered the possibility that loss of Hmx1 might have a direct effect on early muscle specification. In order to test this, we examined the expression of Isl1, a marker for mesoderm-derived muscle precursor cells in BA1 and BA2 [87, 88]. Immunohistochemistry of Isl1 cryosections (16-20 μm) of the E10.5 mouse embryo was performed by Jessica Rosin. During development, these muscle precursor cells in BA1 and BA2 give rise to the ventral/distal branchiomeric (stylohyoid, mylohyoid, digastric) muscles, laryngeal muscles and to a lesser extent, contribute to the development of masticatory muscles (masseter, pterygoid, and temporalis). Using dmECR activity as a surrogate, it was demonstrated that the regions with Hmx1 expression did not include the endogenous mouse Isl1 cells (data not shown). This indicates that Hmx1-expressing cells do not directly contribute to developing muscles. However, there are complex interactions between neural crest cells (NCCs) and nearby cells from the

mesoderm, ectoderm, and endoderm during development. Vital signals like fibroblast growth factors (FGFs), bone morphogenetic proteins (BMPs) and sonic hedgehog (SHH) provided by endoderm and surface ectoderm positively regulate skeletogenesis of NCCs [89–91]. NCCs also play instructive roles in patterning cranial muscles [92, 93]. It is unclear at this stage whether the primary cause of the functional deficits in the Hmx1 *dumbo* mutant animals is the result of a primary sensory nerve deficit or reflective of a lateral facial muscle disturbance. In future experiments, an inducible CreER(T2)/LoxP system may help to facilitate fate-mapping experiments to understand the structural contribution of the Hmx1 cells, as well as selecting Hmx1 cells at critical developing time points for downstream targets analysis. Considering the complex interaction between the neural crest and the surrounding tissues during development, mice carrying a conditional knockout allele of Hmx1 [38] would be a valuable tool to analyze the cell types which are responsible for the *dumbo* phenotype.

Molecular mechanisms of dmECR function. Even though more experiments are still needed, we have gained insight into Hmx1's gene regulation pathway with help from other team members and collaborators. After we introduced the dmECR-LacZ reporter to the *dumbo* (*Hmx1*$^{dm/dm}$) line, we noticed a consistent expansion of the dmECR-driven β-galactosidase staining region in the mesenchyme between the eye and ear of E11.5 to E14.5 *Hmx1*$^{dm/dm}$ embryos when compared to littermate controls (see **Fig. 33 H-O**). Dr. Jessica Rosin quantified the dmECR staining region in E12.5 control and *Hmx1*$^{dm/dm}$ embryos (see **Fig. 33 P-Q**), displaying an expansion of dmECR-LacZ positive tissue to almost double its size (see **Fig. 33 R**), as well as the endogenous *Hmx1* mRNA expression (data not shown). This suggested that Hmx1

negatively regulates its own expression via dmECR.

Our collaborator Dr. Nicoletta Bobola supported us with the ChIP-seq-binding profiles for Hoxa2 and Meis2 surrounding the Hmx1 gene in chromatin isolated from E11.5 BA1 and BA2 tissue, as described previously [94]. Hoxa2 and Meis binding profiles in BA2 showed overlapping prominent peaks ~80kb downstream of the *Hmx1* gene (see **Fig. 36 A**), consistent with putative Hoxa2 and Meis sites within the most highly conserved part of dmECR (see **Fig. 36 C**). Enhanced Meis binding was also observed in BA2 tissue relative to the Hox-negative BA1 (see **Fig. 36 A**). ChIP-qPCR on Hoxa2-selected BA2 chromatin revealed nearly 10-fold enrichment of the Hmx1 dmECR enhancer region (see **Fig. 36 B**) over the established positive control [94], confirming Hoxa2 binds to the core dmECR sequence. Moreover, analysis of microarray data obtained from E11.5 *Hoxa2* mutant and control BA2 tissue [95] showed a 1.6 fold down-regulation of *Hmx1* expression ($p < 0.005$). This suppression of *Hmx1* expression in E11.5 *Hoxa2* mutant embryos was validated by qRT-PCR in five technical replicates (see **Fig. 36 D**) and *in situ* hybridization for *Hmx1* on E11 *Hoxa2* mutant embryos (see **Fig. 36 E**). Dr. Jessica Rosin also used the luciferase assay to demonstrate that the highest level of enhancer activation requires the presence of the complete Hox-Pbx-Meis complex (data not shown here). These three transcription factors are known cofactors of each other. The Hox-Pbx-Meis trimer can be found in the cell as a stable complex in the absence of DNA binding. The trimer helps Meis bind to a site that does not otherwise accommodate Meis binding [96]. DNA-binding complexes formed by Meis with Hox proteins dissociate much more slowly than DNA-binding complexes with Meis alone, suggesting that Hox proteins stabilize the interactions of Meis proteins with their

DNA targets [97]. Based on our findings, it is concluded that Hox, Pbx and Meis transcription factors were good upstream candidates for activation of the *Hmx1* dmECR enhancer. Deletion of the 32bp sequence encompassing the trimer binding site resulted in a severe reduction in the enhancer activity (data not shown), and repeated transient transgenesis by the Visel group using the 594bp dmECR construct conducted in parallel with the newly generated dmECRdel32 construct demonstrated that the 32bp sequence is required for the enhancer to express in the dorsal aspect of BA1 and throughout BA2.

In summary, our findings support the hypothesis that Hmx1 plays a central role in lateral facial mesenchyme differentiation and that the Hmx1 dmECR has a tissue-specific enhancer function. The discovery of potential upstream regulators and a solution to tackle downstream effectors in future experiments will shine light on poorly understood lateral craniofacial developmental processes. In conjunction with future mutational analysis of relevant patient cohorts, knowledge of Hmx1's function could be applied in prenatal screening, treatment planning of mild auricular and lateral facial anomalies which are commonly seen in clinical practice.

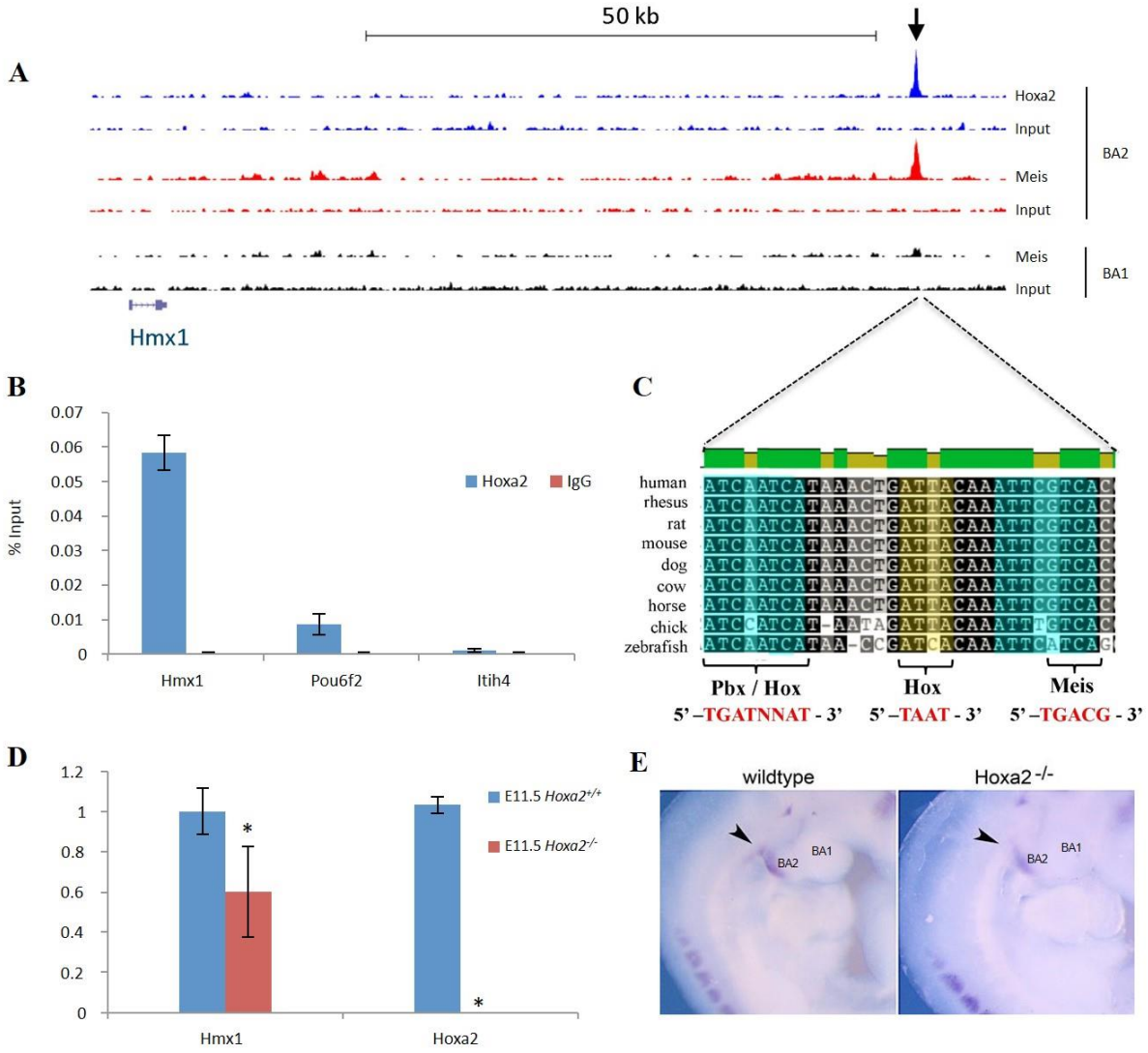

Figure 36. ChIP-seq demonstrates that Hoxa2 and Meis2 bind to the dmECR *in vivo* (courtesy of Dr. Nicoletta Bobola). (A) ChIP-seq-binding profile of Hoxa2 and Meis2 at *Hmx1* gene in chromatin isolated from E11.5 first (BA1) and second branchial arch (BA2). Input tracks represent genomic DNA. Black arrow highlights the binding region tested by qPCR in (B). (B) Analysis of Hoxa2 binding to *Hmx1* enhancer by ChIP-qPCR. Enrichment is calculated as percent input. IgG is a negative control antibody. *Pou6f2* is a positive control and *Itih4* is a negative control. (C) Consensus binding sites within the dmECR are indicated on the 32bp multispecies alignment, which includes multiple mammalian species as well as chick and zebrafish, and highlights potential Hox-Pbx (left, blue), Hox (yellow) and Meis (right, blue) binding sites [94]. (D) qRT-PCR validates suppression of *Hmx1* expression in E11.5 *Hoxa2* mutant embryos (five technical replicates; *Hmx1* $p = 0.0155$, *Hoxa2* $p = 0.0001$). (E, F) Whole-mount *in situ* hybridization for *Hmx1* on E11 embryos shows reduced caudal BA2 expression in *Hoxa2* mutants (F, arrow) when compared to controls (E, arrow).

REFERENCES

1. Luquetti D V, Heike CL, Hing A V, Cunningham ML, Cox TC: **Microtia: Epidemiology and genetics.** *Am J Med Genet A* 2011(November):124–139.

2. Luquetti DV, Leoncini E, Mastroiacovo P: **Microtia-anotia: A global review of prevalence rates**. *Birth Defects Res Part A - Clin Mol Teratol* 2011, **91**:813–822.

3. Suutarla S, Rautio J, Ritvanen A, Ala-Mello S, Jero J, Klockars T: **Microtia in Finland: Comparison of characteristics in different populations**. *Int J Pediatr Otorhinolaryngol* 2007, **71**:1211–1217.

4. Mastroiacovo P, Corchia C, Botto LD, Lanni R, Zampino G, Fusco D: **Epidemiology and genetics of microtia-anotia : a registry based study on over one million births**. 1995:453–457.

5. Harris J, Kallen B, Robert E: **The epidemiology of anotia and microtia**. 1996:809–813.

6. Castilla EE, Lopez-Camelo JS, Campaña H: **Altitude as a risk factor for congenital anomalies**. *Am J Med Genet* 1999, **86**:9–14.

7. Gonzalez-Andrade, Frabricio; Lopez-Pulles, Ramiro; Espin, Victir H.;Paz-y-Mino C: **High altitude and microtia in Ecuadorian patients High altitude and microtia in Ecuadorian patients**. *J Neonatal Perinatal Med* 2010, **3**:109–116.

8. Alasti F, Sadeghi A, Sanati MH, Farhadi M, Stollar E, Somers T, Van Camp G: **A Mutation in HOXA2 Is Responsible for Autosomal-Recessive Microtia in an Iranian Family**. *Am J Hum Genet* 2008, **82**:982–991.

9. Braunstein EM, Crenshaw EB, Morrow BE, Adams JC: **Cooperative function of Tbx1 and Brn4 in the periotic mesenchyme is necessary for cochlea formation**. *JARO - J Assoc Res Otolaryngol* 2008, **9**:33–43.

10. Kawakami K, Sato S, Ozaki H, Ikeda K: **Six family genesÐstructure and function as transcription factors and their roles in development**. 2000:616–626.

11. Ingraham CR, Kinoshita A, Kondo S, Yang B, Sajan S, Trout J, Malik MI, Dunnwald M, Goudy SL, Lovett M, Murray C, Schutte BC: **NIH Public Access**. 2007, **38**:1335–1340.

12. Schorderet DF, Nichini O, Boisset G, Polok B, Tiab L, Mayeur H, Raji B, de la Houssaye G, Abitbol MM, Munier FL: **Mutation in the Human Homeobox Gene NKX5-3 Causes an Oculo-Auricular Syndrome**. *Am J Hum Genet* 2008, **82**:1178–1184.

13. Franceschetti A, Valerio M: **Malformations associées des yeux et des oreilles.** *Stereotact Funct Neurosurg* 1944, **6**:255–257.

14. Gillespie RL, Urquhart J, Lovell SC, Biswas S, Parry NR a., Schorderet DF, Lloyd IC, Clayton-Smith J, Black GC: **Abrogation of HMX1 Function Causes Rare Oculoauricular Syndrome Associated With Congenital Cataract, Anterior Segment Dysgenesis, and Retinal Dystrophy**. *Invest Ophthalmol Vis Sci* 2015, **56**:883–891.

15. Cox TC, Camci ED, Vora S, Luquetti D V., Turner EE: **The genetics of auricular development and malformation: New findings in model systems driving future directions for microtia research**. *Eur J Med Genet* 2014(June):1–8.

16. Rennie CA, Chowdhury S, Khan J, Rajan F, Jordan K, Lamb RJ, Vivian AJ: **The prevalence and associated features of posterior embryotoxon in the general ophthalmic clinic.** *Eye (Lond)* 2005, **19**:396–399.

17. Marcelli F, Boisset G, Schorderet DF: **A Dimerized HMX1 Inhibits EPHA6/epha4b in Mouse and Zebrafish Retinas**. *PLoS One* 2014, **9**:e100096.

18. Stadler HS, Murray JC, Leysens NJ, Goodfellow PJ, Solursh M: **Phylogenetic conservation and physical mapping of members of the H6 homeobox gene family**. *Mamm Genome* 1995, **6**:383–388.

19. Holland PWH, Booth HAF, Bruford EA: **Classification and nomenclature of all human homeobox genes.** *BMC Biol* 2007, **5**:47.

20. Hanes SD, Brent R: **A genetic model for interaction of the homeodomain**

recognition helix with DNA. *Science* 1991, **251**:426–430.

21. Amendt B a., Sutherland LB, Russo AF: **Transcriptional antagonism between Hmx1 and Nkx2.5 for a shared DNA- binding site**. *J Biol Chem* 1999, **274**:11635–11642.

22. Stadler HS, Solursh M: **Characterization of the homeobox-containing gene GH6 identifies novel regions of homeobox gene expression in the developing chick embryo.** *Developmental biology* 1994:251–262.

23. Wang W, Lo P, Frasch M, Lufkin T: **Hmx: An evolutionary conserved homeobox gene family expressed in the developing nervous system in mice and Drosophila**. *Mech Dev* 2000, **99**:123–137.

24. Yoshiura K, Leysens NJ, Reiter RS, Murray JC: **Cloning, characterization, and mapping of the mouse homeobox gene Hmx1.** *Genomics* 1998, **50**:61–68.

25. Quina L a., Tempest L, Hsu Y-W a. WA, Cox TC, Turner EE: **Hmx1 is required for the normal development of somatosensory neurons in the geniculate ganglion**. *Dev Biol* 2012, **365**:152–163.

26. Munroe RJ, Prabhu V, Acland GM, Johnson KR, Harris BS, O'Brien TP, Welsh IC, Noden DM, Schimenti JC: **Mouse H6 Homeobox 1 (Hmx1) mutations cause cranial abnormalities and reduced body mass.** *BMC Dev Biol* 2009, **9**:27.

27. Vaclavik V, Schorderet DF, Borruat F-X, Munier FL: *Retinal Dystrophy in the Oculo-Auricular Syndrome due to HMX1 Mutation. Volume 32*; 2011:114–117.

28. Quina LA, Kuramoto T, Luquetti D V., Cox TC, Serikawa T, Turner EE: **Deletion of a conserved regulatory element required for Hmx1 expression in craniofacial mesenchyme in the dumbo rat: a newly identified cause of congenital ear malformation**. *Dis Model Mech* 2012, **5**:812–822.

29. Kuramoto T, Yokoe M, Yagasaki K, Kawaguchi T, Kumafuji K, Serikawa T: **Genetic analyses of fancy rat-derived mutations.** *Exp Anim* 2010, **59**:147–55.

30. Turner EE, Cox TC: **Genetic evidence for conserved non-coding element function**

across species-the ears have it. *Front Physiol* 2014, **5 JAN**(January):1–6.

31. Koch CT, Bruggmann R, Tetens J, Drögemüller C: **A Non-Coding Genomic Duplication at the HMX1 Locus Is Associated with Crop Ears in Highland Cattle**. *PLoS One* 2013, **8**:1–7.

32. Gendron-Maguire M, Mallo M, Zhang M, Gridley T: **Hoxa-2 mutant mice exhibit homeotic transformation of skeletal elements derived from cranial neural crest**. *Cell* 1993, **75**:1317–1331.

33. Minoux M, Kratochwil CF, Ducret S, Amin S, Kitazawa T, Kurihara H, Bobola N, Vilain N, Rijli FM: **Mouse Hoxa2 mutations provide a model for microtia and auricle duplication.** *Development* 2013, **140**:4386–97.

34. Dixon J, Jones NC, Sandell LL, Jayasinghe SM, Crane J, Rey J, Dixon MJ, Trainor PA: **Tcof1/Treacle is required for neural crest cell formation and proliferation deficiencies that cause craniofacial abnormalities.** *Proc Natl Acad Sci U S A* 2006, **103**:13403–13408.

35. Richter CA, Amin S, Linden J, Dixon J, Dixon MJ, Tucker AS: **Defects in middle ear cavitation cause conductive hearing loss in the Tcof1 mutant mouse**. 2010, **19**:1551–1560.

36. Milunsky JM, Maher TA, Zhao G, Roberts AE, Stalker HJ, Zori RT, Burch MN, Clemens M, Mulliken JB, Smith R, Lin AE: **TFAP2A Mutations Result in Branchio-Oculo-Facial Syndrome**. *Am J Hum Genet* 2008, **82**:1171–1177.

37. Kingsley DM, Bland AE, Grubber JM, Marker PC, Russell LB, Copeland NG, Jenkins NA: **The mouse short ear skeletal morphogenesis locus is associated with defects in a bone morphogenetic member of the TGF beta superfamily.** *Cell* 1992, **71**:399–410.

38. Furlan A, Lübke M, Adameyko I, Lallemend F, Ernfors P: **The transcription factor Hmx1 and growth factor receptor activities control sympathetic neurons diversification.** *EMBO J* 2013, **32**:1613–25.

39. Boulling A, Wicht L, Schorderet DF: **Identification of HMX1 target genes: a predictive promoter model approach.** *Mol Vis* 2013, **19**(August):1779–94.

40. Quina L a, Pak W, Lanier J, Banwait P, Gratwick K, Liu Y, Velasquez T, O'Leary DDM, Goulding M, Turner EE: **Brn3a-expressing retinal ganglion cells project specifically to thalamocortical and collicular visual pathways.** *J Neurosci* 2005, **25**:11595–11604.

41. Rolfe SM, Camci ED, Mercan E, Shapiro LG, Cox TC: **A new tool for quantifying and characterizing asymmetry in bilaterally paired structures**. In *Proceedings of the Annual International Conference of the IEEE Engineering in Medicine and Biology Society, EMBS*; 2013:2364–2367.

42. Limaye A: **Drishti: a volume exploration and presentation tool**. *SPIE 8506, Dev X-Ray Tomogr VIII, 85060X* 2012, **8506**:85060X.

43. Vickerton P, Jarvis J, Jeffery N: **Concentration-dependent specimen shrinkage in iodine-enhanced microCT**. *J Anat* 2013, **223**:185–193.

44. Theiler K: *The House Mouse: Atlas of Embryonic Development*. 1989.

45. Ittner LM, Götz J: **Pronuclear injection for the production of transgenic mice.** *Nat Protoc* 2007, **2**:1206–1215.

46. Koopman P, Gubbay J, Vivian N, Goodfellow P, Lovell-Badge R: **Male development of chromosomally female mice transgenic for Sry.** *Nature* 1991, **351**:117–121.

47. Arenkiel BR, Tvrdik P, Gaufo GO, Capecchi MR: **Hoxb1 functions in both motoneurons and in tissues of the periphery to establish and maintain the proper neuronal circuitry**. 2004:1539–1552.

48. Wilson L, Ching YH, Farias M, Hartford SA, Howell G, Shao H, Bucan M, Schimenti JC: **Random mutagenesis of proximal mouse chromosome 5 uncovers predominantly embryonic lethal mutations**. *Genome Res* 2005, **15**:1095–1105.

49. Stephenson DA, Lee KH, Nagle DL, Yen CH, Morrow A, Miller D, Chapman VM,

Bućan M: **Mouse rump-white mutation associated with an inversion of Chromosome 5**. *Mamm Genome* 1994, **5**:342–348.

50. Wilson L, Ching Y-H, Farias M, Hartford SA, Howell G, Shao H, Bucan M, Schimenti JC: **Random mutagenesis of proximal mouse chromosome 5 uncovers predominantly embryonic lethal mutations.** *Genome Res* 2005, **15**:1095–105.

51. Sharpe J, Ahlgren U, Perry P, Hill B, Ross A, Hecksher-Sørensen J, Baldock R, Davidson D: **Optical projection tomography as a tool for 3D microscopy and gene expression studies.** *Science* 2002, **296**:541–5.

52. Sharpe J: **Optical projection tomography.** *Annu Rev Biomed Eng* 2004, **6**:209–28.

53. Kagurasho M, Yamada S, Uwabe C, Kose K, Takakuwa T: **Movement of the external ear in human embryo**. *Head Face Med* 2012, **8**:2.

54. Knittel T, Kessel M, Kim MH, Gruss P: **A conserved enhancer of the human and murine Hoxa-7 gene specifies the anterior boundary of expression during embryonal development.** *Development* 1995, **121**:1077–1088.

55. Sanger TJ, Norgard E a., Pletscher LS, Bevilacqua M, Brooks VR, Sandell LJ, Cheverud JM: **Developmental and genetic origins of murine long bone length variation**. *J Exp Zool Part B Mol Dev Evol* 2011, **316 B**:146–161.

56. Vora SR, Camci ED, Cox TC: **Postnatal Ontogeny of the Cranial Base and Craniofacial Skeleton in Male C57BL/6J Mice: A Reference Standard for Quantitative Analysis**. *Front Physiol* 2016, **6**(JANUARY).

57. Rolfe SM, Shapiro LG, Cox TC, Maga AM, Cox LL: **A landmark-free framework for the detection and description of shape differences in embryos.** *Conf Proc . Annu Int Conf IEEE Eng Med Biol Soc IEEE Eng Med Biol Soc Annu Conf* 2011, **2011**:5153–6.

58. Leamy LJ, Klingenberg CP, Sherratt E, Wolf JB, Cheverud JM: **A search for quantitative trait loci exhibiting imprinting effects on mouse mandible size and shape.** *Heredity (Edinb)* 2008, **101**:518–526.

59. De Souza Faloni AP, Schoenmaker T, Azari A, Katchburian E, Cerri PS, De Vries TJ,

Everts V: **Jaw and long bone marrows have a different osteoclastogenic potential**. *Calcif Tissue Int* 2011, **88**:63–74.

60. JUDEX S, CARLSON KJ: **Is Bone's Response to Mechanical Signals Dominated by Gravitational Loading?** *Med Sci Sport Exerc* 2009, **41**:2037–2043.

61. Santagati F, Minoux M, Ren S-Y, Rijli FM: **Temporal requirement of Hoxa2 in cranial neural crest skeletal morphogenesis.** *Development* 2005, **132**(October):4927–4936.

62. Rieder MJ, Green GE, Park SS, Stamper BD, Gordon CT, Johnson JM, Cunniff CM, Smith JD, Emery SB, Lyonnet S, Amiel J, Holder M, Heggie A a, Bamshad MJ, Nickerson D a, Cox TC, Hing A V, Horst J a, Cunningham ML: **A human homeotic transformation resulting from mutations in PLCB4 and GNAI3 causes auriculocondylar syndrome.** *Am J Hum Genet* 2012, **90**:907–14.

63. Herring SW: **Mechanical Influences on Suture Development and Patency**. *Front Oral Biol* 2008, **7446**:1–15.

64. Rafferty KL, Liu ZJ, Ye W, Navarrete AL, Nguyen TT, Salamati A, Herring SW: **Botulinum toxin in masticatory muscles: Short- and long-term effects on muscle, bone, and craniofacial function in adult rabbits**. *Bone* 2012, **50**:651–662.

65. Rafferty KL, Sun Z, Egbert M, Bakko DW, Herring SW: **Changes in growth and morphology of the condyle following mandibular distraction in minipigs: overloading or underloading?** *Arch Oral Biol* 2007, **52**:967–76.

66. da Silva Guerreiro F, Diniz P, Carvalho PEG, Ferreira EC, Avancini SRP, Ferreira-Santos RI: **Effects of masticatory hypofunction on mandibular morphology, mineral density and basal bone area**. *Brazilian J Oral Sci* 2013, **12**:205–211.

67. Pennacchio L a, Ahituv N, Moses AM, Prabhakar S, Nobrega M a, Shoukry M, Minovitsky S, Dubchak I, Holt A, Lewis KD, Plajzer-Frick I, Akiyama J, De Val S, Afzal V, Black BL, Couronne O, Eisen MB, Visel A, Rubin EM: **In vivo enhancer analysis of human conserved non-coding sequences.** *Nature* 2006, **444**:499–502.

68. Dickel DE, Visel a, Pennacchio L a: **Functional anatomy of distant-acting mammalian enhancers.** *Philos Trans R Soc Lond B Biol Sci* 2013, **368**:20120359.

69. **Manipulating the Mouse Embryo: A Laboratory Manual, Fourth Edition** [http://cshlpress.com/default.tpl?cart=144216589941501674&action=full&--eqskudatarq=982]

70. Cary LC, Goebel M, Corsaro BG, Wang HG, Rosen E, Fraser MJ: **Transposon mutagenesis of baculoviruses: Analysis of Trichoplusia ni transposon IFP2 insertions within the FP-locus of nuclear polyhedrosis viruses**. *Virology* 1989, **172**:156–169.

71. Fraser MJ, Ciszczon T, Elick T, Bauser C: **Precise excision of TTAA-specific lepidopteran transposons piggyBac (IFP2) and tagalong (TFP3) from the baculovirus genome in cell lines from two species of Lepidoptera.** *Insect Mol Biol* 1996, **5**:141–51.

72. Ferguson HJ, Neven LG, Thibault ST, Mohammed A, Fraser M: **Genetic transformation of the codling moth, Cydia pomonella L., with piggyBac EGFP**. *Transgenic Res* 2011, **20**:201–214.

73. Lobo N, Li X, Fraser MJ: **Transposition of the piggyBac element in embryos of Drosophila melanogaster, Aedes aegypti and Trichoplusia ni**. *Mol Gen Genet* 1999, **261**:803–810.

74. Ding S, Wu X, Li G, Han M, Zhuang Y, Xu T: **Efficient transposition of the piggyBac (PB) transposon in mammalian cells and mice**. *Cell* 2005, **122**:473–483.

75. Owens JB, Urschitz J, Stoytchev I, Dang NC, Stoytcheva Z, Belcaid M, Maragathavally KJ, Coates CJ, Segal DJ, Moisyadi S: **Chimeric piggyBac transposases for genomic targeting in human cells**. *Nucleic Acids Res* 2012, **40**:6978–6991.

76. Keng VW, Yae K, Hayakawa T, Mizuno S, Uno Y, Yusa K, Kokubu C, Kinoshita T, Akagi K, Jenkins N a, Copeland NG, Horie K, Takeda J: **Region-specific saturation germline mutagenesis in mice using the Sleeping Beauty transposon system.** *Nat*

Methods 2005, **2**:763–769.

77. Bowen CJ, Zhou J, Sung DC, Butcher JT: **Cadherin-11 coordinates cellular migration and extracellular matrix remodeling during aortic valve maturation**. *Dev Biol* 2015, **407**:145–157.

78. Bjork BC, Fujiwara Y, Davis SW, Qiu H, Saunders TL, Sandy P, Orkin S, Camper S a., Beier DR: **A transient transgenic RNAi strategy for rapid characterization of gene function during embryonic development**. *PLoS One* 2010, **5**:1–11.

79. Kothary R, Clapoff S, Darling S, Perry MD, Moran L a, Rossant J: **Inducible expression of an hsp68-lacZ hybrid gene in transgenic mice.** *Development* 1989, **105**:707–14.

80. Nagy A: **Cre recombinase: The universal reagent for genome tailoring**. *Genesis* 2000, **26**:99–109.

81. DeMayo JL, Wang J, Liang D, Zhang R, DeMayo FJ: **Genetically Engineered Mice by Pronuclear DNA Microinjection**. In *Current Protocols in Mouse Biology*. *Volume 121*. Hoboken, NJ, USA: John Wiley & Sons, Inc.; 2012:19–26.

82. Crispo M, Schlapp G, C??rdenas-Rodr??guez M, Gonz??lez-Maciel D, Rumbo M: **Optimization of transgenesis conditions for the generation of CXCL2-luciferase reporter mice line**. *Electron J Biotechnol* 2013, **16**:10–17.

83. Sumiyama K, Kawakami K, Yagita K: **A simple and highly efficient transgenesis method in mice with the Tol2 transposon system and cytoplasmic microinjection**. *Genomics* 2010, **95**:306–311.

84. Liu C: **Strategies for Designing Transgenic DNA Constructs**. *Volume 1027*; 2013:183–201.

85. Feil S, Valtcheva N, Feil R: **Inducible Cre mice.** *Methods Mol Biol* 2009, **530**:343–63.

86. Engström C, Kiliaridis S, Thilander B: **The relationship between masticatory function and craniofacial morphology. II A histological study in the growing rat fed**

a soft diet. *Eur J Orthod* 1986, **8**:271–279.

87. Nathan E, Monovich A, Tirosh-Finkel L, Harrelson Z, Rousso T, Rinon A, Harel I, Evans SM, Tzahor E: **The contribution of Islet1-expressing splanchnic mesoderm cells to distinct branchiomeric muscles reveals significant heterogeneity in head muscle development.** *Development* 2008, **135**:647–657.

88. Gopalakrishnan S, Comai G, Sambasivan R, Francou A, Kelly RG, Tajbakhsh S: **A Cranial Mesoderm Origin for Esophagus Striated Muscles**. *Dev Cell* 2015, **34**:694–704.

89. St-Jacques B, Hammerschmidt M, McMahon AP: **Indian hedgehog signaling regulates proliferation and differentiation of chondrocytes and is essential for bone formation.** *Genes Dev* 1999, **13**:2072–2086.

90. Merrill AE, Eames BF, Weston SJ, Heath T, Schneider R a: **Mesenchyme-dependent BMP signaling directs the timing of mandibular osteogenesis.** *Development* 2008, **135**:1223–1234.

91. Pan A, Chang L, Nguyen A, James AW: **A review of hedgehog signaling in cranial bone development**. *Front Physiol* 2013, **4 APR**(April):1–14.

92. Schilling TF, Walker C, Kimmel CB: **The chinless mutation and neural crest cell interactions in zebrafish jaw development.** *Development* 1996, **122**:1417–1426.

93. Han A, Zhao H, Li J, Pelikan R, Chai Y: **ALK5-mediated transforming growth factor β signaling in neural crest cells controls craniofacial muscle development via tissue-tissue interactions.** *Mol Cell Biol* 2014, **34**:3120–31.

94. Amin S, Donaldson IJ, Zannino D a., Hensman J, Rattray M, Losa M, Spitz F, Ladam F, Sagerström C, Bobola N: **Hoxa2 selectively enhances Meis binding to change a branchial arch ground state.** *Dev Cell* 2015, **32**:265–77.

95. Donaldson IJ, Amin S, Hensman JJ, Kutejova E, Rattray M, Lawrence N, Hayes A, Ward CM, Bobola N: **Genome-wide occupancy links Hoxa2 to Wnt-β-catenin signaling in mouse embryonic development.** *Nucleic Acids Res* 2012, **40**:3990–4001.

96. Shen WF, Rozenfeld S, Kwong a, Köm ves LG, Lawrence HJ, Largman C: **HOXA9 forms triple complexes with PBX2 and MEIS1 in myeloid cells.** *Mol Cell Biol* 1999, **19**:3051–3061.

97. Shen WF, Montgomery JC, Rozenfeld S, Moskow JJ, Lawrence HJ, Buchberg AM, Largman C: **AbdB-like Hox proteins stabilize DNA binding by the Meis1 homeodomain proteins.** *Mol Cell Biol* 1997, **17**:6448–6458.

ACKNOWLEDGEMENTS

Frist, I would like to thank my committee for their guidance with my training at the University of Washington. I would like to thank my mentor Dr. Timothy Cox for giving me this opportunity to come to the US and welcoming me to his lab. His invaluable support and advice during my training made me stronger in every possible way. I would also like to thank my co-supervisor Dr. Eric E Turner's for sharing his knowledge and wisdom with me about science, career and also life. I would like to thank Dr. Richard Presland's amazing support through the years, and I am especially honored to finish one full Marathon and a half Marathon together with him. I would like to thank Dr. Anne-Marie Bollen and former committee member Dr. Daniela Luquetti for agreeing to be on my committee and providing their valuable advice.

I would like to thank the past and present members of the Cox lab: Liza, Kai, Yongzhao, Sid, Jess, Sara, Emily, Cathy, Esra, Basma, Suhaib, Tina, Matt; past and present members of the Turner lab: Lely, Tony, Glenn, Si; Scott Houghtaling and Anna Lindsay from the Beier lab. I am grateful to receive their generous offer with training/resources/assistance/knowledge.

I would like to thank our collaborators: Dr. Axel Visel's group in Lawerence Berkeley lab supported us with all transient transgenic studies. Dr. Nicoletta Bobola's in vivo ChIP-seq data was curial to our research paper got accepted by Development journal. Dr. Kuramoto's group from Kyoto University did the characterization work of the dumbo rat downstream deletion region. UW transgenic core Bob Hunter and La'Akea helped out with the transgenic line injection. Even though our first collaboration with Dr. David R. Beier didn't work out, I am really thankful for his generosity and kind support. I am grateful to have the strong support from the Seattle Children's Research Institution Office of Animal Care (Staff members: Maia Chan, Stephanie Slater, Devin Margolies).

Also, many thanks go to the wonderful people that supported me, encouraged me and inspired me through the years:

From our research institution: Dr. Michael Cunningham; Dr. Murat Maga; our center business manager Wendy Kramer; the past and current program coordinator Mackenzie Krouse, Aimy Pham, Ellen Coyle; colleagues from other labs Sarah Park, Seungshin Ha, Jabier Llamas, Chris Brewer, Chris Clarke, Jennifer Gustafson, Xiurong Dong,.

From our dental school Dr. Joel Berg, Dr. Timothy DeRouen, Dr. Norma Wells, Dr. Richard Darveau, Dr. Susanne Kölare Jeffrey, Dr. Whasun Oh Chung, Dr. Lisa Heaton, Dr. Donald Chi, Dr. Tracy Popwics, Dr. Charles Spiekerman, Dr. Linda LeResche, Dr. Timothy Rose, Dr. Beatrice Gandara, Dr. Rolf Christensen, Dr. Steve Albright, and Dr. Johan Aps; our wonderful staff member Jennifer Kohn, Kathy Hobson, Rosale Meriales, Mary Beth Cunningham, Kseniya Savva. I would want to express my sincere thanks to Dr. Sue Herring and Dr. Douglas Ramsay for their continuous encouragement and guidance with my career development. I would also like to thank Dr. Greg Huang and other faculties from the Orthodontics department for having me at the clinical journal club sessions. I am especially grateful to learn from Dr. Vincent Kokich, and will always treasure the two AJODO journals he personally handed over to me.

The enormous support from the Northwest Chinese Dentist Association (NWCDA): Dr. Ying Guo, Dr. Shengyi Teng, Dr. Erjia Mao, Dr. Allen Chen, Dr. Wei Tian, Dr. Yu Mao, Dr. Zijun Liu, Dr. Hai Zhang, Dr. Janice Chen, Dr. Cindy Du.

I am heavily blessed to have all the prayers and love from my church UPC and ICF Fellowship and many dear friends who made the past years the most enjoyable and memorable time in my academic life: Oral Biology department, “Big bro” Kajohnkiart Janebodin (KJ), Juliet Dang, Thao (Jenny) To, Diane Daubert, Worakanya Buranaphatthana (Ice), Nutthapong Kantrong

(Tom), Anusha Reddy Etikala, Atriya Salamati, Jonathan An, and Michael Baldwin; other departments: Shean Han Soh, David Ludwig, Heidi Sarff.

I would like to convey my sincere thanks to my funding support: NIH R90 training grant, Seattle Children's Research Institute InterCenter Grant generously support for my work.

Last but not least, I want to thank my whole family, especially my parents who always support me, believe in me, and love me.

FORMAL PRESENTATIONS

I have presented my work

Conference oral presentations:

1. 2015 IADR/AADR/Canadian Association for Dental Research (CADR) General Session & Exhibition, Models of Craniofacial Development and Disorders Session, Boston, MA, USA. (Mar 13, 2015)
   Hmx1 enhancer function in lateral facial development. **Li W**, Quina L, Turner EE, Visel A, Cox TC.
2. 2014 Graduate Student/Trainee Symposium, AADR Seattle Section, Seattle, WA, USA. (Sep 16, 2014)
   Hmx1 enhancer function in craniofacial development. **Li W**, Quina L, Turner EE, Visel A, Cox TC.

Conference abstract and poster presentations:

3. 2016 AADR/CADR Annual Meeting & Exhibition, Cleft Lip and Palate II Session, Los Angeles, CA, USA. (Mar 16-19, 2016)
   Hmx1- a regulator of lateral facial development. **Li W**, Rosin J, Cox LL, Rolfe S, Visel A, Turner EE, Cox TC.
4. Dental Research Day, School of Dentistry, UW, Seattle, WA, USA. (Sep 19, 2014)
   Common phenotypes in multiple species identify an Hmx1 enhancer important for lateral facial development. **Li W**, Quina L, Turner EE, Visel A, Cox TC.
5. 73rd Annual Meeting, Society for Developmental Biology, Seattle, WA, USA (Jul 17-21, 2014)
   Common phenotypes in multiple species identify an Hmx1 enhancer important for lateral facial development. **Li W**, Quina L, Turner EE, Visel A, Cox TC.
6. 2014 AADR/CADR Annual Meeting & Exhibition, National Institute of Dental and Craniofacial Research (NIDCR) Trainee Day, Charlotte, N.C., USA. (Mar 19-22, 2014)
   Hmx1 enhancer function in lateral facial development. **Li W**, Quina L, Turner EE, Visel A, Cox TC.
7. Dental Research Day, School of Dentistry, UW, Seattle, WA, USA. (Sep 20, 2013)
   Generation of Hmx1 enhancer transgenic mouse using the PiggyBac system. **Li W**, Quina L, Houghtaling S, Turner EE, Beier DR, Cox TC.

As part of our collaborative research, my work has also been presented

1. Craniofacial Morphogenesis & Tissue Regeneration (GRS) Gordon Research Seminar – from Bench to Bedside in Craniofacial Biology, Ventura, CA, USA (Mar 12-13, 2016)
   A Distal 594bp ECR Specifies Hmx1 Expression in Pinna and Lateral Facial Morphogenesis and Is Regulated by Hox-Pbx-Meis. Rosin J, **Li W**, Cox LL, Rolfe S, Latorre V, Akiyama JA, Visel A, Kuramoto T, Bobola N, Turner EE, Cox TC.

2. 37th Annual Meeting, Society of Craniofacial Genetics and Developmental Biology, Sanford Consortium for Regenerative Medicine, La Jolla, CA, USA. (Oct 18, 2014)
Common phenotypes in multiple species identify an Hmx1 enhancer important for lateral facial development. **Li W**, Quina L, Turner EE, Visel A, Cox TC.

PUBLICATIONS

1. *A distal 594bp sequencing containing an evolution conserved region specifies Hmx1 expression in pinna and lateral facial morphogenesis and is regulated by Hox-Pbx-Meis.* Rosin J, **Li W**, Rolfe S, Cox LL, Latorre V, Akiyama JA, Visel A, Kuramoto T, Bobola N, Turner EE, Cox TC. Development. 2016 Jun 10. pii: dev.133736. [Epub ahead of print]
2. *Common phenotypes in multiple species identify an Hmx1 enhancer important for lateral facial development.* **Li W**, Quina L, Turner EE, Visel A, Cox T. Conference Paper in *American Journal of Medical Genetics Part A*, June 2015, Volume 167.

TO

the memory of Qiuzhuan Chen, my beloved grandma